Phase Transitions in Dipole-Dipole Interacting Atomic Systems

by

Qingyang Wang

B.Sc., The University of Tokyo (2013)

Submitted to the Department of Physics
in partial fulfillment of the requirements for the degree of

Doctor of Philosophy in Physics

at the

MASSACHUSETTS INSTITUTE OF TECHNOLOGY

February 2022

Author .....
Department of Physics
December 30, 2021

Certified by .....
Susanne Yelin
Professor of Physics, Harvard
Thesis Supervisor

Certified by .....
Vladan Vultić
Professor of Physics
Thesis Supervisor

Accepted by .....
Deepto Chakrabarty
Associate Department Head of Physics

Phase Transitions in Dipole-Dipole Interacting Atomic Systems

by

Qingyang Wang

Submitted to the Department of Physics
on December 30, 2021, in partial fulfillment of the
requirements for the degree of
Doctor of Philosophy in Physics

Abstract

Phase transitions are generally a many-body phenomenon, and in order to access the full range of interesting physics of phase transitions, one needs interactions between the microscopic constituents. In this thesis, the phase transitions of atomic systems with interparticle dipole-dipole interaction controlled by laser fields are studied.

In the first half of the thesis, a system with externally polarized dipole molecules at half-filling moving along a one-dimensional zigzag chain is studied, including ground-state phase diagrams. The dipoles are oriented in-plane. Together with the geometry of the chain, this gives rise to a bond-alternating nearest-neighbor interaction due to simultaneous attractive and repulsive interactions. By tuning the ratio between the nearest-neighbor interaction and hopping, various phases can be accessed by controlling the polarization angle. In the ultrastrong coupling limit, the system simplifies to a frustrated extended axial Ising model. For the small coupling limit, a qualitative discussion of the ordering behavior using effective field theory arguments is provided. We show that when the chain angle is small, the system mostly exhibits a phase transition from the gappless phase into the gapped phase, whereas a large chain angle would drive the system into a dimerized phase, where the hopping strength is closely related to the orientation of the dimerized pairs of the molecules.

In the latter part of the thesis, the interatomic correlations of a semiclassical driven dissipative Dicke model are studied. By numerically examining the genuine multiparticle entanglement of the reduced systems of various particle numbers, we show that the entanglement is built up at the transition point, even when the system makes transitions into a highly mixed state. This suggests that the phase transition is of quantum nature. Additionally, the quantum discord of the system is computed. By the use of the full permutation invariance of the system, we show that the numerical complexity in computing quantum discord is significantly reduced. The result indicates that when the dissipation becomes dominant, the system is not entangled but possesses large quantum discord.

Thesis Supervisor: Susanne Yelin
Title: Professor of Physics, Harvard

Thesis Supervisor: Vladan Vultić
Title: Professor of Physics

Acknowledgments

I would not have come this far without warm supports from many people. First and foremost, I would like to express my deepest gratitude to my academic supervisor Prof. Susanne Yelin for providing me the freedom of pursuing my interests and helping me challenge many difficult problems of atomic physics. Susanne never failed to make me feel cheerful in our meetings. Any time I visit her, either at the office or on zoom, she gives me a big smile. I cannot forget the words Susanne told me when I was feeling down in a difficult situation – "The more you are struggling, the more I am here to help, because I am not the boss whipping my students to work, but a true supporter of you and your research." I would also like to thank my colleagues in Susanne's group. All of them are equally smart and passionate, at the same time, lively and joyful.

I am also grateful for my friends outside of the research group. Akira Sone, Jian Feng Kong, Cipriano Romero, Yongwhan Lim, David Theurel, Austin Mei, Seon Kinrot, Sami Dress, Yohei Sato, Taka Ihara, Daichi Hayakawa and many others, who made my years in Cambridge fruitful and enjoyable. Big part of my friends are from the soccer team Bosbaka FC that I gave my biggest passion to outside of MIT. Even if I face hardships during midweeks, I magically become happy just by imagining about playing soccer as a member of my favorite team on weekends. Let me give my teammates a big hug just like what we do when we score a goal.

Most of all, I would like to thank my loving and supportive family: my brother Qingbo, my mother Hongyu, and my father Yunhai. Qingbo is not only my beloved family, but also my best friend and my fellow researcher who pursued PhD in the same city. No matter how blessed I was with friends and colleagues in a foreign country, having a member of my family by my side always filled me with an extra sense of security and trust. My parents have sacrificed a great deal raising us. The longer I stay in the US, the more I realized how difficult it would have been for them to move from their home country and to rebuild a foundation for life abroad, all at the same time raising two mischievous boys. I am extremely grateful for their inexhaustible

support and faith in us even when we were more than 10,000km away from them. At the end of my PhD journey, I hope that I have made you proud.

Contents

List of Figures

List of Tables

Chapter 1

Overview

What is a phase transition? Perhaps the most common way to explain it is to give an example of different states of water. Water in a teapot is boiled and transformed into steam, the Charles River that we walk by everyday is no longer running in winter as the water is completely frozen. The list of such examples can go on and on. The seemingly complex concept of phase transition is actually deeply rooted in our daily lives. Therefore, historically, phase transitions have often been the subject of matter and phenomena that exist ubiquitously in nature. Water is the best example of this, and other examples such as the sudden disappearance of magnetism of certain magnets were no exception. Theories involving phase transitions were often used to determine the properties of materials in nature under certain conditions and in many cases the condition that is variable, and often is the parameter that induces phase transitions, is the temperature, as one would easily imagine in examples of water. Accordingly, thermodynamic and statistical mechanical arguments have become at the center stage for analyzing such phase transitions.

On the other hand, with the rise of quantum theory, it has become necessary to discuss some phase transitions in a way that is distinct from pure thermodynamic arguments. The class of such phase transitions that are beyond classical thermodynamics and are often induced by quantum fluctuations rather than thermal fluctuations, is called quantum phase transitions.

Quantum mechanics is in general a microscopic theory, and phase transitions are

macroscopic phenomena. Accordingly, to decipher the full picture of quantum phase transitions, one must deploy both microscopic and macroscopic viewpoints regardless of whether the information that is targeted to extract from the system is macroscopic or microscopic. Quantum statistical mechanics is usually the theory that bridges these two opposing realms of physics. In the early days, this theoretical framework mainly allowed physicists to go from macro to micro; explaining certain phases of matter through the dynamics of microscopic constituents of that matter. The BCS theory that enabled the explanation of the superfluidity of helium is categorized as such macro-to-micro achievements. However, the bridge between the two opposing regions further resulted in the formation of a flow that is logically opposite; starting from the micro and ending in macro. That is, physicists can, in principle, first design and propose a model with specific microscopic properties and then theoretically investigate the macroscopic ones including the phase of the model. This is exactly the approach we took throughout this thesis.

When discussing the microscopic aspect of a state of matter, it is the interparticle interactions that usually play the central role. Phase transitions, whether classical or quantum, are generally a many-body phenomenon, and to open the door to the full scope of the exciting physics of phase transitions, one needs interactions between the microscopic constituents. In this thesis, the key to the door is the dipole-dipole interaction; we explore novel physical systems and their phase properties that are not previously known, by taking the dipole-dipole interacting as the starting point of the microscopic end.

The heart of the peculiarity of dipole-dipole interaction is its anisotropic and long-range nature. Since the dipole interaction is a low-order term in multipole expansion, it exists universally in nature. However, there are not numerous materials that embody these properties in the context of phase transitions, partly because in those systems, other interactions are usually dominant.

If we shift our perspective to experimental physics, one of the turning points that followed the flow of micro to macro was the advent of laser technologies and their influence on atomic physics. In particular, certain technologies of cold atoms

have made it possible to artificially create systems with properties that are difficult to exist in nature. From a microscopic point of view, by controlling atoms at the individual level, it has become possible to realize a wide variety of atomic interactions and arrangements of atoms. Consequently, it has widened the possibilities of experimentally designing a system with more interesting phase transitions that are artificially creatable in the lab. Dipole-dipole interactions, for example, are no longer the interaction that happens to exist in particles in certain materials, but rather, it is a type of interaction that can be artificially created and controlled in the lab. In atomic and molecular physics, the interaction of atoms is not limited to interparticle ones, but also is applied to atoms and external fields that are difficult to mimic in natural systems. Such fine tuning of atom-field interaction leads to artificial lattices such as optical lattices, as we discuss in the first part of the thesis.

From a broader perspective, the concept of phase transition has been found to be deeply related to information theory. The idea is that regardless of the microscopic interactions, the phase transition should ultimately be classifiable by the information theoretic description of the relationships of the microscopic constituents. This is particularly useful in discussing phase transition points, where the correlation length is known to diverge infinitely, as first shown by the Landau-Ginzburg theory. In thermal phase transitions, these correlations were classical correlations (probabilistic correlations), but as research on quantum phase transitions has progressed, it has become clear that quantum correlations, or quantum entanglement to be precise, also behave in a peculiar way in quantum phase transitions. Less known is the correlation behavior of phase transitions of hybrid systems whose description involves both quantum and classical. Chapter 3 of the thesis mainly discusses the phase transitions of atomic systems from this perspective.

Chapter 2

Interacting in-plane molecular dipoles in a zig-zag chain

2.1 Introduction and Motivation

The efficient production of ultracold dipolar systems hanonequilibrium to a wide range of interesting effects, for example, strongly correlated systems, chemical reactions at ultracold temperatures, precision tests of fundamental symmetries, possibly new schemes of quantum information processing, just to mention a few [9, 3]. Additionally, there has been great progress in the creation of new techniques for nonstandard optical lattices [5, 64] and optical tweezers [44] that would make a quantum simulator using systems of ultracold atoms even more promising and unique. The vast tunability offered by molecules and lattice configurations has introduced many ideas to simulate interesting unsolved quantum models motivated by solid-state physics. In particular, low-dimensional systems in this context are of great interest, partly because of the recent development in creating real solid state systems that can be described in theoretical models studied in the past, and because an ultracold system may provide a test ground that is beyond the actual material we have access to today. Topics in low-dimensional physics range from frustrated systems in 1D, 2D [37, 1, 31, 59, 32, 18], and coupled one-dimensional setups [50, 25, 61, 4], to non-equilibrium behavior in certain systems [58, 21].

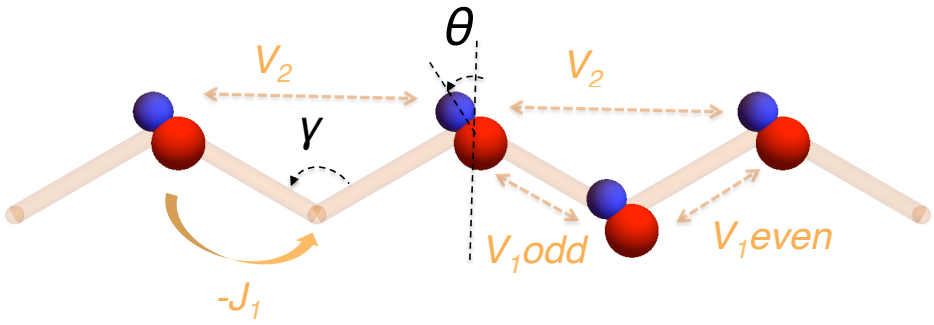

Figure 2-1: (Color online) Schematic setup of dipoles moving on a zig-zag chain with an opening angle γ.
The dipoles are polarized by an external field enclosing an angle θ with the normal of the chain axis

For this, we consider a quasi-1D system, where the dipolar particles, regardless of whether they are fermions or hardcore bosons, are confined in a zig-zag optical lattice and are polarized in-plane, leading to simultaneous attractive and repulsive interactions (Fig. 2-1). This means that, while hopping can be limited to nearest neighbors (NN) in the same way that this is the case for strictly 1D models, at least one order more (i.e., next nearest neighbor, NNN) has to be taken into account for interactions. Depending on the angle of the zig-zag opening, this model can be viewed as the 1D building block of, for instance, a hexagonal or kagomé lattice. In this manuscript, we show that this is a model that, despite its small deviation from a strictly 1D system, leads to a qualitatively different and much richer phase diagram (Fig. 2-2), especially for the two limiting cases – very small and very large inter-site hopping. This model can, in principle, be explored with typical species of polar particles, fermions or bosons, as one of the first models – and also a very simple model– in the field of ultracold atoms that add a particular variety of phases (see Fig. 2-2) to the traditional linear chain by introducing a dimerization parameter in the chain.

Our main result, which shows the ground state phase diagram of the system for various zig-zag opening angle γ and θ is summarized in Fig. 2-2. We observe a zig-zag chain introducing, in particular, a dimerized phase whose orientation can be tuned by the depth of the optical lattice.

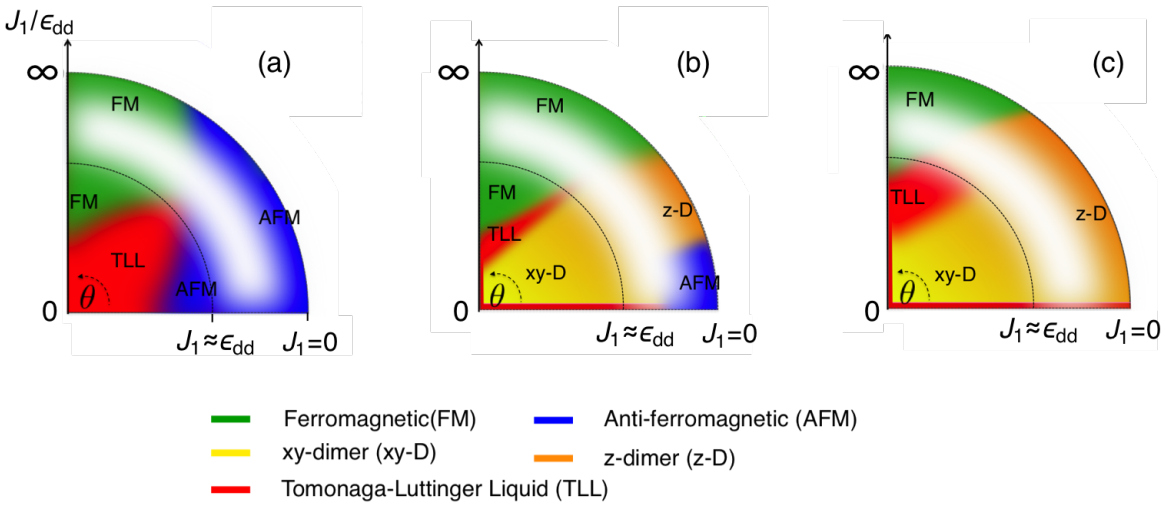

Figure 2-2: (Color online) Qualitative ground state phase diagram of our system with different opening angles of the lattice γ.
The radial degree of freedom shows the inverse of the hopping parameter of the system, and the argument θ is the angle of the polarized molecules. (a) $\gamma = \pi$ (straight lattice), (b) $\gamma = 5\pi/6$, (c) $\gamma = 2\pi/3$. Each color shows a different phase. The white shaded area is the region whose ordering behavior is not studied in this paper.

2.2 The model

Throughout the paper, we set the temperature to be zero. The model we consider is conceptually described in Fig. 2-1. This system consists of hard-core dipoles sitting at the vertices of the zig-zag chain with chain opening angle γ ($0 < \gamma \leq \pi$, cf. Fig. 2-1). The dipoles can be realized using heteronuclear molecules [35, 55, 67] or dipolar atoms [26, 10, 18, 3]. The dipolar particles are polarized in-plane, leading to simultaneous attractive and repulsive interactions from dipole-dipole interactions

$$V_{dip} = \epsilon_{dd}(1 - 3\cos^2\theta_{\mathbf{r_1}-\mathbf{r_2}})$$

with the dipolar coupling strength $\epsilon_{dd} = \mu_e/(4\pi\epsilon_0|\mathbf{r_1} - \mathbf{r_2}|^3)$, where ϵ_0, μ_e are the vacuum permittivity and electric dipole moment of the molecules, respectively, $\mathbf{r_1}$ and $\mathbf{r_2}$ are the position of the molecules, $\theta_{\mathbf{r_1}-\mathbf{r_2}}$ is the angle between $(\mathbf{r_1} - \mathbf{r_2})$ and the external electric field that polarizes the molecules. Additionally, the particles are mobile and can propagate.

In actual experiments, the lattice can be created by appropriately angled standing wave laser fields with the correct intensity to create single-chain strands. The molecules can then be loaded by applying an electric field $\vec{E}$ perpendicular to the zig-zag plane, and subsequently changing the orientation of $\vec{E}$ adiabatically until it becomes parallel to the plane, followed by the process of changing $\vec{E}$ in plane (to vary θ). This way, there should never be more than one molecule per site, fulfilling the hardcore condition throughout the experiment (see the next subsection for more details).

The most general Hamiltonian that describes our system is

$$\begin{aligned} H = &- \sum_{j} \sum_{j'>j} J_{j'-j} \hat{a}_j^\dagger \hat{a}_{j'} + \text{h.c.} \\ &- \mu \sum_{j} \hat{n}_j + \sum_{j'>j} \sum_{j} V_{j'-j}^{[j/2]} \ \hat{n}_j \hat{n}_{j'} \end{aligned} \tag{2.1}$$

where $J_{j-j'}$ is the hopping parameter between sites j and j', μ is the chemical potential. Note again that we will only consider NN hopping, and in this case, the creation (destruction) operator $\hat{a}_j(\hat{a}_j^\dagger)$ can either be fermionic or bosonic without any essential difference as there is an exact mapping from fermion to hardcore boson systems [27] . $V_{j-j'}^{[j/2]}$ denotes the non-local dipole-dipole interactions between particles at site j and j', respectively. Note that due to the anisotropic nature of dipole-dipole interaction and the nontrivial geometry of the chain, this interaction term $V_{j-j'}^{[j/2]}$ depends not only on the range $j-j'$ but also on the even-odd of j (expressed by $[j/2]$). This $V_{j-j'}^{[j/2]}$ can be varied dynamically from negative to positive value with θ and γ. As an example, using the standard form of the dipole interaction, we find, after simple trigonometric manipulations, the following explicit expressions for the NN interaction and the next

nearest neighbor (NNN) interaction.

$$V_1^{\text{even}} = \epsilon_{dd}\left[1 - 3\cos^2\left(\pi - \frac{\gamma}{2} - \theta\right)\right], \tag{2.2}$$

$$V_1^{\text{odd}} = \epsilon_{dd}\left[1 - 3\cos^2\left(\frac{\gamma}{2} - \theta\right)\right], \tag{2.3}$$

$$V_2 = \frac{\epsilon_{dd}}{[2(1-\cos(\gamma))]^{3/2}}\left[1 - 3\cos^2\left(\frac{\pi}{2} - \theta\right)\right] \tag{2.4}$$

2.2.1 Simplification of the Hamiltonian

We simplify the model Eq. (2.1) by assuming that there are exactly half as many molecules as the lattice sites. This is a less specific assumption than it looks at first glance, since the remaining parameters can be mostly rescaled for relatively small filling imbalances. In addition, we further impose that the lattice opening angle $\gamma \geq 2\pi/3$. This allows us to safely ignore longer-range hopping (beyond J_1, i.e., NN hopping) as the overlap between the NNN Wannier orbitals and beyond is significantly smaller than the nearest-neighbor ones. Likewise, we make the simplification on the (dipolar) interaction terms by only taking NN and NNN interactions. All contribution from longer-range interactions is small because of the $1/r^3$ nature of the dipolar interaction, and we assume it can be ignored. To this we introduce the dimerization parameter δ:

$$\begin{aligned} H &= -J_1 \sum_j \hat{a}_{j+1}^\dagger \hat{a}_j + \text{h.c.} - \mu \sum_j \hat{n}_j \\ &\quad + V_{\text{NN}} \sum_j [1 + \delta(-1)^j] \hat{n}_j \hat{n}_{j+1} + V_2 \sum_j \hat{n}_j \hat{n}_{j+2} \end{aligned} \tag{2.5}$$

where V_{NN} and δ are related to V_1^{even} and V_1^{odd} as $\delta = (V_1^{\text{even}} - V_1^{\text{odd}})/(V_1^{\text{odd}} + V_1^{\text{even}})$ and $V_{\text{NN}} = (V_1^{\text{odd}} + V_1^{\text{even}})/2$. In this paper, we study the model described by this Hamiltonian.

We restrict the region of parameters θ and δ by symmetry arguments. First, we note that the interactions exhibit symmetries with respect to $\theta = 0$ (cf. Fig. 2-3), which translate directly into symmetries of the Hamiltonian. Performing the transformation $\theta \to \theta + \pi$ leaves the Hamiltonian Eq.(2.6) unchanged and we can

restrict ourselves to the range $\theta \in [-\pi/2, \pi/2]$. Another symmetry is changing the sign of the dimerization parameter as $\delta \to -\delta$ while at the same time inverting theta $\theta \to -\theta$. However, inverting the sign of δ can be achieved merely by shifting the summation index by ± 1. Therefore, we can further restrict ourself to $\delta > 0$ and $\theta \in [0, \pi/2]$. This implies that the translational invariance is broken, yet as we will see shortly, these symmetries will be reproduced in the systems' ground states.

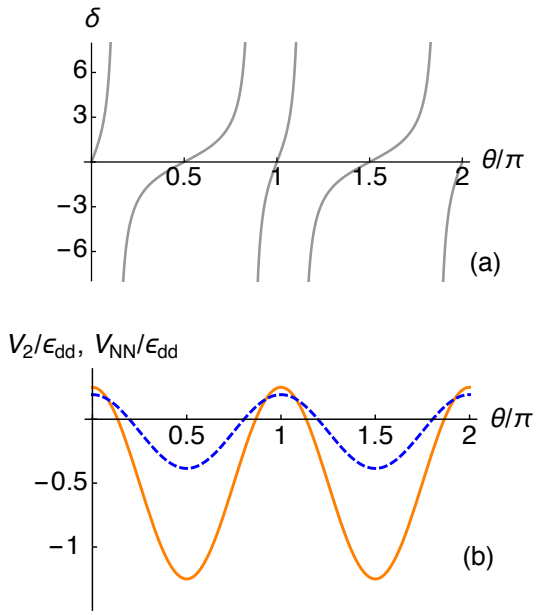

Figure 2-3: (Color online) (a) Dimerization parameter δ and (b) interactions V_{NN}, V_2 with respect to θ. The chain opening angle is set to be $\gamma = 2\pi/3$.

2.2.2 On-site contribution and stability

In general, the models of particles in optical lattices have an on-site interaction term $Un_i(n_i - 1)/2$. This term is often abandoned when the molecules are polarized by an external electric field and thus they can be regarded as hard core bosons. This results from the infinite on-site repulsion of two parallel dipoles sitting in the same space, thus creating a substantial barrier. This simplification process, however, needs extra care in our case since, once the E field is in plane, the orientation of the dipoles changes between strong attractive and strong repulsive interactions, depending on the (in-plane) polarization angle. Here we argue that in most of cases the on-site term

can still be ignored mainly because of the quantum Zeno effect.

To explain, we first give an estimate on the on-site interaction energy U. This is computed as

$$\begin{aligned} U &= U_{ct} + U_{dip} \\ &= g \int d^3r \rho(\boldsymbol{r})^2 + \int d^3r d^3r' \rho(\boldsymbol{r}) U_{dd}(\boldsymbol{r} - \boldsymbol{r}') \rho(\boldsymbol{r}') \end{aligned} \tag{2.6}$$

where the first term is the effective contact potential and the second is the potential coming from the dipole interaction. $\rho(\mathbf{r}) = |\mathbf{w}(\mathbf{r})|^{\mathbf{2}}$ is the Wannier function density, U_{dd} is the dipolar interaction, and g is the depth of contact potential that is related to s-wave scattering length. The second term is expressed in Fourier-transformed $\tilde{\rho}$ and $\tilde{U}_{dd}$ as, $1/(2\pi)^2 \int d^2\boldsymbol{k} \tilde{\rho}(\boldsymbol{k})^2 \tilde{U_{dd}}(\boldsymbol{k})$ Here we assume a strong trapping potential in the z-direction, thereby treating the lattice site as 2D, and further assume that in this plane each site in the trap is isotropic. The polarizing E field is also in this plane, and thus the direction of E field in the xy-plane is irrelevant in the discussion. If treating Wannier functions as Gaussians with length scale l_{HO}, then $\tilde{\rho}(\boldsymbol{k}) = \exp\{(-l_{\mathrm{HO}}^2 k^2/4)\}$, and $\tilde{U_{dd}}(\boldsymbol{k}) = -\pi d^2(1/\epsilon - k) + \pi d^2 q \cos(2\phi_k)$, where d is the electric dipole moment and ϵ is the cutoff length that is on the order of molecule length in true 2D confinement. From this we arrive at

$$\begin{aligned} U_{dip} &= \int d\boldsymbol{k}^2 \left[-\pi d^2 \left(\frac{1}{\epsilon} - q \right) + \pi d^2 q \cos(2\phi_k) \right] e^{-\frac{1}{2} l_{\mathrm{HO}}^2 k^2} \\ &= \frac{2\pi^2 d^2}{l_{\mathrm{HO}}^2} \left(\frac{\sqrt{2\pi}}{l_{\mathrm{HO}}} - \frac{1}{\epsilon} \right) \end{aligned} \tag{2.7}$$

Typically, $l_{\mathrm{HO}} \approx 1\mu$m and $\epsilon \approx 0.1$nm In real experiments the confinement is not truly flat which will essentially magnify the value of ϵ. Because of this, depending on the design of the confinement, U_{dip} may be somewhat comparable to other energy scales and therefore on-site terms cannot be neglected. In this case one needs to tune the depth of contact potential g (in Eq. (2.6)) to exclude on-site terms if the molecules are nonreactive. If the molecules are reactive then because of the Zeno effect the on-site term are ignored regardless of the ϵ. (The Zeno effect is briefly explained in the next

paragraph.) Therefore the on-site energy U is negative with an absolute value at least several orders of magnitude larger than the other energy scales such as J_1, V_{NN} and V_2, which are at most on the order of d^2/l_{HO}^3. If we naively ignore the dynamics and internal structure of the molecules and assume the system initially is prepared with one molecule per site, at most, we can neglect the part of the Hilbert space with more than one molecule per site. This can be done because in the ultracold regime, there would be no process to dissipate the energy gained from this on-site contribution.

Often, however, the molecules are reactive and hence will be kicked out of the optical lattice once they come to occupy the same lattice site. In these situations, attractive dipole directions enhance such reactive processes and the appropriate dissipative picture is necessary to describe those systems. This contrasts with the case where molecules are polarized to be repulsive and consequently feel the large potential barrier generated by the dipole interactions before they can approach close enough to start inelastic processes. Even with the dissipation process, we point out that when the dissipation is strong, the decay process of molecules is frozen out. This counterintuitive result is due to the continuous Zeno effect [53, 67, 16]. When $\gamma \gg J$, where γ is the 2-body on-site loss rate and J is the hopping parameter, the molecules may again be treated as hard-core, with much slower dissipation rate of the system $\gamma_{eff} \approx J^2/\gamma \ll 1/J$. Thus, it is necessary to choose the system parameters such that the tricky cases are avoided. In what follows this is assumed.

2.3 Ultrastrong coupling case

In this section, we consider the ultrastrong coupling limit $J_1 \to 0$ with an even number of particles, i.e. $N \in 2\mathbb{N}$, where we observe that Hamiltonian (2.6) reduces to a purely classical one. We project the system onto a spin-1/2 system where the spin degree of freedom is encoded in the occupation number of a single lattice site, which is explicitly done by the Jordan-Wigner transformation, $S_j^+ = a_j^\dagger e^{i\pi O_j}$, $S_j^- = a_j e^{-i\pi O_j}$, $S_j^z = a_j^\dagger a_j - \frac{1}{2}$, with $O_j = \sum_{l<j} a_l^\dagger a_l$. Here, the S^+ and S^- operators are spin raising and lowering operators, respectively. The phase diagram of $J_1 = 0$ is shown

in Fig. 2-4 and the numerical result of the energy density of each phase for small J_1 can is shown in Fig. 2-5

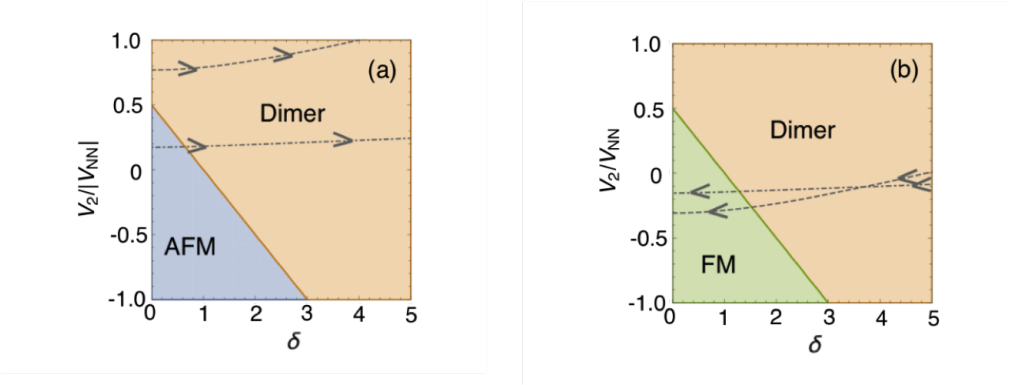

Figure 2-4: (Color online) Phase diagram of the ultrastrong coupling limit. (a) $V_{\mathrm{NN}} > 0$, (b) $V_{\mathrm{NN}} < 0$. The dashed lines show the actual trace of the parameter space when θ is varied from 0 to $\pi/2$.

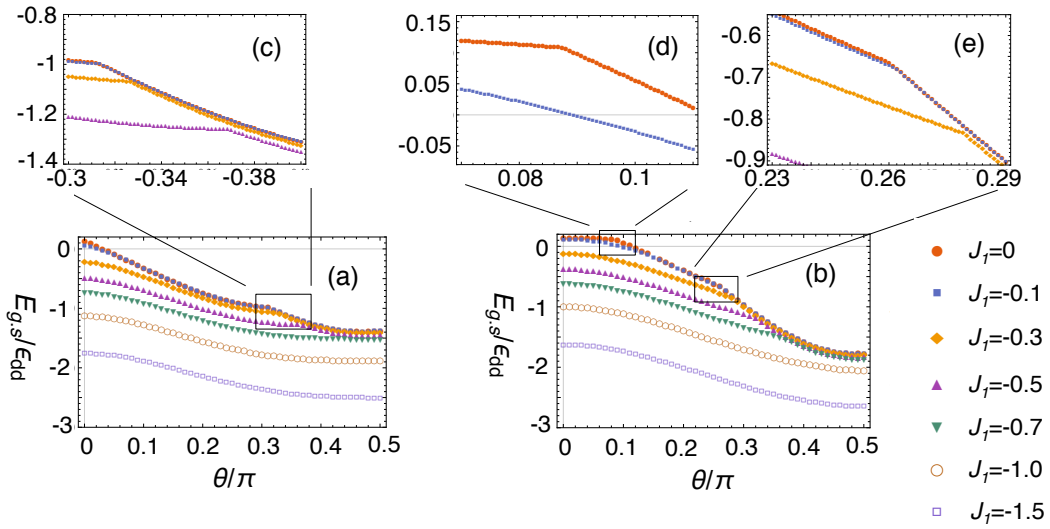

Figure 2-5: (Color online) Ground state energy per particle plotted against $\theta \in [-\pi/2, \pi/2]$ with various hopping parameter J_1 by exact diagnolization method Number of sites L=18. (a) $\gamma = 2\pi/3$ (b) $\gamma = 5\pi/6$. (c)-(e) are magnified areas of the figures. The kinks show the first order phase transition points.

2.3.1 Ordering of the ground state

Since the Hamiltonian (2.6) without the hopping term is classical, it is not difficult to completely identify the lowest energy configuration. The ground states are classified into these three phases: anti-ferromagnetic, dimer and ferromagnetic, depending on the parameters δ, $V_{\rm NN}$ and V_2. To explicitly write down the states, the antiferromagnetic state $|\text{AFM}\rangle = |\ldots\uparrow\downarrow\uparrow\downarrow\ldots\rangle$, $|\text{dimer}\rangle = |\ldots\uparrow\uparrow\downarrow\downarrow\uparrow\uparrow\ldots\rangle$, and ferromagnetic state $|\text{FM}\rangle = |\ldots\uparrow\uparrow\uparrow\downarrow\downarrow\downarrow\ldots\rangle$. To ensure half-filling, the ferromagnetic order $|\text{FM}\rangle$ exhibits domain walls, dividing the system by half, corresponding to a domain wall soliton [33]. We can derive the condition for the system in each of the phases by comparing the energy per site.

Here, the symbols such as $\boxed{\text{n L}}$ (or $\boxed{\text{n R}}$) $n = 1, 2, 3...$ are used to denote a "building block" of the system, whose meaning is n left (right) sites are filled with the molecules and n right (left) sites are vacant. For example, $\boxed{\text{1, L}}$ is $\bullet\circ$ with the black circles being the filled sites and white circle being vacant sites. $\boxed{\text{3, R}}$ is $\circ\circ\circ\bullet\bullet\bullet$ for instance.

Using these "blcok" notations, the three presumable ground states, ferromagnetic,

anti-ferromagnetic, and dimer state, are described as

$$\begin{aligned} |AFM\rangle &= \boxed{1,\ \mathrm{L}} - \boxed{1,\ \mathrm{L}} - \boxed{1,\ \mathrm{L}} - \boxed{1,\ \mathrm{L}} - .... \\ |FM\rangle &= \boxed{\mathrm{N}/2,\ \mathrm{L}} \\ |Dimer\rangle &= \boxed{2,\ \mathrm{L}} - \boxed{2,\ \mathrm{L}} - \boxed{2,\ \mathrm{L}} - \boxed{2,\ \mathrm{L}} - ... \end{aligned} \tag{2.8}$$

and their average energy per site is

$$\begin{aligned} E_{p.s.}^{AFM} &= \frac{V_2}{2} \\ E_{p.s.}^{FM} &= \frac{V_1^{even} + V_1^{odd} + 2V_2}{4} \\ E_{p.s.}^{Dimer} &= \frac{V_1^{even}}{4} \end{aligned} \tag{2.9}$$

It is useful to investigate the energy density of these "building blocks" for the later comparison. It is easy to convince oneself that the average energy per site is different depending on whether N is odd or even. To write it explicitly with the coupling constants $V_1^{odd}, V_1^{even}, V_2$,

$$\begin{aligned} E_{p.s.}(\boxed{2\mathrm{m},\ \mathrm{L}}) &= \frac{mV_1^{even} + (m-1)V_1^{odd} + (2m-2)V_2}{4m} \\ E_{p.s.}(\boxed{2\mathrm{m}{+}1,\ \mathrm{L}}) &= \frac{mV_1^{even} + mV_1^{odd} + (2m-1)V_2}{4m+2} \end{aligned} \tag{2.10}$$

The differences of these energies are computed as

$$\begin{aligned} \Delta E_{p.s.}^{2mL} &\equiv E_{p.s.}(\boxed{2(\mathrm{m}{+}1),\ \mathrm{L}}) - E_{p.s.}(\boxed{2\mathrm{m},\ \mathrm{L}}) \\ &= \frac{2V_1^{odd} + V_2}{2m(m+1)} \\ \Delta E_{p.s.}^{2m+1L} &\equiv E_{p.s.}(\boxed{2(\mathrm{m}{+}1){+}1,\ \mathrm{L}}) - E_{p.s.}(\boxed{2\mathrm{m}{+}1,\ \mathrm{L}}) \\ &= \frac{V_1^{odd} + V_1^{even} + 4V_2}{2(2m+3)(2m+1)} \end{aligned} \tag{2.11}$$

We see that depending on the sign and magnitude of the interaction parameters, $\Delta E_{p.s.}$ can be positive or negative (or 0), regardless of the value of m (or equivalently

N). This means that when we fix $V_1^{odd}, V_1^{even}, V_2$ the energy per site of the building blocks are either monotonic increased or decreased, or just a constant with respect to m and thus we can find a unique building block that has the lowest energy per site. We can presume that the ground state is built with these building blocks that have the lowest energy per site.

However, we need to take into account the "connection energy" arising from the additional interaction between the connecting building blocks. For example $\boxed{1, \text{L}}$ – $\boxed{\text{N, L}}$ with $N \geq 2$ ($\bullet\circ$ – $\bullet\bullet\bullet...\circ\circ$) generates V_2 upon connecting (Remember $\bullet$ is filled and $\circ$ is empty site.) Since the range of the interaction is at most 2 sites, the contribution of the connection is the same for all $N \geq 2$. Therefore when we consider the connection, it is sufficient to classify the building blocks into 4 cases: $\boxed{1, \text{L}}$, $\boxed{1, \text{R}}$, $\boxed{\text{N, L}}$, $\boxed{\text{N, R}}$, with $N \geq 2$. To list up all possible connections, there are $4 \times 4 = 16$ possible possibilities – one of those 4 building blocks on the left and one of those 4 on the right. All connections are shown in Table (2.1)

Before moving onto the next step, we note that the role of V_1^{odd} and V_1^{even} can be flipped by inserting an empty site at the left edge of the chain. Instead of performing this, we remove this redundancy by deliberately forcing $V_1^{odd} \geq V_1^{even}$ or vice versa, depending on in each case. For example, $|Dimer\rangle$ has average energy $V_1^{even}/4$ per site. By inserting an additional site (or translating by 1 site) the energy is $V_1^{odd}/4$. In this situation we will just assume $V_1^{odd} < V_1^{even}$. With all of these information, we would like to explicitly construct a state that has the lowest energy with given interaction constants and prove that either one of the 3 phases (dimer, ferromagnetic, or anti-ferromagnetic) has the lowest energy in any case. From now on, we use n to be general integer that is larger than or equal to 0, and N to be the integer that is larger than or equal to 2.

When the interaction parameters fulfill these conditions, the ground state is obvious.

1. $V_1^{even} < 0, V_1^{odd} < 0, V_2 < 0 \Rightarrow |FM\rangle$

2. $V_1^{even} > 0, V_1^{odd} < 0, V_2 > 0$ or $V_1^{even} < 0, V_1^{odd} > 0, V_2 > 0 \Rightarrow |Dimer\rangle$

Table 2.1: the building blocks on the left are the left component of the connection. The top ones are right component of the connection. For example (3,2) element of the table, V_1^{odd}, indicates [1,R]–[N, L] connection of gives V_1^{odd} energy.

	[1, L]	[1, R]	[N, L]	[N, R]
[1, L]	V_2	0	V_2	0
[1, R]	V_1^{odd}	V_2	V_1^{odd}	0
[N, L]	0	0	0	0
[N, R]	$V_1^{odd} + V_2$	V_2	$V_1^{odd} + 2V_2$	0

3. $V_1^{even} > 0, V_1^{odd} > 0, V_2 < 0 \Rightarrow |AFM\rangle$

Now let us tackle the less obvious case. We need to consider these 4 cases:

1. $V_1^{even} > 0, V_1^{odd} > 0, V_2 > 0$

2. $V_1^{even} < 0, V_1^{odd} < 0, V_2 > 0$

3. $V_1^{even} > 0, V_1^{odd} < 0, V_2 < 0$

4. $V_1^{even} < 0, V_1^{odd} > 0, V_2 < 0$

First, let us look into Case 1. $(V_1^{even}, V_1^{odd}, V_2 > 0)$. For simplicity, we can impose another condition, that is, $V_1^{even} < V_1^{odd}$. Then we prove that when $V_2 > V_1^{even}/2$ the lowest energy state is Dimer with average energy per site $E_{p.s.}^{Dimer} = V_1^{even}/4$ and when $V_2 < V_1^{even}/2$ it is in anti-ferromagentic order and $E_{p.s.}^{AFM} = V_2/2$ just by explicitly computing the energy.

Now consider a general state

$$\underbrace{[\text{n', L}] - ...}_{\text{made of [L]}} - \underbrace{[\text{n", R}] - ...}_{\text{made of [R]}} - [\text{n"', L}] - .... \tag{2.12}$$

When all interactions are positive, from Eq.(2.11), we know that the average energy per site of the building blocks is the smallest when $n = 1$. This let us exclude the possibility of $n, n', n'' > 2$ that appears in Eq.(2.12). Therefore, the ground state must be built with "building blocks" whose n is either 1 or 2.

Let us assume all n appears in Eq.(2.12) are 1. Looking at the Fig. 2.1, we see that the possible lowest energy state is either |1, L|-|1, R|-|1, L|-|1, R|-|1, L|.... whose average energy per site is $V_1^{odd}/4$, or |1,L|-|1,L|-|1, L|-.... (or equivalently |1, R|-|1, R|-...) whose average energy per site is $V_2/2$.

Similarly, when we set all $n = 2$, possible lowest energy state is |2,L|-|2,L|-|2, L|...or |2,R|-|2,R|-|2,R|- and the average energy per site is $V_1^{even}/4$.

From these analysis, we set an upper bound for the ground state average energy per site:

$$\begin{aligned} V_1^{even} < V_1^{odd} \wedge V_2 < V_1^{even}/2 \Rightarrow E_{G.S} \leq V_2/2 \\ V_1^{even} < V_1^{odd} \wedge V_2 > V_1^{even}/2 \Rightarrow E_{G.S} \leq V_1^{even}/4 \end{aligned} \tag{2.13}$$

Now we need to take into account the third case – state with $n = 1$ and $n = 2$ "building blocks" combined. One can come up with low energy states such as |2, L|-|1, R|-|2, R| - repetition of this set of 3 blocks, whose energy per site is $\frac{2V_1^{even}+V_1^{odd}+2V_2}{10}$ and |1, L|-|1, R| -|2, L| -repetition of this set of 3 blocks, whose energy per site is $\frac{V_1^{odd}+V_1^{even}}{8}$. Both of these energy exceeds the upper bound we set previously at Eq.(2.13) and cannot be the ground state. Therefore the ground state configuration must be either |2,L|-|2,L|-|2, L|...or |2,R|-|2,R|-|2,R|-, meaning the ground state is the (Ising) dimer phase.

The other ground states for less obvious cases can be identified the same way and we will not list the derivation here. Again, the results that summarize this section is shown in Fig. 2-4.

To summarize, the phases of the ultracoupling case and their condition are : anti-ferromagnetic: $E_{GS}/L = V_2/2$, ferromagnetic: $V_2/2 + V_{\mathrm{NN}}/2$, dimer: $V_{\mathrm{NN}}(1-\delta)/4$. When $V_{\mathrm{NN}} < 0$, V_2 is not relevant and the transition point still lies at $\delta = 1$. For the case $\delta > 1$ the system is in the dimer phase, and for $\delta < 1$, it is in the ferromagnetic phase. When $V_{\mathrm{NN}} > 0$, V_2 significantly affects the phase. When $V_2/V_{\mathrm{NN}} < (1-\delta)/2$, the system is in the anti-ferromagnetic phase and when $V_2/V_{\mathrm{NN}} < (1-\delta)/2$, it is

in the dimer phase. The phase diagram that summarizes the argument is shown in Fig. 2-4. Note that interactions and δ cannot be tuned completely independently. The possible traces are indicated by the gray dashed lines in Fig. 2-4 with $\gamma = 2\pi/3$ and $5\pi/6$ and θ varied from 0 to $\pi/2$. It suggests for $\gamma = 2\pi/3$ only one phase transition whereas for $\gamma = 5\pi/6$ there would be two. This can be checked by calculating the derivative with respect to θ or observing the kinks in the $J_1 = 0$-curve of Fig. 2-5.

To finish the discussion of the strong coupling limit, we remark that for an odd number of particles the nature of the anti-ferromagnetic and ferromagnetic phases are not altered and merely the ground-state energy will be different. However, in the dimer phase, it is easy to see that the additional particle will tend to localize at the edge of the system with a smaller bond energy. Hence, the bulk state will still show the dimerized structure.

Before concluding , we would like to mention the case of a small but finite J_1 contribution. From the results of the exact diagonalization, we see that the cusp at $\theta \sim 0.09\pi$ for $\gamma = 5\pi/6$ (cf. Fig. 2-5 graph C), corresponding to the boundary between the anti-ferromagnetic and the dimer-configuration vanishes as soon as $J_1 \neq 0$ turning into a smooth crossover. This can be understood intuitively by observing that both states break translational invariance but exhibit a discrete Z_2 symmetry, thus belonging to the same symmetry class. On the other hand, the ferromagnetic phase preserves translational invariance and belongs to a different symmetry class. Hence the dimer- and ferromagnetic states cannot be related by a continuous distortion and the cusp remains, as can be seen in Fig. 2-5. Moreover, the numerical results suggest that the phase transition stays of first order even for finite J_1 until it vanishes in the TLL phase (see the next section). The transition point is continuously shifted towards large values of θ with increasing J_1. However, the question whether the first-order line and the BKT line meet, and how they close is beyond the scope of this manuscript.

2.4 Weak coupling case

Now we will derive a qualitative ground-state phase diagram of this model in the opposite limit – the case of small dipolar coupling. We assume a finite hopping term J_1 and regard the dipolar interaction as a small perturbation, using field-theoretic arguments and a bosonization formalism. In this section, we take the large size ($L \to \infty$) and continuum (lattice spacing $a \to 0$) limits. The discussion below is a well-studied topic that can be found in standard textbooks in this literature (see, for example [17]) which we closely followed.

2.4.1 Low energy effective theory of non-interacting fermions

Rewriting the system in the low energy effective form and in the spin picture, thenon-interactingg Hamiltonian becomes

$$\begin{aligned} H_{XX} &= \sum_j \left[-J_1(\mathcal{S}_j^+\mathcal{S}_j^- + \mathcal{S}_j^-\mathcal{S}_j^+)\right] \\ &= \sum_j \left[-J_1(\hat{a}_j^\dagger \hat{a}_{j+1} + \hat{a}_{j+1}^\dagger \hat{a}_j)\right] \\ &= -J_1 \int_{-\pi/a}^{\pi/a} dk \cos(ak)\, \tilde{a_k}^\dagger\, \tilde{a_k} \end{aligned} \tag{2.14}$$

where in the third line we go into Fourier space. For the case of half-filling, the Fermi points are at $k = \pm\pi/2a$. In the low energy regime, we can linearize the energy spectrum around these Fermi points and introduce slowly varying fields. The ground state of this model is now gapless and can be treated as Tomonaga-Luttinger liquid (TLL). Mapping the XX model into an effective low energy model is a well-studied subject, and here we will only summarize the basic relations to clarify the notations used in this paper.

The Fermi operators can be written as field operator

$$\frac{a_j}{\sqrt{a}} = e^{ik_F x}\psi_R(x) + e^{-ik_F x}\psi_L(x) \tag{2.15}$$

where, $k_F = \pi/2a$ and the index j and x are related as $x = ja$. $\psi_R(x)$ and $\psi_L(x)$ are (slowly varying) right and left mover operators. These operators can be described using Boson fields $\varphi_L(x)$ and $\varphi_R(x)$:

$$\psi_R(x) = \frac{e^{i\varphi_R(x)}}{\sqrt{2\pi\alpha}} \tag{2.16}$$

$$\psi_L(x) = \frac{e^{-i\varphi_L(x)}}{\sqrt{2\pi\alpha}} \tag{2.17}$$

The α appearing here is an undetermined regularization parameter that has the dimension of length. This mapping from Fermi operator to the boson field operator is called bosonization. While 1D Fermi systems in general show various peculiarities that would make perturbative calculation difficult, the mapped boson system may be easier to treat. Thus, bosonization generally is an effective method in 1D systems.

It is customary to define the (bosonic) field operators as

$$\begin{aligned} \phi(x) &= \frac{1}{\sqrt{4\pi}}[\varphi_L(x) + \varphi_R(x)], \\ \Pi(x) &= \frac{d}{dx}\frac{1}{\sqrt{4\pi}}[\varphi_L(x) - \varphi_R(x)]. \end{aligned} \tag{2.18}$$

These operators are conjugate and obey the commutation relation $[\phi(x), \Pi(x')] = \delta(x - x')$. Thus, the effective Hamiltonian of the noninteracting spinless fermions (or hard core Bosons) is expressed as

$$\tilde{H}_{XX} = \frac{aJ_1}{2}\int_{-\infty}^{\infty} dx \left[\left(\frac{d\phi}{dx}\right)^2 + \Pi^2\right] \tag{2.19}$$

To obtain this form, we removed the minus sign that should appear in front of J_1. This can be done in this case as long as the hopping range is NN only: we (passively) transform the system by the commutation-conserving transformation of spin operators $\mathcal{S}_j^x \to \tilde{\mathcal{S}}_j^x = (-1)^j \mathcal{S}_j^x, \mathcal{S}_j^y \to \tilde{\mathcal{S}}_j^y = (-1)^j \mathcal{S}_j^y$, $\mathcal{S}_j^z \to \tilde{\mathcal{S}}_j^z = \mathcal{S}_j^z$. This point is important when interpreting the results of the phase of the system in this effective theory argument. The tilde mark on the spin and Hamiltonian indicates the transformed expression.

2.4.2 Bosonization of Ising coupling terms

Now, the dipolar interaction terms can be added. In spin language, the dipolar interactions are in the form of Ising coupling. The constituent, S^z, can be written using the Bose field $\phi(x)$ as

$$\begin{aligned}\tilde{\mathcal{S}}^z_j &= a^\dagger_j a_j - \frac{1}{2} \\ &= \frac{a}{\sqrt{\pi}}\frac{d\phi(x)}{dx} + \frac{a(-1)^j}{\pi\alpha} : \sin\sqrt{4\pi}\phi(x) :\end{aligned} \tag{2.20}$$

where : . . . : denotes normal ordering. The nearest neighbor interaction is expressed by expanding in a, as

$$\begin{aligned}&\sum_j \tilde{\mathcal{S}}^z_j \tilde{\mathcal{S}}^z_{j+1} = \\ &a\int_{-\infty}^{\infty} dx \left[\frac{1}{\pi}\left(\frac{d\phi}{dx}\right)^2 + \frac{1}{2\pi^2\alpha^2} : \cos\left(\sqrt{16\pi}\phi\right) : + ...\right]\end{aligned} \tag{2.21}$$

where ... donotes the terms we ignore, which includes quadratic or higher order terms in a and less relevant terms in the context of renormalization group argument such as $: \cos^2\left(\sqrt{16\pi}\phi\right) :$ (this point will be explained later).

The dimerization part of the nearest neighbor interaction ($V_{\mathrm{NN}}\,\delta(-1)^j$) requires a different bosonization calculation, due to its oscillatory nature that can lead to back-scattering of a single particle. [17, 39]. Expanding in a, the bosonized form is expressed as

$$\sum_j (-1)^j \tilde{\mathcal{S}}^z_j \tilde{\mathcal{S}}^z_{j+1} = \frac{a}{\pi\alpha}\int_{-\infty}^{\infty} dx : \cos\left(\sqrt{4\pi}\phi\right) : + ... \tag{2.22}$$

Similarly, the NNN interaction term can be written as

$$\begin{aligned}\sum_j \tilde{\mathcal{S}}^z_j \tilde{\mathcal{S}}^z_{j+2} =& a\int_{-\infty}^{\infty}\left[-\frac{3}{\pi}\left(\frac{d\phi}{dx}\right)^2 - \frac{1}{2\pi^2\alpha^2} : \cos\Big(\sqrt{16\pi}\phi\Big) :\right] \\ &+ ...\end{aligned} \tag{2.23}$$

Thus, the form of the zig-zag Hamiltonian (density) is expressed as

$$\begin{aligned}\tilde{\mathcal{H}}_{\mathrm{zig-zag}} &= \frac{aJ_1}{2}\left[\left(1+\frac{4V_{\mathrm{NN}}}{\pi J_1}-\frac{6V_2}{\pi J_1}\right)\left(\frac{d\phi(x)}{dx}\right)^2+\Pi(x)^2\right] \\ &\quad+\frac{a}{2\pi^2\alpha^2}(V_{\mathrm{NN}}-V_2):\cos\left(\sqrt{16\pi}\phi\right): \\ &\quad+\frac{\delta V_{\mathrm{NN}}}{\pi\alpha}:\cos\left(\sqrt{4\pi}\phi\right): \\ &= \frac{u}{2}\left(\frac{1}{K}\left(\frac{d\phi}{dx}\right)^2+K\Pi^2\right) \\ &\quad+g_1:\cos\left(\sqrt{16\pi}\phi\right):+g_\delta:\cos\left(\sqrt{4\pi}\phi\right):\end{aligned} \tag{2.24}$$

where again we ignore the higher order terms in a, and operators with higher oscillation frequencies that are less relevant in terms of the following renormalization group argument. K and u are the Luttinger parameters, calculated to be

$$\begin{aligned}K &= \frac{1}{\sqrt{1+\frac{4\Delta_1-6\Delta_2}{\pi}}}, \\ u &= aJ_1\sqrt{1+\frac{4\Delta_1-6\Delta_2}{\pi}},\end{aligned} \tag{2.25}$$

where $\Delta_1 = V_{\mathrm{NN}}/J_1, \Delta_2 = V_2/J_1$. The result is accurate up to the first order in Δ_1 and Δ_2. The treatment so far does not deviate from textbook methodology, yet the expression for K may look uncommon. Both Δ_1 and Δ_2 affect K, yielding unpredictable results. g_1, g_δ are nonuniversal coupling constants. This "non-universality" stems from the remaining cut-off parameters a and α appearing in these constants. To accurately determine these constants, one would need to take into account all orders of expansion in Eqs. (2.21) – (2.23). In most cases, this is impossible analytically. This solution, however, gives a good qualitative picture of the system.

We observe that, as the angle of molecules θ changes, Δ_1 and Δ_2 dramatically change, and consequently the Luttinger parameter K can take a wide range of values, resulting in a rich phase diagram. K determines the asymptotic behavior of

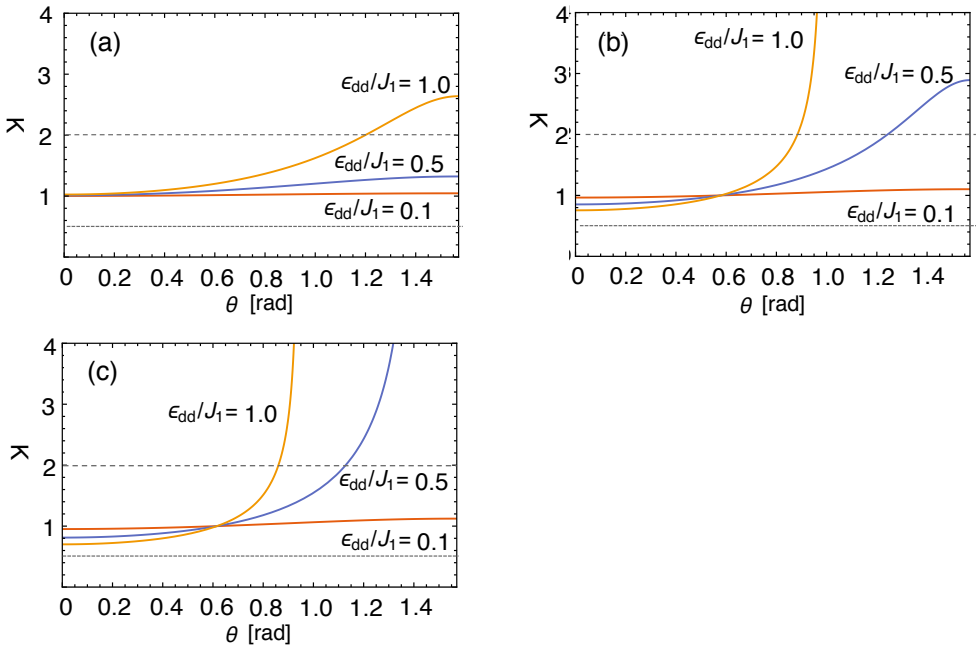

Figure 2-6: (Color online) Luttinger parameter plotted vs. θ of the molecules, for different hopping parameters J_1 and for different zig-zag angles γ. (a)$\gamma = \pi$, (b) $\gamma = 5\pi/6$, $\gamma = 2\pi/3$. These results are based on Eq. (2.25), calculated using perturbative renormalization group arguments.

the system's correlation function in TLL, such as the charge-density wave (CDW) correlation function c_{CDW}. Working at zero magnetic field, this is given by

$$c_{\mathrm{CDW}} \propto \left\langle \tilde{\mathcal{S}}^z(x)\tilde{\mathcal{S}}^z(0)\right\rangle \sim \frac{K}{2\pi}\frac{1}{x^2} + A\cos(2\pi\rho_0 x)\frac{1}{x^{2K}}, \tag{2.26}$$

with a nonuniversal amplitude, A and $\rho_0 = 1/(2a)$.

2.4.3 Renormalization Group Arguments

The ordering of the system is qualitatively discussed using a first-order renormalization group argument, which enables us to discuss the two nonlinear terms (g_1 : $\cos(\sqrt{16\pi}\phi)$: and g_δ : $\cos(\sqrt{4\pi}\phi)$:) independently and individually as long as one of the terms is irrelevant. We may see our model (2.24) as the Sine-Gordon Hamiltonian in treating the non-linear terms. The renormalization group argument of this model is well known [17] and here we apply the result. Because of the zig-zag nature

of the chain we have both alternating terms (giving rise to g_δ) and non-alternating terms (generating g_1), something that look uncommon in textbook physics. First we investigate the relevance of the non-linear terms $g_1 \cos(\sqrt{16\pi}\phi)$ and $g_\delta \cos(\sqrt{4\pi}\phi)$. In general, the scaling dimension of an operator of $g \exp\left\{(i\sqrt{4n^2\pi}\phi)\right\}$ type is known to be $n^2 K$, where K is the usual Luttinger parameter and g is the coupling constant. The scaling equation is known to be [17]

$$\frac{dg}{dl} = (2 - n^2 K)g, \quad \frac{dK}{dl} = -Cg^2 a^4, \tag{2.27}$$

implying that for $K = 2/n^2$ the $g \exp\left\{(i\sqrt{4n^2\pi}\phi)\right\}$ operator is marginal, while it is irrelevant for smaller values of K. In the case of our Hamiltonian, $n = 2$ for the $g_1 : \cos(\sqrt{16\pi}\phi) :$ term implying this operator changes its relevance at $K = 1/2$, and similarly $n = 1$ for the $g_\delta : \cos(\sqrt{4\pi}\phi) :$ term, changing its relevance at $K = 2$. We therefore may classify the system into these 4 cases: (i) $K > 2$, (ii) $1/2 < K < 2$, (iii) $0 < K < 1/2$, (iv) $K^2 < 0$.

(i) $K > 2$ — Neither of the nonlinear terms are relevant, and the system is described by Gaussian Hamiltonian, whose ground state is TLL.

(ii) $1/2 < K < 2$ — Only the term $g_\delta : \cos(\sqrt{4\pi}\phi) :$ is relevant, and the bosonic field ϕ tries to minimize $g_\delta : \cos(\sqrt{4\pi}\phi) :$. As a result, $\sqrt{4\pi}\phi = \pm\pi$, depending on the sign of g_δ, and thus $\left\langle \tilde{\mathcal{S}}^z_j \right\rangle = 0$ (cf.Eq. (2.20)), and $\vec{S}_i \cdot \vec{S}_{i+1} - \vec{S}_{i+1} \cdot \vec{S}_{i+2} = (-1)^j$, i.e., resulting in dimerized order. The sign of g_δ does not qualitatively change the order. Although the coupling inducing the dimerization is Ising-like, for large $J_1 \gg \epsilon_{dd}$ this dimerized state is a *valence bond state* (VBS), which is explicitly expressed as $(|\uparrow\downarrow\rangle - |\downarrow\uparrow\rangle/\sqrt{2}) \otimes (|\uparrow\downarrow\rangle - |\downarrow\uparrow\rangle/\sqrt{2}) \otimes ...$, in contrast to the Ising type dimer state ($|\text{dimer}\rangle = |\ldots\uparrow\uparrow\downarrow\downarrow\uparrow\uparrow\ldots\rangle$) that appeared in previous sections. For our system, we see that $K < 2$ is satisfied in a broad region (dashed line in Fig. 2-6). In particular, this is true even if the system is barely interacting, namely when Δ_1 and Δ_2 are both close to 0. This implies that $g_\delta \cos(\sqrt{4\pi}\phi)$ term is relevant and the system is governed by this term no matter how small the interaction and dimerization are, as long as they remain finite. This behavior has been described as "Spin-Peierls instability" [11, 38]

– even a tiny distortion of the lattice (in our case the dimerization) will open an energy gap. The gap scales as $E_g \propto \delta$, when δV_{NN} is small compared to J_1 and V_{NN} $E_g \propto (\delta V_{NN})^{1/(2-K)}$ otherwise. These two limits are smoothly connected.

(iii) $0 < K < 1/2$ — Both $g_1 : \cos(\sqrt{16\pi}\phi) :$ and $g_\delta : \cos(\sqrt{4\pi}\phi) :$ become relevant. Treating these terms individually no longer holds and the scaling behavior from the equation Eq. (2.27) is not valid. We therefore do not know the ordering behavior of this region. However as we will see later, as long as the dipolar-interaction terms are small compared to hopping term ($V_{NN}, V_2 < J_1$) the luttinger parameter usually stays away from the region (See Fig. 2-6). Hence, we do not intend to look further into this case.

(iv) $K^2 < 0$ — In this situation,the system is not in Luttinger liquid to start off, and the system is clearly in a gapped phase. Eq. (2.25) indicates that $K^2 < 0$ is realized for both strong attractive NN interaction and repulsive NNN interaction, implying that the system will be in the dimerized or ferromagnetic phase depending on the parameters θ, γ and J_1, but not in the anti-ferromagnetic state.

Thus far, we have excluded the case $\delta = 0$ (see Eq. (2.6) and Eq. (2.24)), that is when lattice opening angle $\gamma = \pi$. In this situation, the $g_\delta : \cos(\sqrt{4\pi}\phi) :$ term does not exist. The ordering behavior discussed so far has to be modified. Since the only non-linear term in this case is $g_1 : \cos(\sqrt{16\pi}\phi) :$, which changes its relevance at $K = 1/2$, we need to take into account these 3 cases: (i') $K > 1/2$, (ii') $0 < K < 1/2$, (iii')$K^2 < 0$.

(i') $K > 1/2$ — In this case, the non-linear term $g_1 : \cos(\sqrt{16\pi}\phi) :$ is not relevant and the system is described as TTL.

(ii') $0 < K < 1/2$ — The $g_1 : \cos(\sqrt{16\pi}\phi) :$ term becomes relevant and the system is entirely governed by this term. The system in this case is driven to either anti-ferromagnetic or dimer order, depending on the sign of the coupling constant g_1. When $g_1 > 0$, the bosonic field $\phi(x)$ appearing in the $g_1 : \cos(\sqrt{16\pi}\phi) :$ tries to minimize this term and takes the value such that $\sqrt{16\pi}\phi(x) = \pi$ or $\phi(x) = \sqrt{\pi}/4$. From Eq. (2.20) we see that $\tilde{\mathcal{S}}^z \approx (-1)^j \sin(\pi/2 + n\pi) \approx (-1)^j$, i.e., spin changes its sign at every each site. On the other hand if $g_1 < 0$, the bosonic field is pinned to

$\phi = 0$, leading to $\left\langle \tilde{\mathcal{S}}_j^z \right\rangle = 0$ and the finite dimer value of $\vec{S}_i \cdot \vec{S}_{i+1} - \vec{S}_{i+1} \cdot \vec{S}_{i+2} = (-1)^j$. As mentioned earlier, perturbative theory cannot in general determine the sign of g_1, thus the differentiation between dimer and anti-ferromagnetic phases has to be done numerically. We will see (cf. Fig. 2-6), however, that in our system for large J_1 at $\gamma = \pi$, K is always larger than $1/2$, implying $g_1 : \cos(\sqrt{16\pi}\phi) :$ is always irrelevant, and thus we do not go further to discuss this point.

(iii') $K^2 < 0$ — As before, the system is in a gapped phase. $K^2 < 0$ is realized when angle (θ) of the molecules is relatively large, leading to strong attractive NN interaction and NNN interaction. Hence the system is in Ferromagnetic order.

We would like to emphasize again that the analysis is perturbative. Going beyond perturbation in Δ_1, Δ_2, the Luttinger parameter K has to be found numerically. There are, however, special points in the parameter space where K and u can be obtained analytically. For example, for $\Delta_2 = 0, \delta = 0$ the model reduces to the XXZ model which allows for an exact calculation, using, e.g., Bethe-Ansatz techniques [51].

$$\begin{aligned} K &= \frac{1}{2(1 - \pi^{-1}\cos^{-1}(\Delta_1))} \\ u &= \frac{\pi\sqrt{1-\Delta_1^2}}{2\cos^{-1}\Delta_1} \end{aligned} \tag{2.28}$$

and thus $K \in [1/2, \infty)$. To check, it can be seen that K in Eq. (2.28) has the same form up to first order in Δ_1 as Eq. (2.25)

2.4.4 Phase Diagrams

The phase diagrams that sum up the discussion are shown in Fig. 2-2. The phase diagrams are the result of field theoretical analysis using bosonization techniques and first-order perturbative renormalization group arguments. They inevitably involve approximations and therefore unspecified constants, resulting in an overall qualitative picture of the system rather than a quantitative one. At this point, numerical methods are needed to accurately determine many exact transitions in the phase diagram. The qualitative discussion so far, however, provides a good picture of the overall behavior

of the system. Each pie in Fig. 2-2 shows the ground state phases for three different zig-zag angles γ, where the first, $\gamma = \pi$, is just the solution of a straight chain. The diagrams are depicted in polar coordinates, showing the ratio of lattice depth to hopping as the radius and he angle argument as the actual polarization angle θ of the molecules.

The border between the TLL phase and other phases indicates the Berezinsky-Kosterlitz-Thouless (BKT) transition. When J_1 is large, the gapped phases border to the gapless TLL phase, and the system is expected to be dominated by BKT transitions, as θ changes from 0 to $\pi/2$. In contrast to that, when J_1 is small, the phases are connected with first-order transition lines. We have not adequately studied the region around $J_1 \approx 1$, and hence the details of the crossing of first order and the BKT lines are beyond the scope of this paper.

We here remind ourself that we transformed the spin operators in the beginning of the bosonization treatment. For going back to the original (untransformed) system, one simply needs to perform the same spin operator transformation again $\tilde{\mathcal{S}}_j^x \rightarrow \mathcal{S}_j^x = (-1)^j \tilde{\mathcal{S}}_j^x, \tilde{\mathcal{S}}_j^y \rightarrow (-1)^j \mathcal{S}_j^y$, $\tilde{\mathcal{S}}_j^z \rightarrow \mathcal{S}_j^z = \tilde{\mathcal{S}}_j^z$. Therefore, the reinterpretation is simply equivalent to acting with a unitary operator $U = U^{-1} = \sigma_z = |\uparrow\rangle\langle\uparrow| - |\downarrow\rangle\langle\downarrow|$ on every other lattice site. The phase diagram shows the result in the language of untransformed spins. An important consequence of this remapping is that the VBS state is now remapped into a triplet bound state, or explicitly, $(|\uparrow\downarrow\rangle + |\downarrow\uparrow\rangle/\sqrt{2}) \otimes (|\uparrow\downarrow\rangle + |\downarrow\uparrow\rangle/\sqrt{2}) \otimes ....$ We call this state an "xy-dimer" as the dimerized pairs can be seen as polarized in the xy-plane as opposed to the dimerized order for $J_1 \approx 0$ where the dimerized pairs are polarized in the z-direction (we call this type "z-dimer"). One observes that when the opening angle γ is smaller than π, the system is predominantly in the xy-dimer state when $J_1 \rightarrow \infty$ where each dimer in spin language is $|L, M_L\rangle = |1, 0\rangle$. (Here, L is the total spin of the dimerized pair). As the optical lattice deepens (i.e., a move in radial direction in phase diagram) the dimer pair will gradually polarize into the z-direction by picking up the $M_L = 1$ component until it becomes completely polarized in the z-direction, becoming $|1, 1\rangle$. Thus, the depth of the optical lattice tunes the polarization direction of the dimerized pairs.

Before concluding, let us briefly discuss the effect of the doping of the system, which corresponds to the system being slightly away from half-filling. When the system is in the gapless TLL phase, doping creates a finite magnetic field and this simply results in a finite shift in the bosonic field $\phi(x) = \phi'(x) - \beta x$. Here $\beta = \pi m$, because the magnetization m is related to ϕ as $m = \left\langle \tilde{\mathcal{S}}_j^z \right\rangle = -1/\pi \left\langle \Delta\phi \right\rangle$. Hence, there would be no significant effect on this phase. For the gapped phase, moving away from half-filling creates mobile excitons that essentially make the system gapless. Yet, we will call these phases as ferromagnetic, antiferromagnetic, or dimer due to the large overlap of the wavefunction with one of these states. There might be, however, other physics emerging which we will not discuss in this paper. the test

2.5 Conclusion

The zigzag nature of the chain induces bond-alternating nearest-neighbor interactions as a function of the molecules' aligned angle with the chain axis. We also have taken up to NNN interaction of the dipole interaction, introducing (Ising-type) frustration in the system. In the strong coupling limit, the ground state ordering is exactly identified, where the system lies in either anti-ferromagnetic, ferromagnetic, or Ising-dimer, depending on the coupling parameters. In the weak coupling limit, the effective field theory additionally predicts TLL phase and dimerized phase, whose dimerized pairs have different polarized directions than the strong coupling case. The polarization of dimerized pairs should be closely affected by the depth of the optical lattice. Our methods do not accurately predict the ordering in the region of intermediate hopping and this should be included in future works.

The goal is to utilize this simple quasi-1D model to see phases beyond typical 1D physics. While we here discuss the phase diagram of polarized hard-core dipoles at half-filling moving on a 1D zig-zag chain, first, the richness of the system is obvious in the phase diagrams shown above. Second, the extension to other filling ratios and not only longer-range interactions but also longer-range hopping is obvious and very experimentally feasible. This should lead to very interesting quantum fluctuations

that can lead to unconventional quantum phases [15, 14]. Exploring similar phases with smaller γ in our model will be subject to future studies. Moving away from half-filling and taking longer-range parts of the dipolar interaction into account can lead to an interesting modification of the Devil's staircase [8].

Chapter 3

Non-classical correlations over the Dicke phase transition

3.1 Introduction and Motivation

In general, the two concepts of phase transition and correlation are inseparable. In classical statistical mechanics, the phase transitions are induced by fluctuations of the system. The fluctuation is described by a probabilistic distribution, which formally leads to the correlation length diverging at the phase transition point [46]. The idea is that probabilistic fluctuations are responsible for these phase transitions and the divergence of the correlation function at the critical point. In contrast to classical phase transitions, the fluctuations in quantum phase transitions are fully quantum [60, 41]. This is seen by the peculiar behavior of quantum entanglement, manifested in the form of divergence of entanglement entropy [7]. Quantum entanglement is responsible for these phase transitions and the divergence of the entanglement entropy. However, if we consider that entanglement is incorporated into the correlation in pure quantum systems, which does not accompany the description of porbabilistic distribution, then quantum phase transitions can be treated as the phenomenon associated with large correlations over the phase transitions in parallel with the thermal cases.

As we already know, not all system is uniquely either quantum or classical. There are many hybrid systems of these two. A quantum system with information flow or

loss, an open quantum system, belongs to such class. The questions we ultimately would like to answer are: What is the behavior of correlations in a phase transition in a system that requires both classical and quantum descriptions? Is the fluctuation probabilistic? Or is it entanglement-like? Unfortunately, finding a general answer to this highly abstract question seems very difficult. Rather than tackling the general question, we aim to obtain the answer in a concrete model, as a case study. That is, we pick a model and study the relationship between correlation and phase transition. What kind of model is appropriate for this goal? First of all, it should be a model that shows the phase transition. Second, it should be an open quantum mechanical model as opposed to a pure closed quantum system. Thirdly, the model should be simple enough that complex calculations can be realistically accomplished. The driven-dissipative Dicke model is ideal to this end. In this chapter, we first review the semi-classical drive-dissipative Dicke model and its known properties. We then continue the discussion by investigating quantum entanglement and non-classical correlations of the model, especially those around the phase transition points.

3.2 Review of the semi-classical driven-dissipative Dicke model

In this section, we introduce and highlight the known properties of the semi-classical driven-dissipative Dicke model. In the later chapters, we discuss our own findings on this model in the context of (quantum) information theory. This section, however, is solely devoted to highlighting the established results from past studies by other researchers.

3.2.1 The model

Fig. 3-1 Conceptually pictorializes our model. The 2-level atoms are exposed to a resonant semi-classical EM field and its rabi frequency is ω_R. They are subject to spontaneous emission; the collective spontaneous decay rate is expressed as Γ. The

atoms are further assumed to be in Dicke state, which is justified by imposing the complete permutation invariance of the atoms, and that the states of the atoms perpetually stay in the highest symmetry of the Hilbert space. Experimentally, this constraint amounts to each atom feeling the same phase of the EM field. Often cases, this is realized when the atoms are confined in a space whose length scale is significantly small compared to that of the wavelength of the EM field. Furthermore, dephasing of the atoms, often from the dipole-dipole interaction between the atoms, that breaks the symmetry, is assumed to be non-existent.

With the spontaneous decay (dissipation), the system is no longer a closed system. To quantitatively describe the system, we deploy the density matrix formalism with the Lindblad operators describing the dissipation. Using the Rotating Wave Approximation and Born-Markov approximation, the master equation which expresses the dynamics of the semi-classical driven-dissipative Dicke model is

$$\frac{\partial \rho}{\partial t} = \Gamma \left(J_- \rho J_+ - \frac{J_+ J_- \rho + \rho J_+ J_-}{2} \right) - i[H, \rho] \tag{3.1}$$

where

$$H = \frac{\omega}{2} \left(J_+ + J_- \right) \tag{3.2}$$

and

$$J_+ = \sum_{k=1}^{N} \underbrace{\mathbb{1} \ldots \mathbb{1}}_{k-1} \otimes (|0\rangle\langle 1|) \otimes \underbrace{\mathbb{1} \ldots \mathbb{1}}_{N-k}. \tag{3.3}$$

The term J_+ is the collective raising operator with $J_- = (J_+)^\dagger$

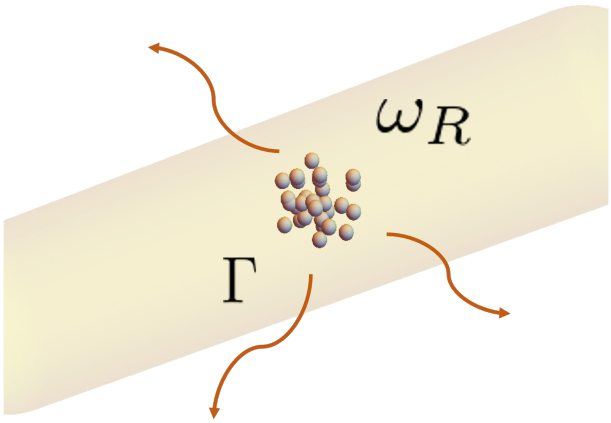

Figure 3-1: (Color online) Schematic setup of semi-classical driven-dissipative Dicke model.
Atoms are subject to EM field (light yellow) and their Rabi frequency is ω_R. Γ is the collective decay rate of the atoms.

3.2.2 Exact solution of the steady state

3.1 is known to be guaranteed to have an steady solution [12]. i.e. the solution to

$$\frac{\partial \rho}{\partial t} = 0 \tag{3.4}$$

always has a single solution, regardless of the choice of the parameter ω and Γ. The solution is expressed as

$$\rho_{ex} = \frac{1}{D} \sum_{l=0}^{2j} \sum_{l=0}^{2j} \left(\frac{J_-}{g} \right) \left(\frac{J_+}{g^*} \right) \tag{3.5}$$

where $g = i\omega/\Gamma$ and D is the normalizing factor that ensures $\mathrm{Tr}(\rho) = 1$. Throughout this chapter, we are interested in the steady state of the model. The reader should be reminded that the word "system" and ρ used in this chapter refer to the steady state of the model, unless otherwise specified. Since the steady state is essentially governed by the ratio of and γ, we define a unitless parameter $\Omega = \omega/N\Gamma$

It is often useful to express the Dicke state in the total angular momnetum basis $|J, m\rangle$. Accordingly, we rewrite the density matrix in this basis. First, let us expand

the raising and lowering operators as follows.

$$J_{\pm} = \sum_{m=-J}^{J} \sqrt{(J \mp m)(J \pm m + 1)}\, |J, m \pm 1\rangle \langle J, m| \tag{3.6}$$

After some simple calculations, one can show

$$(J_{+})^{n} = \sum_{m=-J}^{J-n} \sqrt{\frac{(j+m+n)!(j-m)!}{(j+m)!(j-m-n)!}}\, |J, m+n\rangle\, J, m \tag{3.7}$$

$$(J_{-})^{n} = \sum_{m=-J+n}^{J} \sqrt{\frac{(j-m+n)!(j-m)!}{(j+m)!(j+m-n)!}}\, |J, m-n\rangle\, J, m \tag{3.8}$$

Using these relations, the density matrix is readily expressed in this basis. To be concrete, if we write $\rho = \sum_a \sum_b \rho_b^a \, |j, a\rangle \langle j, b|$, the matrix components ρ_b^a is,

$$\rho_b^a = \frac{i^{b-a}}{D} \sum_{l=max\{b-a,0\}}^{j-a} \frac{1}{g^l g^{*(a-b+l)}} \frac{(j+a+l)!}{(j-a-l)!} \sqrt{\frac{(j-b)!(j-a)!}{(j+b)!(j+a)!}} \tag{3.9}$$

3.2.3 Dicke Phase transition of the steady state

This model is known to go through a phase transition by changing Ω []. This can be seen by (for example) the sudden decay of the purity of the system as shown in Fig. 3-2. Purity (γ) is defined as

$$\gamma = \mathrm{Tr}\big(\rho^2\big). \tag{3.10}$$

When $\gamma = 1$ the system is a pure state, and when $\gamma < 1$ the system is a mixed state. Fig. 3-2 suggests that a steady state goes through an apparent phase transition at $\Omega = 0.5$ dividing the system into $\Omega < 0.5$, a mostly pure phase, and $\Omega > 0.5$, a highly mixed state. By taking the limits $\Omega \to 0$ and $\Omega \to$ on the solution of our model, one finds

$$\rho(\Omega \to 0) = |J, -J\rangle \tag{3.11}$$

$$\rho(\Omega \to \infty) = \sum_{m=J}^{J} \frac{1}{2J} |J, m\rangle \langle J, m| \tag{3.12}$$

Therefore, this phase transition is seen to be a transition from the state of the lowest angular momentum into a state of the maximally mixed state of each angular momentum state.

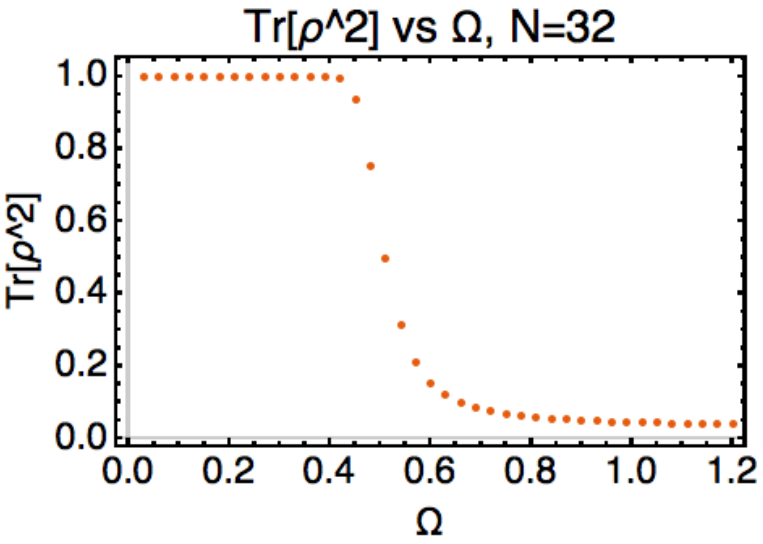

Figure 3-2: (Color online) Purity of the system plotted against Ω. $N = 32$

3.2.4 Summary of the driven Dicke model

In summary, the dynamics of atoms in Dicke stated driven by a classical laser field are decribed by Eq. (3.1). The equation is guaranteed to have a steady state for each Ω. By varying Ω, the system experiences a phase transition at $\Omega = \Omega_c = 0.5$. When $\Omega < \Omega_c$ the system has high purity, suggesting it is in a pure quantum state. When $\Omega > \Omega_c$ the purity becomes small suggesting the system is highly mixed.

3.3 Quantum measures of Dicke phase transition

In this section, several quantum measures are computed and plotted for the driven-dissipative Dicke model as the function of Ω, to inpsect the nature of the phase

transition. As pointed out in [65] and [66], the model is not entangled when the driven field is turned off and is entangled when Ω approaches to Ω_c. Our results in this section reinforce this result and further inform us how the model shows quantumness as well as how the model could in turn be useful for quantum applications. In this section, we summarize some of the quantum measures computed on the model.

3.3.1 Reduced density matrix

In computing quantum measures as well as entanglement and quantum discord in the following sections, obtaining the expression for the reduced density matrix is often required, when the subsystems of the given system are the center stage of the discussion. When the density matrix is written in the qubit basis, that is, when the basis of the density matrix is spanned by the product states of each particle system, this is easily done. However, because we have chosen to use the Dicke basis, the trace of the density matrix has to be carefully taken. In our case, the density matrix is written as,

$$\rho = \sum_{m=-J}^{J} \sum_{n=-J}^{J} \rho_m^n \left|J, m\right\rangle \left\langle J, n\right| \tag{3.13}$$

. To obtain a reduced density matrix, $|J, m\rangle$ has to be expanded using basis that spans Hilbert space of subsystem A ($\mathcal{H}_\mathcal{A}$) and basis that spans Hilbert space of subsystem B ($\mathcal{H}_\mathcal{B}$).

States $|J, m\rangle$ are expressed by dicke states of subsystem of A, $|j_a, \mu_a\rangle \in \mathcal{H}_\mathcal{A}$ and those of subsystem B, $|j_b, \mu_b\rangle \in \mathcal{H}_\mathcal{B}$ using unitary transformation as

$$\left|J, m\right\rangle = \sum_{\mu_a, \mu_b} C(j_a j_b J; \mu_a \mu_b m) \left|j_a, \mu_a\right\rangle \left|j_b, \mu_b\right\rangle . \tag{3.14}$$

The coefficients are the famous Clebsch-Gordon coefficients

$$C(j_a j_b J; \mu_a \mu_b m) = \left\langle J, m\right| \cdot \left|j_a, \mu_a\right\rangle \left|j_b, \mu_b\right\rangle \tag{3.15}$$

In theory, j_a, j_b are constrained by the total angular momentum of the system J by the inequality relation

$$|j_a + j_b| \leq J \leq |j_a - j_b| \tag{3.16}$$

However, in our case, $N = N_A + N_B$ where N, N_A and N_B are the particle number of the entire system, subsystem A and subsystem B, respectively. Therefore $J = j_a + j_b$ because $N = 2J$, $N_A = 2j_a$ and $N_B = 2j_b$. Instead of applying an overly general expression of Clebsh-Gordon coefficients [43], we attempt to derive a simpler expression for $J = j_a + j_b$.

A Dicke state expressed as $|J, M\rangle$ where $M = J - l$ can be interpreted as a state of $2J$ spins, $2J - l$ of which are spin up and l of which are spin down. If the system is divided into subsystems A and B, that has $2j_a$ spins and $2j_b$ spins each ($J = j_a + j_b$), then system A should have k spin down and system B should have $l - k$ spin down, with k ranging from $\max\{0, -2J + 2j_a + l\}$ to $\min\{l, j_a\}$. Therefore, the following relationship stands.

$$\begin{aligned}
&\binom{2J}{l}^{1/2} |J, M = J - l\rangle \\
&= \sum_{k=\max\{0,-2J+2j_a+l\}}^{\min\{l,j_a\}} \left(\binom{2j_a}{k}^{1/2} |j_a, j_a - k\rangle \otimes \binom{2J - 2j_a}{l - k}^{1/2} |J - j_a, J - j_a - l + k\rangle \right)
\end{aligned} \tag{3.17}$$

Here, $\binom{n}{k} = \frac{n!}{k!(n-k)!}$ is the binomial coefficients. Moving the normalization factor

to the right, one finds the total angular momentum state is expanded as

$$
\begin{aligned}
&|J, M = J - l\rangle \\
&= \binom{2J}{l}^{-1/2} \sum_{k=\max\{0,-2J+2j_a+l\}}^{\min\{l,j_a\}} \left(\binom{2j_a}{k}^{1/2} |j_a, j_a - k\rangle \right. \\
&\quad \left. \otimes \binom{2J-2j_a}{l-k}^{1/2} |J - j_a, J - j_a - l + k\rangle \right) \\
&= \binom{2J}{J-M}^{-1/2} \sum_k \binom{2j_a}{k}^{1/2} \binom{2j_b}{J-M-k}^{1/2} |j_a, j_a - k\rangle \, |j_b, -j_a + M + k\rangle \\
&= \binom{2J}{J-M}^{-1/2} \sum_{a=-j_a}^{j_a} \sum_{b=-j_b}^{j_b} \binom{2j_a}{j_a - a}^{1/2} \binom{2j_b}{j_b + a - M}^{1/2} \delta_{a,M-b} \, |j_a, a\rangle \, |j_b, b\rangle
\end{aligned} \tag{3.18}
$$

In the last line, we define $a = j_a - k$ and $b = -j_a + M + k$. The parameter k moves within the range that guarantees $-j_a \leq j_a - k \leq j_a$ and $-j_b \leq M - j_a + k \leq j_b$. Therefore, the ranges of the newly defined parameters a and b are $-j_a \leq a \leq j_a$ and $-j_b \leq b \leq j_b$. This result implies the general expression of the unitary transformation between two representations of the state, and gives the general expression of the Clebsh-Gordan coefficients ($C(j_a, j_b, J; a, b, M)$), for j_a and j_b such that $j_a + j_b = J$. To organize, the angular momentum state is exapnaded as,

$$
|J, M\rangle = \sum_a \sum_b C(j_a, j_b, J; a, b, M) \, |j_a, a\rangle \, |j_b, b\rangle \tag{3.19}
$$

where

$$
C(j_a, j_b, J; a, b, M) = \binom{2J}{J-M}^{-1/2} \binom{2j_a}{j_a - a}^{1/2} \binom{2j_b}{j_b + a - M}^{1/2} \delta_{a,M-b} \tag{3.20}
$$

Again, the reader should be warned that this expression for the unitary transformation is applicable only to j_a and j_b such that $J = j_a + j_b$ while the general addition of angular momnetum states does not have this constraint.

Using Eq. (3.19), the overlap of the two states is immediately obtained:

$$\begin{aligned}\langle j_a, \mu_a| \cdot |J, M\rangle &= \binom{2J}{J-M}^{-1/2} \sum_k \binom{2j_a}{k}^{1/2} \binom{2J-2j_a}{J-M-k}^{1/2} \\ &\quad \times \delta_{\mu_a, j_a-k} \, |J-j_a, M-j_a+k\rangle \\ &= \binom{2J}{J-M}^{-1/2} \binom{2j_a}{j_a-\mu_a}^{1/2} \binom{2J-2j_a}{J-M-ja+\mu_a}^{1/2} \\ &\quad \times |J-j_a, M-\mu_a\rangle \end{aligned} \tag{3.21}$$

At this stage, the reduced density matrix is readily calculated.

$$\mathrm{Tr}_a \, \rho = \sum_{\mu_a=-j_a}^{j_a} \langle \mu_a, j_a| \cdot \sum_{m,n} \rho_{m,n} \, |J, m\rangle \, \langle J, n| \otimes |\mu_a, j_a\rangle$$

$$= \sum_{\mu_a, m, n} \rho_{m,n} \, \langle \mu_a, j_a|J, m\rangle \, \langle J, n|\mu_a, j_a\rangle$$

$$\begin{aligned} &= \sum_{\mu_a, m, n} \rho_{m,n} \binom{2J}{J-m}^{-1/2} \binom{2j_a}{j_a-\mu_a}^{1/2} \binom{2J-2j_a}{J-m-j_a+\mu_a}^{1/2} \\ &\quad \times \binom{2J}{J-n}^{-1/2} \binom{2j_a}{j_a-\mu_a}^{1/2} \binom{2J-2j_a}{J-n-j_a+\mu_a}^{1/2} \\ &\quad \times |J-j_a, m-\mu_a\rangle \, \langle J-j_a, n-\mu_a| \end{aligned} \tag{3.22}$$

$$\begin{aligned} &= \sum_{\mu_a, m, n} \rho_{m,n} \binom{2j_a}{j_a-\mu} \binom{2J}{J-m}^{-1/2} \\ &\quad \binom{2J}{J-n}^{-1/2} \binom{2j_b}{j_b-m+n}^{1/2} \binom{2j_b}{j_b-n+\mu}^{1/2} \\ &\quad \times |j_b, m-\mu_a\rangle \, \langle j_b, n-\mu_a| \end{aligned} \tag{3.23}$$

where $-ja \leq \mu_a \leq j_a$, $-J \leq m, n \leq J$ and $-j_b \leq m-\mu_a, n-\mu_a \leq j_b$.

To further simplify, let us write the term inside the summation as $f(m, n, \mu)$, and then consider transforming the variables as $m' = m-\mu_a$ and $n' = n-\mu_a$ and rewriting

the density matrix. The condition $-J \leq m, n \leq J$ yields $-J - \mu_a \leq m', n' \leq J - \mu$. Combining it with $-j_b \leq m - \mu_a, n - \mu_a \leq j_b$ gives the range of the new parameters m' and n':

$$\begin{aligned} &\max\{-j_b, -J - \mu_a\} \leq m', n' \leq \min\{j_b, J - \mu_a\} \\ \Leftrightarrow &-j_b \leq m', n' \leq j_b \end{aligned} \tag{3.24}$$

Therefore, the reduced density matrix is expressed as

$$\begin{aligned} \mathrm{Tr}_a\, \rho &= \sum_{\mu_a, m, n} f(m, n, \mu_a) \left| j_b, m - \mu_a \right\rangle \left\langle j_b, n - \mu_a \right| \\ &= \sum_{m'=-j_b}^{j_b} \sum_{n'=-j_b}^{j_b} \sum_{\mu_a=-j_a}^{j_a} f(m' + \mu_a, n' + \mu_a, \mu_a) \left| j_b, m' \right\rangle \left\langle j_b, n' \right| \\ &= \sum_{m'=-j_b}^{j_b} \sum_{n'=-j_b}^{j_b} \sum_{\mu_a=-j_a}^{j_a} \rho_{m'+\mu_a, n'+\mu_a} \\ &\quad \times \binom{2j_a}{j_a - \mu_a} \binom{2J}{J - \mu_a - m'}^{-1/2} \\ &\quad \times \binom{2J}{J - \mu_a - n'}^{-1/2} \binom{2j_b}{j_b - m'}^{1/2} \binom{2j_b}{j_b - n'}^{1/2} \left| j_b, m' \right\rangle \left\langle j_b, n' \right| \end{aligned} \tag{3.25}$$

This result shows that taking a trace of a density matrix expressed in Dikce basis is simply equivalent to taking the following transformation in matrix components

$$\begin{aligned} &\rho_{m,n} \to \rho^B_{m,n} \\ &\quad = \sum_{\mu=-j_a}^{j_a} \rho_{m+\mu, n+\mu} \binom{2j_a}{j_a - \mu_a} \\ &\qquad \times \binom{2J}{J - \mu_a - m'}^{-1/2} \binom{2J}{J - \mu_a - n'}^{-1/2} \binom{2j_b}{j_b - m'}^{1/2} \binom{2j_b}{j_b - n'}^{1/2} \end{aligned} \tag{3.26}$$

With this transformation rule, we are able to compute various quantum measures that are associated with this model.

Fidelity susceptibility

Fidelity is the quantity to describe the "similarity" of the two states. Because a quantum phase transition accompanies a sudden change of the state (or by definition, the sudden change is the phase transition itself), one should expect to observe a dramatic change in fidelity. In general, fidelity is defined as follows

$$f(\theta, \theta + \delta\theta) := \mathrm{Tr}\sqrt{\sqrt{\rho(\theta)}\rho(\theta + \delta\theta)\sqrt{\rho(\theta)}} \tag{3.27}$$

It shows the distinguishability between state $\rho(\theta)$ and state $\rho(\theta + \delta\theta)$. It clearly depends on the small parameter $\delta\theta$. To avoid this dependence, it is common to define its susceptibility, namely, the fidelity susceptibility (FS). In general, first-order term of $\delta\theta$ is believed to be 0. Therefore, FS is defined with the 2nd derivative of the fidelity defined above.

$$\chi_f := -\frac{\partial^2 f(\theta, \theta + \delta\theta)}{\partial(\delta\theta)^2} \tag{3.28}$$

As can be seen in Fig. 3-3, the dicke model shows the peak around the phase transition point $\Omega = 0.5$.

3.3.2 Quantum Fisher Information

Another approach to visualize and analyze the quantum phase transition is the quantum Fisher information (QFI). Here we follow a similar idea from Wang [62] where they used QFI to detect the phase transition of N two-level atoms interacting with a single-mode bosonic field, described by the Dicke model. A review on the general theory of quantum Fisher information can be found [13]. The quantum Fisher information is a quantity to quantify the upper bound on the precision of a measurement that a certain state can be used to estimate a measurable parameter. It also gives a sufficient condition for the system to be entangled if the QFI is larger than the number of particles. This condition implies that with the system that has high QFI,

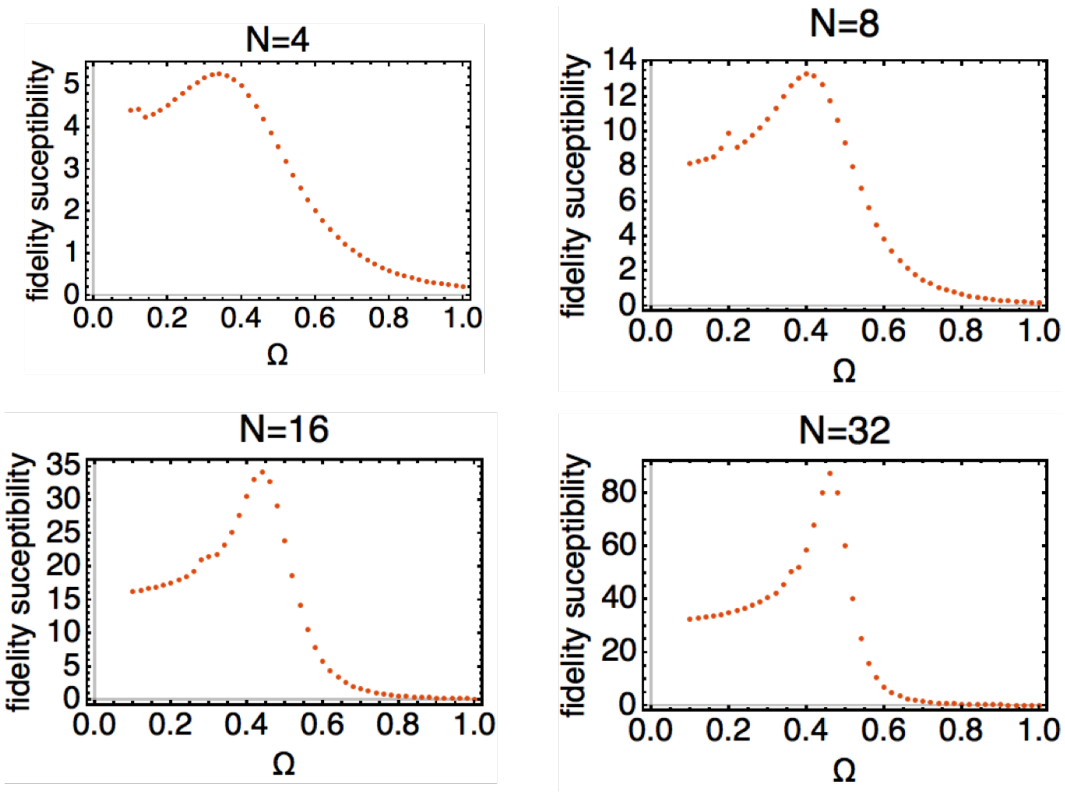

Figure 3-3: (Color online) Fidelity susceptibility of the model, plotted against Ω

one can measure a quantity that is more precise than the shot noise limit.

In an open quantum system, the QFI can be computed by the following expression

$$F(\rho, \hat{G}) = 4 \sum_n p_n \left(\Delta G\right)_n^2 - \sum_{m \neq n} \frac{8 p_m p_n}{p_m + p_n} |\left\langle \psi_n \middle| \hat{G} \middle| \psi_m \right\rangle|^2 \tag{3.29}$$

Here p_n are nonzero eigenvalues of the density matrix of the system $\hat{\rho}$ and $|\psi_n\rangle$ are the corresponding eigenvectors. $\hat{G}$ is the phase-shift generator. With $\hat{G}$, the density operator of the system is phase-shifted by an unknown amount ϕ: $\hat{\rho}(\phi) = \exp\left\{(-i\phi\hat{G})\right\} \hat{\rho} \exp\left\{(i\phi\hat{G})\right\}$. In many literature, $\hat{G}$ is the spin x operator. However in our work We generalize it to take $\hat{G}$ to be $J_{\vec{n}}$ (spin operator in $\vec{n}$ direction), following the approach that appears in [13].

$$J_{\vec{n}} = \frac{1}{2} R^\dagger n_\alpha R \tag{3.30}$$

where R is the rotation operator. By using $J_{\vec{n}}$, it is more convenient to write the

quantum Fisher information in a symmetric matrix as as

$$F(\rho, J_{\vec{n}}) = \sum_{i \neq j} \frac{2(p_i - p_j)^2}{p_i + p_j} |\langle i | J_{\vec{n}} | j \rangle|^2 \tag{3.31}$$

where p_i and $|i\rangle$ represent the eigenvalues and eigenvectors of the density matrix ρ

The quantum Fisher information is defined as the maximum value of F with respect to the rotation appeared in spin operator $J_{\vec{n}}$ averaged over the number of particles. Written explicitly,

$$\overline{F}_{\max} = \frac{1}{N} \max_{\vec{n}} F(\rho, J_{\vec{n}}) \tag{3.32}$$

The plot of quantum Fisher information is plotted in Fig. 3-4. As can be seen, qfi becomes larger than 1 when, Ω approaches Ω_c, suggesting in that parameter region, the system is entangled.

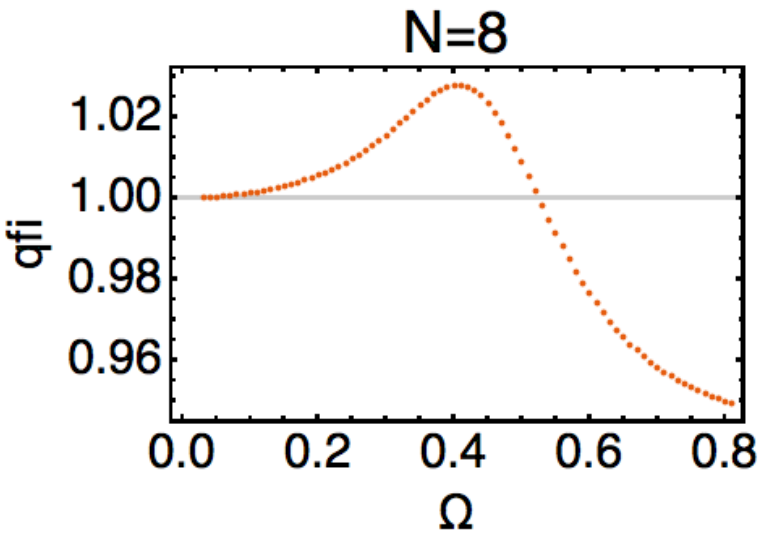

Figure 3-4: (Color online) Quantum fisher information of the model.

3.3.3 Spin squeezing

Spin squeezing of the model is first studied by E.Wolfe and S. Yelin [66]. Here results from their work are briefly touched upon to affirm and compare with our previous

results of fidelity susceptibility and quantum Fisher information. The metric of spin squeezing, ξ, that can be applied to our model is defined as [29],

$$\xi^2 = \frac{\left\langle \bar{J}_1^2 + \bar{J}_2^2 \right\rangle - \sqrt{\left\langle \bar{J}_1^2 - \bar{J}_2^2 \right\rangle^2 + \left\langle \bar{J}_1 \bar{J}_2 + \bar{J}_2 \bar{J}_1 \right\rangle^2}}{2/N} \tag{3.33}$$

where,

$$\bar{J}_1 = \bar{J}_y \cos\phi - \bar{J}_x \sin\phi \tag{3.34}$$

$$\bar{J}_2 = \bar{J}_x \cos\theta \cos\phi + \bar{J}_y \cos\theta \sin\phi - \bar{J}_z \sin\theta. \tag{3.35}$$

The angeles and are expressed as

$$\theta = \cos^{-1}\left(\left\langle \bar{J}_z \right\rangle / \sqrt{\left\langle \bar{J}_x \right\rangle^2 + \left\langle \bar{J}_y \right\rangle + \left\langle \bar{J}_z \right\rangle^2} \right) \tag{3.36}$$

$$\phi = \tan^{-1}\left(\left\langle \bar{J}_y \right\rangle / \left\langle \bar{J}_x \right\rangle \right) \tag{3.37}$$

Spin squeezing is known to detect the entanglement of the system[57] [52]. That is, when $\xi < 1$, the system is entangled. This is a sufficient condition for the entanglement and the opposite is not true. In Fig. 3-5, that is taken from [66], the spin squeezing parameter is plotted against Ω. Their results are consistent with our results from the quantum Fisher information. When $\Omega \approx 0.4$ the system appears to be entangled. But when the system is in the mixed state region, no informative result on entanglement is obtained.

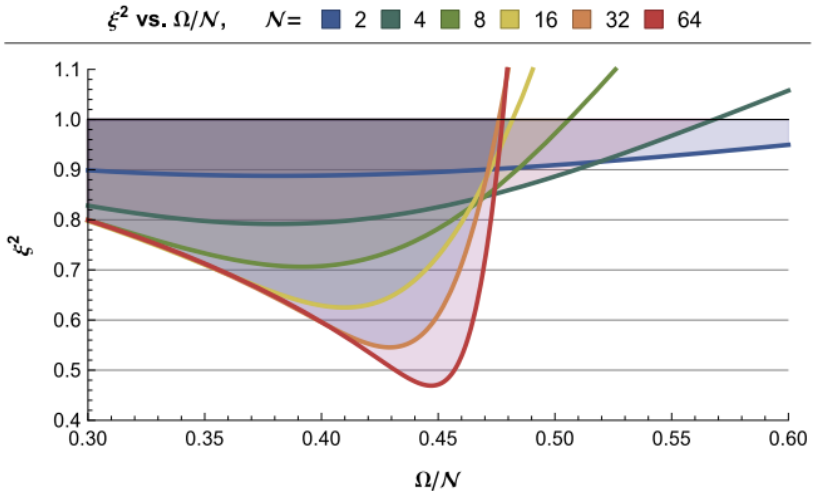

Figure 3-5: (Color online) Spin squeezing plotted against Ω
This plot is taken from the paper by E.Wolfe and S. Yelin [66]. Ω/N that appears in this plot is equivalent to Ω used in this thesis.

3.4 Entanglement of driven-dissipative Dicke model

As we have witnessed in the previous section, various quantum measures suggest that the quantum mechanically interesting properties are condensed in the region of $\Omega < \Omega_c$, or to be precise, the region where Ω is just below the critical point. If quantum entanglement is the source of the quantumness of this region, does it mean that the system of the model is entangled only at $\Omega \approx \Omega_c$? Is the region where the system is highly impure not entangled? How is the entanglement affected by the phase transition? These are the questions we would like to answer in this section. As we review in the coming subsections, in general, discussing the entanglement of a general mixed quantum state is a very formidable task because it involves sorting all possible pure state decompositions. However, as we assume permutation invariant particles, this operation is much simplified. With that, we are able to give a much more in-depth discussion about the entanglement of the system over the whole region of Ω, thereby connecting the phase transitions and entanglement of the model.

3.4.1 Review of Entanglement

Before we initialize the discussion of the entanglement of our specific model, we would like to review the concept of entanglement of mixed states in this section. A more thorough review on entanglement can be found, for example, in [2].

Definition of Entanglement

What is the entanglement in quantum mechanics? A one-liner answer to this question would be "There is entanglement if certain systems are not separated." For example, if atom A and atom B are entangled, then they cannot be separated. If atom C is not entangled with either atom A and atom B, then it can be separated. This intuitive and simple description is the backbone to understand entanglement; entanglement is ultimately a subject of separability of the state. We need to therefore make it precise what we mean by "atoms being separated". To that end, we shall formally define separable states [34].

Definition 3.4.1 (Separable states, pure)**.** A pure state of N particles described by $|\Psi\rangle$ is separable if it can be described as a product state:

$$|\Psi\rangle = |\Psi_1\rangle \otimes |\Psi_2\rangle \ldots \otimes |\Psi_N\rangle \tag{3.38}$$

where $|\Psi_i\rangle \in \mathcal{H}_i$ is some state of particle i.

N separable states are sometimes called fully-separable states and these states are not entangled. 2-separable state is commonly named as biseparable state. With the definition of separable states, we are immediately ready to define entangled states.

Definition 3.4.2 (Entangled states, pure)**.** Any system that is not separable is entangled.

As an example, 2-qubit bell states (e.g. $|\Psi\rangle = \frac{1}{\sqrt{2}}(|0\rangle_A \otimes |1\rangle_B + |1\rangle_A \otimes |0\rangle_B)$) are famously known entangled state [54]. In fact, for a 2-composite system, whose most general form of the state can be written as $|\Psi_{AB}\rangle = \sum_i \sum_j \Gamma_{i,j} \left|\psi_i^A\right\rangle \left|\psi_j^B\right\rangle$, judging

whether a state is entangled or not is straightforward. That is because Schmidt decomposition of Ψ_{AB} guarantees any 2-composite pure state to be transformed in this form:

$$\begin{aligned} |\Psi_{AB}\rangle &= \sum_i \sum_j \Gamma_{i,j} \left|\psi_i^A\right\rangle \left|\phi_j^B\right\rangle \\ &= (U_A \otimes U_B) \sum_{i=1}^{r} \sqrt{\lambda_i} |\psi_i'^A\rangle \otimes |\phi_i'^B\rangle \end{aligned} \tag{3.39}$$

where $|\psi_i^A\rangle, |\psi_i'^A\rangle \in \mathcal{H}_A$, $|\psi_i^B\rangle, |\psi_i'^B\rangle \in \mathcal{H}_B$ and U_A, U_B are the unitary operators each acting on $\mathcal{H}_A$, $\mathcal{H}_B$. Clearly, if $r = 1$ (that is, the second line of the above equation no longer contains the summation), the system is separable, and if $r > 1$ the system is entangled. The reverse is also true [47].

Unfortunately, the discussion cannot be applied for a system of more than two particles. For instance, $|\psi_{ABC}\rangle = \sum_{i=1}^{N} \sum_{j=1}^{N} \sum_{k=1}^{N} \Gamma_{ijk} |i_A\rangle \otimes |j_B\rangle \otimes |k_C\rangle$ can NOT be always written as similar form in the manner of 2-composite system

$$|\psi_{ABC}\rangle = (U_A \otimes U_B \otimes U_C) \sum_{i=1}^{N} \sqrt{\lambda_i} |i_A\rangle \otimes |i_B\rangle \otimes |i_C\rangle \quad \text{(not always true)} \tag{3.40}$$

This is why physicists often say, in the context of entanglement, "3 is too many". Even for a pure state, knowing whether a system is entangled is generally a very difficult problem. In a bipartite system, entangled means the system is not separable at all. There is no gray zone. However, if the system is more than two particles, one can imagine a situation where the system is entangled, yet the system has a subsystem that is separated from the rest. The definition below describes such cases.

Definition 3.4.3 (k-separable states, pure)**.** A pure state of N particles described by $|\Psi\rangle$ is k-separable if the system is k-factorized states. Here a k-factorable state is $|\Psi\rangle \in \mathcal{H}_1 \otimes \mathcal{H}_2 ... \otimes \mathcal{H}_N$ and can be explicitly written as

$$|\Psi\rangle = |\psi_1\rangle \otimes |\psi_2\rangle \otimes ... |\psi_N\rangle \tag{3.41}$$

Note that (k'-separable states) $\subset$ (k-separable states) if $k > k'$. For example, 3-separable state $|\Psi\rangle \in \mathcal{H}_1 \otimes \mathcal{H}_2 \otimes \mathcal{H}_1$ is also a 2-separable state $|\Psi\rangle \in \mathcal{H}_1 \otimes \mathcal{H}_2'$ if we define $\mathcal{H}_2' = \mathcal{H}_2 \otimes \mathcal{H}_3$.

To rephrase the definition of entanglement, if a system of N particles is not N separable, then the system is said to be entangled. However, even if the system as a whole is entangled, some chunks of subsystems could be separated from the rest, although the systems themselves are entangled within. By examining k-separability, one may gain information of how the system is entangled.

A special case of entanglement is when all particles of the system are entangled with each others, and such class of entanglement is given a special treatment. In the language of separability, such systems are not even 2-separable.

Definition 3.4.4 (Genuine multiparticle entanglement, pure)**.** If the system is not 2-separable, the system is genuine multiparticle entangled.

Up to this point, we have defined the entanglement for pure states. However, throughout the chapter, we treat our model as an open quantum system and need to further understand the definition of entanglement of mixed states. Because mixed states are in essence a statistical mixture of pure quantum states, all definitions are entanglement and separability can be naturally extended to the same settings [63].

Definition 3.4.5 (Separable states, mixed)**.** A state of N particles described by a density matrix ρ is separable if it can be described as a convex sum of pure product states. i.e. if $\rho = \sum_\mu p_\mu |\Psi_{\mu_1}\rangle \langle\Psi_{\mu_1}| \otimes \ldots \otimes |\Psi_{\mu_N}\rangle \langle\Psi_{\mu_N}|$ for $|\Psi_{\mu_i}\rangle \in \mathcal{H}_i$ and $p_\mu > 0$, $\sum_\mu p_\mu = 1$

Definition 3.4.6 (Entangled states, mixed)**.** Any system that is not separable is entangled.

Definition 3.4.7 (k-separable states, mixed)**.** A state of N particles described by a density matrix ρ is k-separable if the system is a convex sum of k-factorized states. The k-partitions of each k-factorized states that are being summed do not have to be unique. Here a k-factorable state is $|\Psi\rangle \in \mathcal{H}_1 \otimes \mathcal{H}_2 ... \otimes \mathcal{H}_k$. The explicit form of the k-separable states is $\rho = \sum_\mu p_\mu |\Psi'_{\mu_1}\rangle \langle\Psi'_{\mu_1}| \otimes \ldots \otimes |\Psi'_{\mu_k}\rangle \langle\Psi'_{\mu_k}|$

Definition 3.4.8 (Genuine multiparticle entanglement, mixed)**.** If the system is not 2-separable, the system is genuine multiparticle entangled.

To put it in simple words, a mixed state is separable if it can be written as a statistical mixture of pure product states. An easy example of such separable state is $|\Psi\rangle = 1/2\,|11\rangle\langle 11| + 1/2\,|00\rangle\langle 00|$.

One should be aware of the definition of k-separable state. It merely states that the pure states that are being summed are all k-factorized, but it does not state that each k-factorized state has to have the same partition of the total Hilbert space. For example, a system that can be expressed as $\rho = 1/3(\rho_{AB|C} + \rho_{AC|B} + \rho_{C|AB})$ is 2-separable (biseparable), because although each term has a different partition of the system, all of them are 2-separated.

With the definition of entanglement of the general mixed state of multiparticles, we are ready to discuss the entanglement and the separability of the driven-dissipative Dicke model. In the rest of the section, we assume the density matrix is that of the steady solution of the model Eq. (3.1).

3.4.2 2-point concurrence of the model

In this subsection, we show the result of the 2-point concurrence plotted against Ω (Fig. 3-7), and then we discuss the implication of such results to the entanglement of the entire system. Similar plots can be found in [48].

Concurrence is an entanglement monotone that quantifies the entanglement of a qubit. Since it is the quantification of the entanglement, it also gives a sufficient and necessary condition for entanglement. Given a 2-qubit density matrix ρ_2, 2-point concurrence is defined as

$$C(\rho) = max\{0, \lambda_1 - \lambda_2 - \lambda_3 - \lambda_4\} \tag{3.42}$$

where λ_i is the i-th largest eigenvalue of $\sqrt{\rho\tilde{\rho_2}}$, with $\tilde{\rho_2} = (\hat{\sigma}_y \otimes \hat{\sigma}_y)\rho_2^*(\hat{\sigma}_y \otimes \hat{\sigma}_y)$ where $\hat{\sigma}_x, \hat{\sigma}_y$ are the Pauli matrices of a qubit. Then, 2-point concurrence gives information on the entanglement of the 2-qubit system as follows.

- $C(\rho) = 0 \iff \rho_2$ is a separable state.
- $C(\rho) > 0 \iff \rho_2$ is an entangled state.
- $C(\rho) = 1 \iff \rho_2$ is a maximally entangled state.

Be aware that, unlike many other quantum measures, concurrence gives a necessary and sufficient condition for entanglement even if the system is a mixed state.

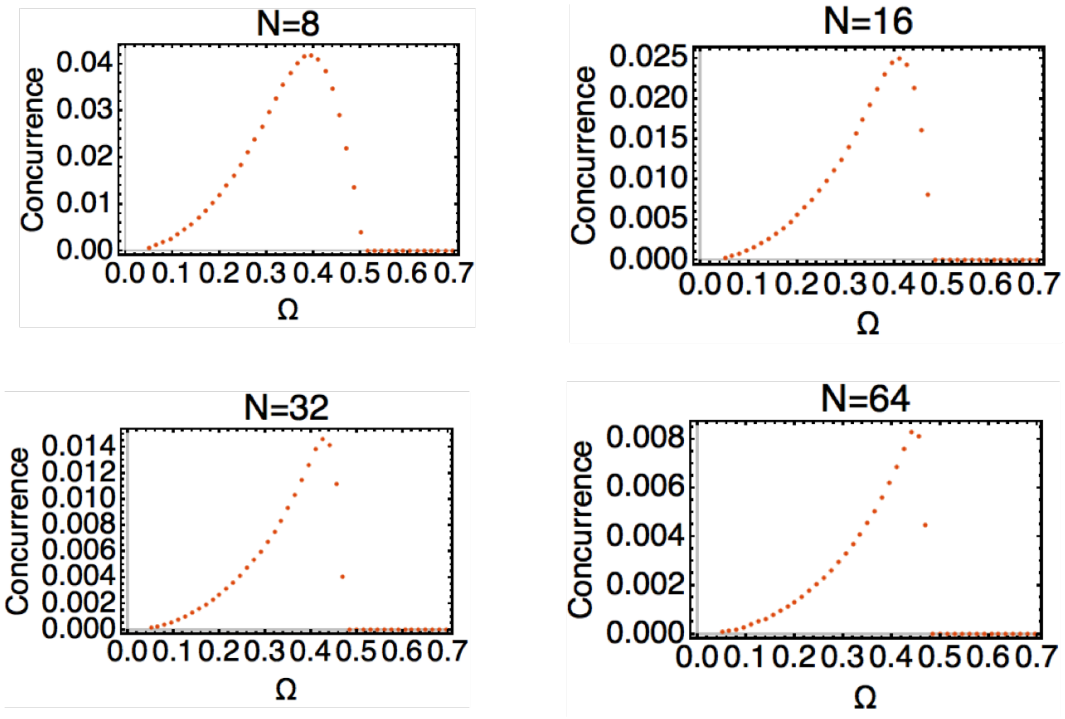

Figure 3-6: (Color online) 2-particle concurrence. $N = 8, 16, 32, 64$ For the plot, we first trace out all but 2 particles, and consequently use the (reduced) density matrix.

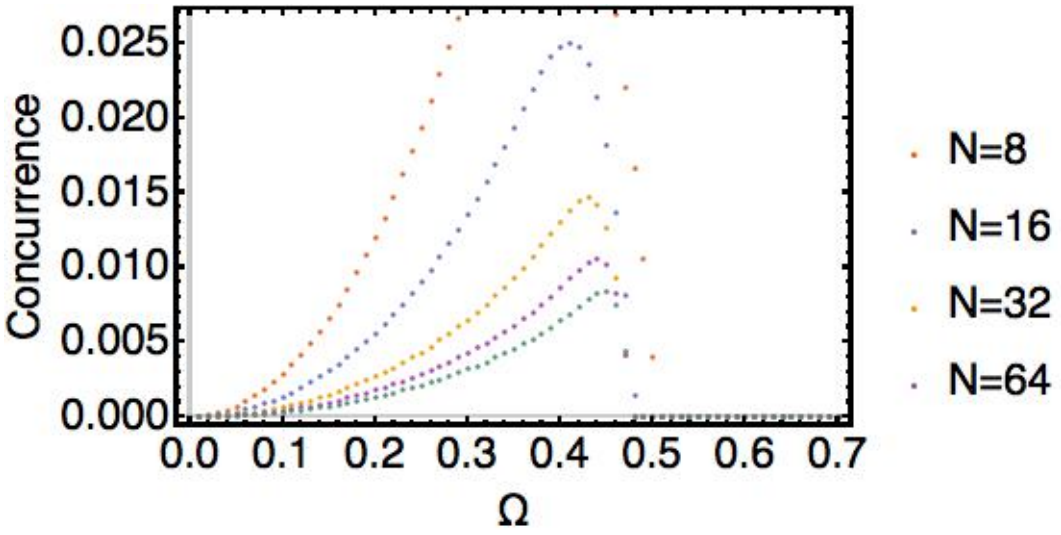

Figure 3-7: (Color online) 2-particle concurrence. For the calculation we first trace out all but 2 particles, and consequently use the (reduced) density matrix.

We have Here are observations of the concurrence plot (Fig. 3-7).

In Fig. 3-6 and Fig. 3-7, we plot of concurrence for varying Ω. The result reveals the following points: Firstly, the concurrence appears to peak below the transition point ($\Omega < \Omega_c$) although as the particle number increases, the peak does seem to shift towards Ω_c . Secondly, the concurrence decreases its value as the particle number increases.

We are tempted to draw a conclusion, similar to the discussion involving entanglement entropy and quantum phasetransitions [23, 40], that entanglement is maximized at the Dicke phase transition point, and less or none entanglement is found beyond the critical point ($\Omega > \Omega_c$). However, this seemingly reasonable conclusion must be carefully reviewed, based on the definition of entanglement introduced in 3.4.1. Clearly, an important factor that must be taken into account is that 2-point concurrence is entanglement monotone for 2-qubit systems. Realistically, computing 2-point concurrence involves the loss of information of the entire system by tracing out all but two particles. This may lead to insensitivity in detecting the entanglement of the entire system.

As an example of such loss, consider the 3-particle GHZ state.

$$|\psi_{GHZ}\rangle = |111\rangle + |000\rangle / \sqrt{2} \tag{3.43}$$

This state is known to be highly entangled. To calculate the 2-point concurrence of this system, one of the particles is traced out. The density matrix that describes the system is

$$\rho_{GHZ} = \frac{1}{2} \left(|111\rangle \langle 111| + |000\rangle \langle 000| + |111\rangle \langle 000| + |000\rangle \langle 111| \right) \tag{3.44}$$

The density matrix that follows after tracing is

$$\begin{aligned} \mathrm{Tr}_3 \ \rho_{GHZ} &= \frac{1}{2} \left(|11\rangle \langle 11| + |00\rangle \langle 00| \right) \\ &= \frac{1}{2} \left(|0\rangle \langle 0| \otimes |0\rangle \langle 0| + |1\rangle \langle 1| \otimes |1\rangle \langle 1| \right) \end{aligned} \tag{3.45}$$

This state is not 2-separable and therefore is not entangled. The result shows that if the system is composed of more than two particles and is entangled, tracing out the particles may leave a system that is separable (not entangled). With this observation, an important question is, what does 2-point concurrence tell us about the *entire* system?

First, consider the case when $C(\rho_2) = 0$. In general, this condition gives no information on the entanglement of the entire system, because, as we have seen,some entanglement classes are destroyed by the tracing operation. Next, let us consider the case when $C(\rho) \neq 0$. Let ρ_2 be the 2-qubit reduced density matrix of the system With $\rho_2 = \mathrm{Tr}_{n-2}\, \rho$, where ρ is the density matrix of the entire system. This case is obvious:

- $C(\rho_2) \neq 0 \Rightarrow \quad \rho$ is not n-separable (i.e., entangled)

This could be easier to be understood by considering the contraposition: If the system is n-separable, $C(\rho_2) = 0$. This must be true because taking the trace of a n-separable state (a product state) is clearly a product state. This in turn implies that the

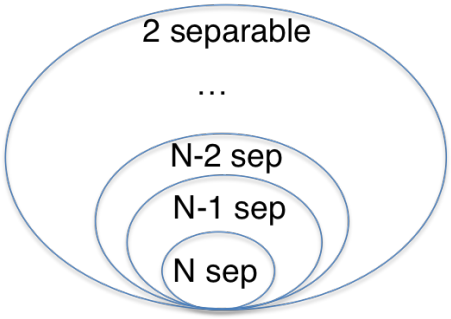

Figure 3-8: (Color online) The hierarchy of separable states.

information on the entire system obtained from 2-point concurrence is very specific, as $C(\rho_2) > 0$ only tells us a small class of separability (see Fig. 3.4.2).

In summary, 2-point concurrence is a rare entanglement monotone that offers a sufficient and necessary condition for entanglement even if the system is mixed. However, it only applies to a 2-qubit system and therefore it has drawbacks in giving insight to the entire system. In the following subsections, we attempt to improve some of the drawbacks by considering genuine multi-particle entanglement of the system.

Before concluding the discussion of concurrence, we would like to point out that there is a generalized multiparticle concurrence defined for *pure* systems

$$\mathcal{C}_{\mathcal{M}}(\rho) = \sqrt{2(1 - Tr(\rho_M^2))} \tag{3.46}$$

This version, however, is not suitable for our model because it offers meaningful information of the system when it is a pure quantum system [45]. [6]

3.4.3 Genuine multiparticle entanglement of the driven-dissipative Dicke model

Implication of genuine multipatricle entanglement of the reduced system

As we have seen, 2-point concurrence of the reduced density matrix detects the n-separability of the original n-particle density matrix of the steady state solution of the driven-dissipative Dicke model. One important factor that should be considered here is that n-separability of a system is the most stringent condition for the system

to be entangled. That, in turn, implies that $C \neq 0$ gives very small information; $C \neq 0$ means the system is k-separable with k ranging from 1 to $n-1$. On top of this, as we have discussed, the nature of the tracing operation of $n-2$ particles leads to 2-point concurrence being very insensitive to many entanglement states.

To overcome these shortcomings, we propose computing genuine multi-particle entanglement of the reduced density with less number of particles traced. That is, to complement the results of the 2-point concurrence, we evaluate the loosest criteria of separability – whether the system is 2-separable or not – of a subsystem whose particle number n_d is larger than 2. The formal procedure is as follows

1. ρ is the steady state solution of the model. Trace out $(n-m)$ particles to obtain a reduced density matrix of d particles ρ_d^m

2. Find a general quantity q that detects when a state is NOT 2-separable

3. Compute q for ρ_d^m

We later show that the quantity q we used is, in most cases, an entanglement witness for genuine-multi particle state (a sufficient condition for a multiparticle state), but in some special cases of our model, it also acts as quantum criteria (sufficient and necessary condition). Below we show that this procedure gives more information than 2-point concurrence on the separability and entanglement of the entire system.

Suppose q is a GME witness. We would like to prove the following:

- If q detects GME of subsystem described by $\rho_d^m \Rightarrow$ The entire system (ρ) is not $n-k+2$ separable

- (Contraposition) $n-k+1$ separable $\Rightarrow$ q does not detect the GME of ρ_d^m

Let us prove by contradiction. Suppose the entire system described by ρ is $n-k+2$ separable. Obtaining ρ_d^k is achieved by tracing out $n-k$ particles. ρ_d^k becomes α-separable where

$$\alpha \geq (n-k+2) - (n-k) = 2 \tag{3.47}$$

However, q detecting GME suggests $\alpha = 1$ and this is a contradiction. In this proof, we have used the following relationship between a trace operation and the separability of the reduced state to obtain the inequality of α.

- If ρ is k-separable $\Rightarrow \mathrm{Tr}_1(\rho)$ is k'-separable where $k' \geq k-1$

Here $\mathrm{Tr}_1(\rho)$ is the reduced density matrix of ρ taking the trace of one particle, regardless of the choice of it. This relation is readily seen if recall the definition of k-separability. The reduced density $\rho_d^n - 1$ matrix can be written as

$$\rho_d^{n-1} = \mathrm{Tr}_1 \left(\sum_\mu p_\mu |\Psi'_{\mu_1}\rangle \langle \Psi'_{\mu_1}| \otimes \ldots \otimes |\Psi'_{\mu_k}\rangle \langle \Psi'_{\mu_k}| \right) \tag{3.48}$$

$$= \underbrace{\sum_\mu p_\mu \left|\Psi'_{\mu_1}\right\rangle \left\langle \Psi'_{\mu_1}\right| \otimes \ldots \otimes \left|\Psi'_{\mu_{k-1}}\right\rangle \left\langle \Psi'_{\mu_{k-1}}\right|}_{(k-1)\text{-separable}} \otimes \mathrm{Tr}_1 \left(\left|\Psi'_{\mu_k}\right\rangle \left\langle \Psi'_{\mu_k}\right| \right) \tag{3.49}$$

Here we define a set of indices μ such that the trace operator acts only on $\left|\Psi'_{\mu_k}\right\rangle \left\langle \Psi'_{\mu_k}\right|$. That is, only $\left|\Psi'_{\mu_k}\right\rangle$ contain the particle that is being traced of. Clearly, the reduced density matrix is at least $(k-1)$-separable. Eq. (3.47) is shown by repeating this procedure.

To summarize, by computing GME of the traced reduced density matrix obtained by tracing out m particles reduced density matrix gives insight into $n-m+2$ separability of the whole system. In addition, the procedure may be more sensitive to some entanglement classes than other quantum measures including 2-point concurrence. This is because, by choosing a small m, some entanglement that was otherwise destroyed in the process of tracing out many particles may be detected. The key to this method is to find a quantity that detects GME, or in other words. We next discuss how to find a sufficient condition that shows the (sub) system is GME.

PPT criteria

In characterising the genuine multiparticle entanglement of the reduced system, we followed the approach appeared in [24] that is based on PPT criteria [42]. Here we

outline the main points of such approach. Most generally, an entangled measure is defined as

$$\mathcal{M}(\varrho) \equiv \inf_{\{p_\mu, \Psi_\mu\}} \sum_\mu p_\mu \mathcal{M}(\Psi_\mu) \tag{3.50}$$

The infimum is taken over all possible decompositions of the quantum states as well as the probabilistic weight of each of the states. This operation is virtually impossible to conduct with exponentially complex optimization processes involved. Even if one gives up quantifying entanglement and focusing only on the criteria of entanglement, similar optimizations are still inevitable. As an example, if we wish to prove k-separability, essentially, we need to examine all possible set of k-separable states and their probabilistic weights and examine if the density matrix can be constructed with them.

The fundamental idea is, instead of exploring possible sets of a mixture of separable states, the problem becomes much simpler if we explore the set of states called PPT states. An state is called PPT when the partial transposed matrix of a state is semidefinite. Given a matrix $\varrho_{j_A,j_B,j'_Aj'_B}$, the partial transpose matrix $\varrho^{T_B}_{j_A,j_B,j'_Aj'_B}$ is defined as,

$$\varrho^{T_B}_{j_Aj_Bj'_Aj'_B} \equiv \left\langle j_A \left| \left\langle j_B \left| \varrho^{T_B} \right| j'_A \right\rangle \right| j'_B \right\rangle \doteq \left\langle j_A \left| \langle j'_B | \varrho | j'_A \rangle \right| j_B \right\rangle = \varrho_{j_Aj'_Bj'_Aj_B} \tag{3.51}$$

If the transposed matrix is positive semidefinite, the state is called a PPT state. The PPT criteria are

Definition 3.4.9 (PPT criteria)**.** If a state is not a PPT mixture $\Rightarrow$ the state is not bi-separable (and is genuine multiparticle entangled).

Note that this is a sufficient condition for GME; the state being PPT does not in turn suggest that it is a bi-separable state, because the set of product states are a subset of PPT states. The process now becomes, instead of finding a decomposition

$$\rho = \sum_i p_i \rho_i^{sep} \tag{3.52}$$

we wish to examine if the given density matrix can be written as

$$\rho = \sum_i p_i \rho_i^{ppt} \tag{3.53}$$

This decomposition process can be further simplified if we attempt to find a witness that detects the PPT. That is, instead of finding ρ^{ppt}, we look for a observable W such that if ρ is a PPT state, $\mathrm{Tr}\,[W\rho] \geq 0$. Taking the contraposition and recall that a non-PPT state is entangled, the witness W gives a sufficient condition for the state to be GME.

- Given ρ, if $\mathrm{Tr}\,[W\rho] \leq 0 \Rightarrow \rho$ is GME.

Finding W is smartly achieved by exploring positive operators P_A and Q_B acting on each of the subsystems A and B. Then, using the properties of positive operators, in general, $W = P_A + Q_B^{T_B}$ is guaranteed to be $\mathrm{Tr}\,[W\varrho_{PPT}] \geq 0$. Further, the decomposition turns out to be sufficient and necessary condition for $\mathrm{Tr}\,[W\varrho_{PPT}] \geq 0$.

- There exists two positive semidefinite operators P_A and Q_B
  $\iff$ $\mathrm{Tr}\,[W\varrho_{PPT}] \geq 0$, where $W = P_A + Q_B^{T_B}$

Therefore, if we can NOT find P_A and Q_B that lead to $\mathrm{Tr}\,[W\rho] \geq 0$, the system ρ must be GME. Computationally, the exploration of GME states can be achieved by implementing numerical programs such as the following.

minimize $\mathrm{Tr}(W\rho)$,

such that for all possible choice of A and B :

$W = P_A + Q_B^{T_B}$,

where Q_M, P_M are positive semidefinite operators

Again, the problem is now, instead of working on the decompoisition of ρ, to find P and Q for all possible choices of subsystems A and B. This approach has several advantages. One of those is that this problem can be solved efficiently by semidefinite programming as opposed to NP hard problem that is involved in decomposition of

ρ. In practice, the procedure 3.4.3 can be computed numerically without too many lines of code, using solver packages for semidefinite programming and optimization. We have used YALMIP package and the SDPT3 as the solver, both of which are the MATLAB package obtainable online. For computing the witness measure of given states, PPTmixer package introduced in [24], is utilized. The witness in general gives a sufficient and necessary condition for a non-PPT state and this in turn gives only a sufficient condition for the state to be GME. However, for permutation invariant states up to three particles, this criteria is known to be necessary and sufficient [36].

Results

In the following discussion we use N_B and the particle number of the reduced system described by ρ_B and N as the particle number of the entire system described by ρ.

The witness ($\mathrm{Tr}\,[W\rho]$) plotted against Ω for each of the reduced density matrices (ρ_B) is shown in Fig. 3-9. The total number of particles is $N = 16$, and each plot corresponds to the size of the reduced density matrix (N_B). Each plot corresponds to different size of ρ_B. For example, the blue-square markers indicate the witness is computed from the reduced density matrix obtained by tracing out $16 - 3 = 13$ particles, leaving three particle in the subsystem B ($N_B = 3$). Note that for the case where $N_B = 2$, the plot and the result of concurrence Fig. 3-7, Fig. 3-6 should give identical information on entropy because both $W < 0$ plotted here and 2-point concurrence $C > 0$ give a necessary and sufficient condition for 2-point entanglement of the (reduced) 2-particle system.

The most unexpected and notable finding from the plot is that even for $\Omega > 0.5$ the reduced system is genuine multiparticle entangled, sequentially suggesting that the entire system is also entangled. This is in stark contrast with the results of, for example, spin squeezing, quantum Fisher information, or the 2-point concurrence which only shows and detects entanglement when $\Omega < 0.5$. Contrary to our intuition, the dissipative Dicke model becomes highly mixed at $\Omega = 0.5$, yet the entanglement of the system does not immediately disappear.

As a complimentary study, we have also plotted the GME for systems of $N = 2, 3, 4$

without taking the trace (Fig. 3-10). The difference between Fig. 3-9 and Fig. 3-10 is that in Fig. 3-9, the system is $N = 16$ and then we obtained reduced system of $N_B = 2, 3, 4, 5$ by taking the trace and then we computed the GME, whereas in Fig. 3-10, we started with $N = 2, 3, 4$ without taking the trace and plotted GME. We observe that GME tend to decay slower in the region $\Omega > 0.5$ for the case of $N = 2, 3, 4$ compared to $N_B = 2, 3, 4$. This is partly because In Fig. 3-10, no entanglement is destructed by the process of taking the trace that is inevitable in plotting Fig. 3-9. In figure Fig. 3-11, the contrast of GME for each N and N_B is further highlighted.

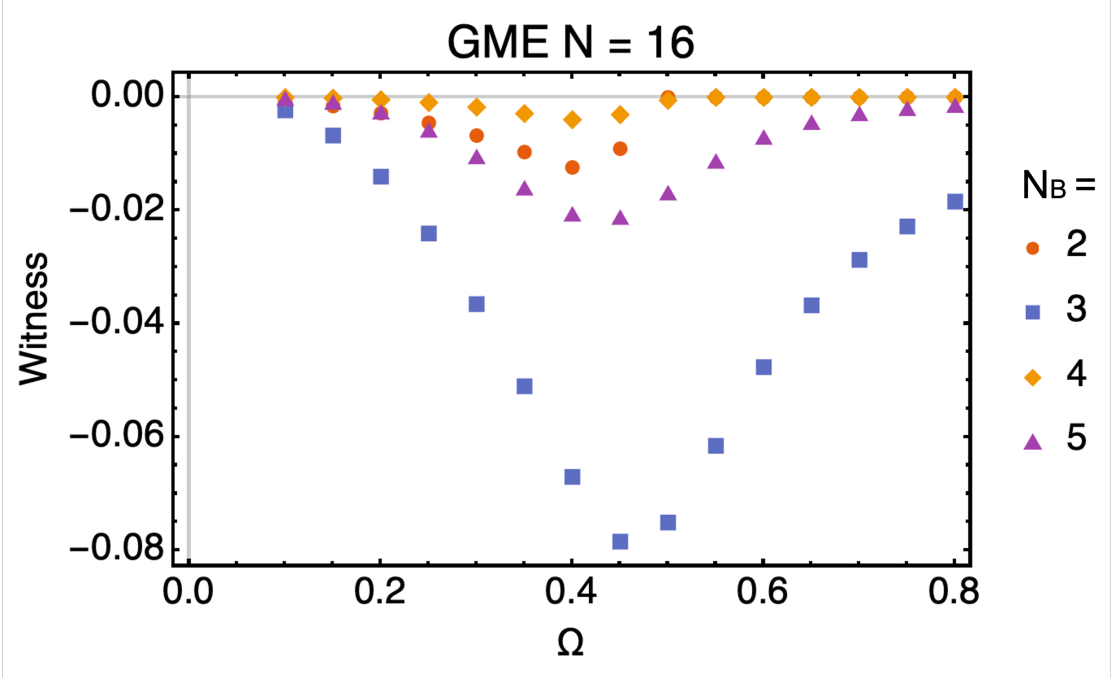

Figure 3-9: (Color online) Genuine multi-partite Entanglement $N = 16$, plotted against Ω for $N_B = 2, 3, 4, 5$

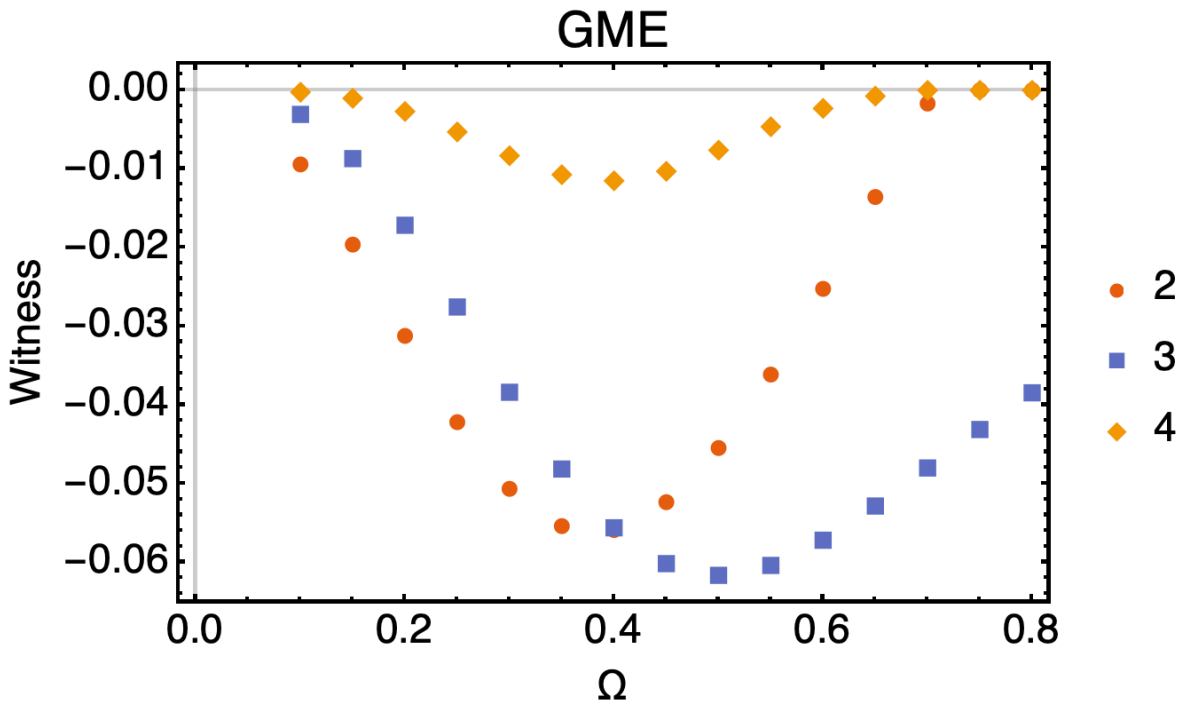

Figure 3-10: (Color online) Genuine multi-partite Entanglement of $N = 2, 3, 4$, plotted against Ω

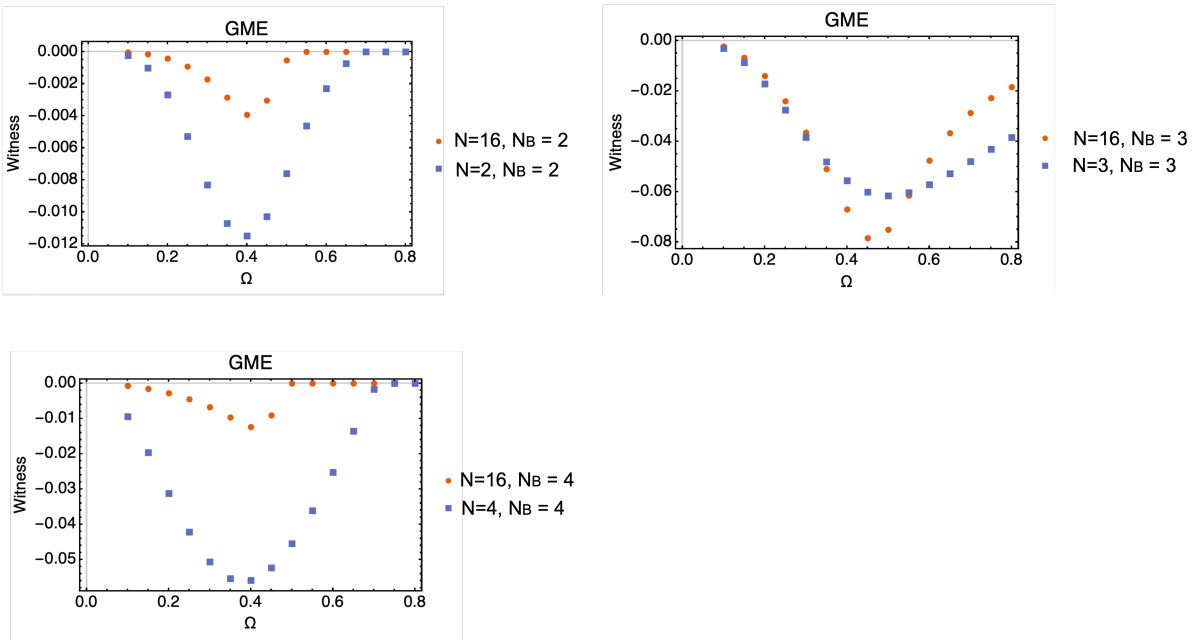

Figure 3-11: (Color online) Comparison of genuine multi-partite Entanglement of the reduced system and the whole system, plotted against Ω

3.4.4 Separability of Dicke state at two limiting cases

In this subsection, we show that the system is NOT entangled in two limiting cases, namely at $\Omega \to 0$ and $\Omega \to \infty$. Here we assume the system is N particles, and the total angular momentum $J = N/2$.

Small Ω limit

When $\Omega \to 0$, the solution to Eq. (3.1) approaches,

$$\lim_{\Omega \to 0} \rho_{ex}(\Omega) = |J, -J\rangle \langle J, -J| \tag{3.54}$$

This is clearly a n-separable state and is not entangled, because

$$|J, -J\rangle = |g\rangle \otimes |g\rangle \otimes ... \otimes |g\rangle \tag{3.55}$$

Large Ω limit

When $\Omega \to \infty$, the solution to Eq. (3.1) approaches,

$$\lim_{\Omega \to \infty} \rho_{ex}(\Omega) = \frac{1}{N} \sum_{m=-J}^{J} |J, m\rangle \langle J, m| \tag{3.56}$$

This state belongs to the diagonal symmetric state, which is the probabilistic mixture of Dicke states. The general form of such states are commonly written as

$$\rho = \sum_{n=0}^{N} \chi_n |D_{N,n}\rangle \langle D_{N,n}| \tag{3.57}$$

Here the basis $|D_{N,n}\rangle$ are the unnormalized Dicke states,

$$|D_{N,n}\rangle := \begin{pmatrix} N \\ n \end{pmatrix} P_{\text{sym}} \left(|1\rangle^{\otimes n} \otimes |0\rangle^{\otimes N-n} \right) \tag{3.58}$$

and is related to our angular momentum basis as

$$|J,m\rangle = \begin{pmatrix} N \\ n \end{pmatrix}^{-1} |D_{N,J-m}\rangle \tag{3.59}$$

There is a proof that the necessary and sufficient condition for the separability of such a diagonal symmetric state is that the Hankel matrix described as follows is positive semi-definite [68].

$$H_0 := \begin{pmatrix} \chi_0 & \cdots & \chi_{m_0} \\ \cdots & \cdots & \cdots \\ \chi_{m_0} & \cdots & \chi_{2m_0} \end{pmatrix} \quad H_1 := \begin{pmatrix} \chi_1 & \cdots & \chi_{m_1} \\ \cdots & \cdots & \cdots \\ \chi_{m_1} & \cdots & \chi_{2m_1-1} \end{pmatrix}$$

Here, the components are from Eq. (3.57). Our goal is to test whether the Hankel matrices are positive semidefinite in our case.

The matrix components of the Hankel matrices are readily obtained with Eq. (3.56) and Eq. (3.59) as,

$$\chi_k = \frac{1}{N+1} \begin{pmatrix} N \\ k \end{pmatrix}^{-2} \tag{3.60}$$

Assuming the smallest eigenvalue of a Hankel matrix is ϵ, the necessary and sufficient condition for the matrix to be positive-semidefinite is $\epsilon \geq 0$. Here we plot ϵ for different particle number N in Fig. 3-12. We rescaled the Hankel matrix as the following by multiplying certain positive factors to set ϵ to be around the same value with different N.

$$H_0 \to (N+1) \begin{pmatrix} N \\ \left[\frac{N}{2}\right] \end{pmatrix}^2 H_0 \tag{3.61}$$

$$H_1 \to (N+1) \begin{pmatrix} N \\ \left[\frac{N}{2}\right] \end{pmatrix}^2 H_1 \tag{3.62}$$

We see that $\epsilon \geq 0$ is indeed satisfied and therefore it suggests that in $\Omega \to \infty$ limit, the density matrix of the steady state solution of Eq. (3.1) is separable and

therefore the system is not entangled.

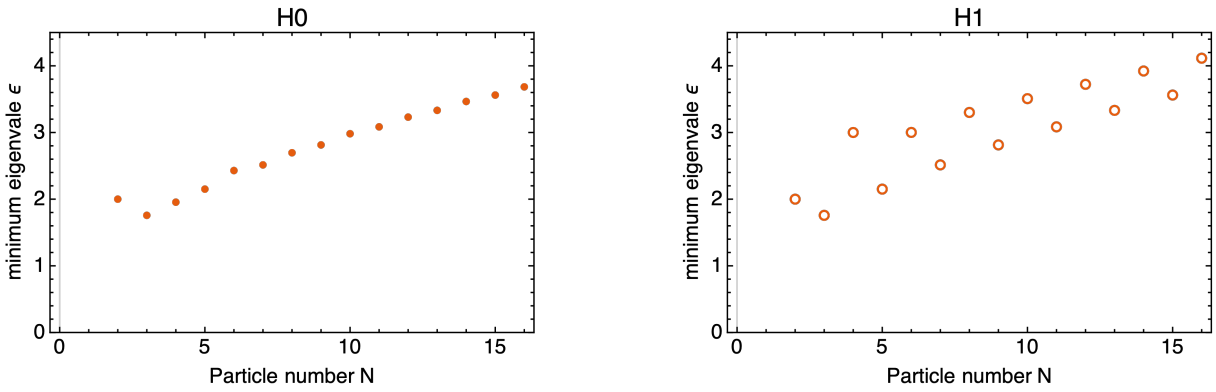

Figure 3-12: (Color online) minimum eigenvalue of the rescaled Hankel matrices plotted against N. $\epsilon > 0$ suggests the system is separable.

3.5 Quantum discord of Dicke state

In the context of quantum correlations, it would be difficult to deny that quantum entanglement has played the most central and most technologically important role in modern quantum physics [30] [52] [56]. However, this does not mean that quantum entanglement manifests itself as the only form of quantum correlation. Quantum entanglement therefore should be regarded as *one of the* approaches to quantum correlation, as opposed to *the only* approach. The formalism of entanglement we have seen in the previous sections was solely based on the separability of the physical system and was not connected with the notion of correlation. Quantum discord is one of the different approaches to quantum correlation [69]. Historically, quantum discord is introduced in the context of indistinguishability of quantum states.

3.5.1 Review of quantum discord

In this subsection, we review the definition of Measurement-based Quantum discord (QD). QD, in simple words, is essentially the difference of two classically equivalent definitions of mutual information [20]. Let us see first consider mutual information of two classical random variables A and B with the possible measurement outcomes $a \in A$ and $b \in B$. The mutual information between A and B is

$$I(A:B) = H(A) + H(B) - H(A,B) \tag{3.63}$$

where $H(A), H(B)$ are the Shannon entropy of marginal distributions over A, B and $H(A,B)$ is the Shannon entropy of the joint distribution over $A \times B$. An identical quantity can be expressed as

$$I(A:B) = H(B) - H(B \mid A) \tag{3.64}$$

where $H(B \mid A)$ is the conditional entropy. The equality of the two expressions can be easily seen if we note that,

$$H(B \mid A) = \sum_a p_a H\left(P_{b|a}\right) \tag{3.65}$$

$$= -\sum_a p_a \sum_b \frac{p_{ab}}{p_a} \log\left(\frac{p_{ab}}{p_a}\right) \tag{3.66}$$

$$= -\sum_{ab} p_{ab} \log\left(p_{ab}\right) + \sum_{ab} p_{ab} \log\left(p_a\right) \tag{3.67}$$

$$= H(A, B) - H(A) \tag{3.68}$$

Now let us observe how the mutual information can be formalized in the quantum domain. The natural extension of the classical mutual information into quantum one is to replace the Shannon entropy by von Neumann entropy and classical probability distributions by the quantum density matrix. That is, with ρ the density matrix of a quantum system, von Neumann entropy $S(\rho)$ is defined as

$$S(\rho) = -\rho \log(\rho) \tag{3.69}$$

Transporting Eq. (3.63) to quantum domain is straightforward, and it is defined as

$$I^t_{AB} = S(\rho_A) + S(\rho_B) - S(\rho_{AB}) \tag{3.70}$$

where $\rho_A = Tr_B(\rho_{AB})$ and $\rho_B = Tr_A(\rho_{AB})$.

Eq. (3.64) is, in a similar manner, expressed as

$$I^c_2 = S(\rho_B) - S_{B/A} \tag{3.71}$$

where $S_{B|A}$ is the quantum conditional entropy of subsystem B after making a measurement on subsystem A.

Eq. (3.71), which at first, appears to be very simple, highlights the complexity and mystery of quantum mechanics in the context of quantum discord. Because in quantum mechanics, making a measurement on a system disturbs the system (back

action), Eq. (3.71) is affected by the choice of such measurements. Moreover, replacing Shannon entropy by von Neumann entropy in Eq. (4) could lead to a quantity which can be positive as well as negative [22], suggesting such naive replacement does not give a meaningful physical quantity.

Accordingly, the formal definition of the quantum conditional entropy reflects such insights,

$$S_{B|A} = \min_{\Pi_k^A \in \mathcal{M}^A} \sum_k p_k S(\rho_{B/k}) \tag{3.72}$$

here, π_k^A is the measurement operator acting on subsystem A with possible out come k. $\mathcal{M}^A$ is the set of all such possible operators in cluding all possible k. $p_k = \mathrm{tr}_{AB}[I_m^B \otimes \Pi_k^A \rho_{AB}\, I_m^B \otimes (\Pi_k^A)^\dagger]$ is the probability of outcome of the measurement yielding k and $\rho_{B/k} = \mathrm{tr}_A[I_m^B \otimes \Pi_k^A\, \rho_{AB}\, I_m^B \otimes (\Pi_k^A)^\dagger]/p_k$ is the density matrix of the subsystem B after the measurement. One can easily confirm the following relationship between I_{AB}^t and I_{AB}^c

- $I_{AB}^c \leq I_{AB}^t$
- When the system is a probablistic mixture of product states,, $I_{AB}^t = I_{AB}^c$

As such, there are suggestions that I_{AB}^t and I_{AB}^c should be treated as the total correlation([19] and the classical correlation [20] of bipartite state ρ_{AB} respectively. If we accept that the difference of those two should yield the quantum portion of the correlation and it is called the quantum discord, which is defined as

$$\begin{aligned} D^{\rightarrow}(\rho_{AB}) &\equiv I_{AB}^t - I_{AB}^c \\ &= S(\rho_A) + S_{B/A} - S(\rho_{AB}) \end{aligned} \tag{3.73}$$

Here are some basic properties of quantum discord

- $D^{\rightarrow}(\rho_{AB}) = 0 \Leftrightarrow$ There exists measurement on A that does not disturb the state

- If ρ_{AB} is a pure state $\Rightarrow D^{\rightarrow}(\rho_{AB}) = S(\rho_B)$
  i.e. QD is equal to von Nuemann entropy of the subsystem.

- $D^{\rightarrow}(\rho_{AB}) \leq S(\rho_A)$ [28]

To summarize, intuitively, QD is measuring the "non-classicality" of the correlation of the system. Here, QD makes the assumption that the "non-classicality" is captured by how much a state is disturbed by measurements of the state. When the system is a pure state, this is exactly coming from the entanglement; therefore, when a system is pure, the discord equals to the von Neumann entropy of the system. However, when the system is mixed, some nonclassical correlation that is not detected by the entanglement can be sensed by QD. Werner state, for example, is a state which can possess nonzero QD, but no entanglement [63].

3.5.2 Quantum Discord of the Dicke model

The difficulty of computing quantum discord lies in the process of taking the minimization of all possible measurement sets that appear in Eq. (3.71).

Possible measurement set

Since we are assuming the system is in Dicke state, we further assume that there is no measurement that breaks the permutation symmetry of the atoms, i.e., the measurement operators are spanned by the Dicke basis, and they cannot change the total spin of the subsystem such that the measurement operators act on. To look at this argument in a different way, if there is a measurement that breaks the symmetry of the subsytem A, for intstance by operating the measurement only on one particle when the subsystem A contains more than one particle, we redefine the subsystem A such that A is made of only the particle that is being measured. Therefore, $\mathcal{M}^A$, the complete set of measurements on subsystem A is described by the conserved quantity J_A in the $SU(2J_A + 1)$ space, where J_A is the total spin of the subsystem A. $\mathcal{M}^A$ is formally expressed as

$$\mathcal{M}^A = \{\pi_m^{J_A}(\phi, \theta, \chi) : 0 \leq \chi, \theta, \phi \leq 2\pi, -J_A \leq m \leq J_A\} \tag{3.74}$$

where ϕ, θ, χ are the parameters that appear from the rotation operation in the $SU(2J_A+1)$ space. Let (R) be the rotation operation, then the measurement operator in $SU(2J_A + 1)$ is expressed as

$$\pi_m^j = \mathcal{D}(\mathcal{R}) \left|j, m\right\rangle \left\langle j, m\right| \mathcal{D}(\mathcal{R})^\dagger \tag{3.75}$$

One handy rotation operation is the Euler rotation, and its matrix components are computed as follows

$$\left\langle j, m\right| \mathcal{D}(\mathcal{R})^\dagger = \sum_{m'} \left\langle j, m'\right| \mathcal{D}^{(j)*}_{m',m}(R) \tag{3.76}$$

$$= \sum_{m'} \left\langle j, m'\right| \exp\{(i(m'\alpha + m\gamma))\} d^{(j)}_{m',m}(\beta) \tag{3.77}$$

Using Wigner d matrices, the measurement operators can be explicitly described as,

$$\begin{aligned}
\pi_m^j(\phi, \theta, \chi) &= \mathbf{R}(\phi, \theta, \chi) \left|J, M\right\rangle \left\langle J, M\right| \mathbf{R}(\phi, \theta, \chi) \\
&= \sum_{n,\mu} \left|J_A, n\right\rangle e^{-i(n\phi + m\chi)} d^{J_A}_{n,m}(\theta) e^{i(\mu\phi + m\chi)} d^j_{\mu,m}(\theta) \left\langle j, \mu\right| \\
&= \sum_{n,\mu} e^{i\phi(\mu - n))} d^j_{n,m}(\theta) d^j_{\mu,m}(\theta) \left|j, n\right\rangle \left\langle j, \mu\right|
\end{aligned} \tag{3.78}$$

Here, $-\pi \leq \alpha, \beta \leq \pi$. Interestingly, gamma does not play a role according to this calculation. $d^{(J)}_{\mu,m}$ is the Wigner matrix and its exact expression is given as

$$d^{(J)}_{\mu,m}(\theta) = [(J+M)!(J-M)!(J+\mu)!(J-\mu)!]^{1/2} \times \sum_{\nu} \frac{(-1)^{\nu}}{(J-\mu-\nu)!(J+m-\nu)!(\nu+\mu-m)!\nu!} \times \left[\cos(\frac{\theta}{2})\right]^{2J+m-\mu-2\nu} \left[-\sin(\frac{\theta}{2})\right] \tag{3.79}$$

The next step of obtaining the quantum discord for the steady state of the Dicke model is to compute the probability of the outcome of the measurement, as well as the resultant density matrix of subsystem B that suffers the back action of measurement operations on the subsystem A. Suppose the density matrix is expressed as

$$\rho = \sum_{m=-J}^{J} \sum_{n=-J}^{J} X(J)^{n}_{m} \left|J,m\right\rangle \left\langle J,n\right| \tag{3.80}$$

. We ideally want to rewrite the density matrix in $\mathcal{H}_{\mathcal{A}} \otimes \mathcal{H}_{\mathcal{B}}$. This is relatively straightforward to do as, as any states $|J,m\rangle$ has a unitary transformation that connects $|j_a,\mu_a\rangle \in \mathcal{H}_{\mathcal{A}}$, $|j_b,\mu_b\rangle \in \mathcal{H}_{\mathcal{B}}$.

$$\left|J,m\right\rangle = \sum_{\mu_a,\mu_b} C(j_a j_b J;\mu_a\mu_b m) \left|j_a,\mu_a\right\rangle \left|j_b,\mu_b\right\rangle \tag{3.81}$$

the coefficients are the famous Clebsch-Gordon coefficients

$$C(j_a j_b J;\mu_a\mu_b m) = \left\langle J,m\right| \cdot (\left|j_a,\mu_a\right\rangle \left|j_b,\mu_b\right\rangle) \tag{3.82}$$

In theory, j_a, j_b are constrained by the total angular momentum of the system J by the inequality relation

$$|j_a + j_b| \leq J \leq |j_a - j_b| \tag{3.83}$$

and one has the freedom to choose whatever j_a and j_b that satisfies the inequality for the unitary transformation. However, as the particle number of the system is related as $n = 2J$, and $n = n_a + n_b$, we only consider the j_a and j_b such that $J = j_a + j_b$.

Now the density matrix is rewritten as

$$\rho_{AB} = \sum_{m=-J}^{J} \sum_{n=-J}^{J} X(J)_m^n \left|J, m\right\rangle \left\langle J, n\right|$$

$$= \sum_{m=-J}^{J} \sum_{n=-J}^{J} X(J)_m^n \sum_{\mu_a', \mu_b'} C(j_a j_b J; \mu_a' \mu_b' m) \left|j_a, \mu_a'\right\rangle \left|j_b, \mu_b'\right\rangle$$
$$\times \sum_{\mu_a, \mu_b} C(j_a j_b J; \mu_a \mu_b n) \left\langle j_a, \mu_a\right| \left\langle j_b, \mu_b\right|$$

$$= \sum_{\mu_a, \mu_b, \mu_a', \mu_b'} \left(\sum_{m,n} X_m^n(J) C(j_a j_b J; \mu_a' \mu_b' m) C(j_a j_b J; \mu_a \mu_b n) \right)$$
$$\times \left|j_a, \mu_a'\right\rangle \left\langle j_a, \mu_a\right| \otimes \left|j_b, \mu_b'\right\rangle \left\langle j_b, \mu_b\right|$$

$$= \sum_{\mu_a, \mu_b, \mu_a', \mu_b'} \gamma_{a,b}^{a'b'} \left|j_a, \mu_a'\right\rangle \left\langle j_a, \mu_a\right| \otimes \left|j_b, \mu_b'\right\rangle \left\langle j_b, \mu_b\right| \tag{3.84}$$

Here we use γ as the matrix component of this matrix, where

$$\gamma_{a,b}^{a'b'} = \sum_{m,n} X_m^n(J) C(j_a j_b J; \mu_a' \mu_b' m) C(j_a j_b J; \mu_a \mu_b n) \tag{3.85}$$

We have expressed the density matrix by a direct product of subspace $\mathcal{H}_\mathcal{A}$ and $\mathcal{H}_\mathcal{B}$. Now we are ready to compute the various quantities with a measurement performed on A (that is, to perform a measurement operator that lies in $\mathcal{H}_\mathcal{A}$.

Assuming the result of the measurement result A yielded the physical value m (for example, imagine the spin value of your chose quanization axis was m), then the affected density matrix of the total system $\rho_{AB|k=m}$ is the following

$$\rho_{AB|m} = \pi_m^{j_a}(\alpha,\beta) \otimes I_B \, \rho \, \pi_m^{j_a} \otimes I_B$$

$$= \sum_{n,\mu} \mathrm{e}^{i\alpha(\mu-n)} d^{j_a}_{n,m}(\beta) d^{j_a}_{\mu,m}(\beta) \left|j_a, n\right\rangle \left\langle j_a, \mu\right|$$
$$\times \sum_{a,a',b,b'} \gamma_{a,b}^{a'b'} \left|j_a, a\right\rangle \left|j_a, a'\right\rangle \left\langle j_{a'}, a'\right| \left\langle j_{b'}, b'\right|$$
$$\times \sum_{l,k} \mathrm{e}^{i\alpha(k-l)} d^{j_a}_{l,m}(\beta) d^{j_a}_{k,m}(\beta) \left|j_a, l\right\rangle \left\langle j_a, k\right|$$

$$= \sum_{n,\mu,l,k=j_a}^{j_a} \sum_{a,a'=-j_a}^{j_a} \sum_{b,b'=-j_b}^{j_b} e^{i\alpha(\mu-l-n+k)} \times d^{j_a}_{n,m}(\beta) d^{j_a}_{\mu,m}(\beta) d^{j_a}_{l,m}(\beta) d^{j_a}_{k,m}(\beta) \gamma_{a,b}^{a',b'}$$
$$\times \left|j_a, n\right\rangle \left\langle j_a, \mu | j_a, a\right\rangle \left\langle j_a, a' | j_a, l\right\rangle \left\langle j_a, k\right| \left\langle j_b, b'\right|$$

$$= \sum_{n,\mu,l,k=-j_a}^{j_a} \sum_{b,b'=-j_b}^{j_b} \mathrm{e}^{i\alpha(\mu-l-n+k)} \gamma_{\mu,b}^{l,b'} d_{n,m} d_{\mu,m} d_{l,m} d_{k,m} \left|j_a, n\right\rangle \left|j_b, b\right\rangle \left\langle j_a, k\right| \left\langle j_b, b'\right|$$

$$= \sum_{n,k=-j_a}^{j_a} \sum_{b,b'=-j_b}^{j_b} \underbrace{\left(\sum_{\mu,l} \mathrm{e}^{i\alpha(\mu-l-n+k)} \gamma_{\mu,b}^{l,b'} d_{n,m} d_{\mu,m} d_{l,m} d_{k,m} \right)}_{\equiv P_{n,b}^{k,b'}(\alpha,\beta)_m^{j_a}} \left|j_a, n\right\rangle$$
$$\times \left|j_b, b\right\rangle \left\langle j_a, k\right| \left\langle j_b, b'\right| \tag{3.86}$$

By changing the indices $k \to a', n \to a$, we arrive at

$$\rho_{AB/k} = \sum_{a,a'=-j_a}^{j_a} \sum_{b,b'=-j_b}^{j_b} P_{a,b}^{a',b'}(\alpha,\beta)_m^{j_a} \left|j_a, a\right\rangle \left|j_b, b\right\rangle \left\langle j_a, a'\right| \left\langle j_b, b'\right| \tag{3.87}$$

Using this expression, we may immediately compute the probability of the measurement result yielding k, which we denote as p_k. (For example if $k = 1$ then p_1 is the probability that the measurement gives the value 1)

$$
\begin{aligned}
p_k &= \mathrm{Tr}_{AB}(\rho_{/A}) \\
&= \sum_{a=-ja}^{j_a} \sum_{-j_b}^{j_b} P_{a,b}^{a,b}(\alpha,\beta)_k^{j_a}
\end{aligned} \tag{3.88}
$$

Now the conditional density operator $\rho_{B/m}$, which is the density operator of the subsystem B after the measurement on A gives the result m) is,

$$
\begin{aligned}
\rho_{B/m} &= p_m^{-1} Tr_A(\rho_{/A_m}) \\
&= p_m^{-1} \sum_{b,b'=-j_b}^{j_b} \left(\sum_k P_{k,b}^{k,b'}(\alpha,\beta)_m^{j_a} \right) |j_b, b\rangle \langle j_b, b'|
\end{aligned} \tag{3.89}
$$

Note that this expression is function of α and β, which were the Euler angles. This means that the conditional density operator should depend on the measurement basis we choose, hence the conditional entropy also depends on this measurement set. This is the essence of discord.

Computing conditional entropy

Our next step is to compute the conditional entropy Eq. (3.71). The flow of such computation is graphically described in Fig. 3-13. To remind the reader, the conditional entropy is defined as

$$
S_{B|A} = \min_{\Pi_k^A \in \mathcal{M}^A} \sum_k p_k S(\rho_{B|k}) \tag{3.90}
$$

Note that p_k and $\rho_{B|k}$ we have computed are dependent of two variables α and β, each of which were used to parameterize the rotation operation. Let us concretely observe how the term that is minimized ($\sum_k p_k S(\rho_{B|k})$) depends on these parameters. For different choice of subsystems A and B.

$N_A = 1$, $N_B = 1$ case: We first examine the case where the system consists of only two particles. subsystem A consists of one particle and subsystem B is the other

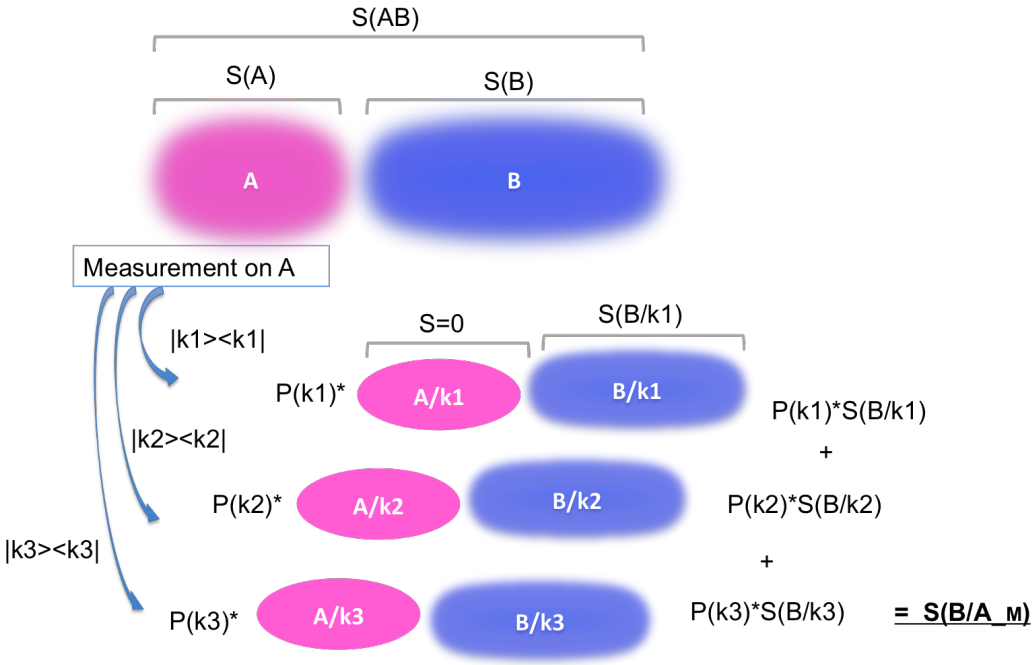

Figure 3-13: (Color online) Illustration of the flow of computing conditional entropy.

particle.

$$\begin{cases} \pi^{1/2}_{-1/2}(\alpha,\beta) = \sum_{n,\mu} \mathrm{e}^{i\alpha(\mu-n)} d^{(1)}_{n,-1/2}(\beta) d^{(1)}_{\mu,-1}(\beta) \left|j,n\right\rangle \left\langle j,\mu\right| \\ \\ \pi^{1/2}_{1/2}(\alpha,\beta) = \sum_{n,\mu} \mathrm{e}^{i\alpha(\mu-n)} d^{(1)}_{n,1/2}(\beta) d^{(1)}_{\mu,0}(\beta) \left|j,n\right\rangle \left\langle j,\mu\right| \end{cases} \tag{3.91}$$

where in spin $1/2$ case, the Wigner matrix has the familiar form.

$$\begin{pmatrix} d^{(1)}_{-1/2,-1/2}(\beta) & d^{(1)}_{1/2,-1/2}(\beta) \\ d^{(1)}_{-1/2,1/2}(\beta) & d^{(1)}_{-1/2,1/2}(\beta) \end{pmatrix} = \begin{pmatrix} \cos(\beta/2) & -\sin(\beta/2) \\ \sin(\beta/2) & \cos(\beta/2) \end{pmatrix},$$

Using these expressions, the probabilistic sum of the von Neumann entropy of the subsystem B based on each of the operator basis, labeled by α and β, $(\sum_k p_k S(\rho_{B|k}))$ is computed (Fig. 3-14).

$N_A = 1$, $N_B = N - 1$ case: Let us next examine the case where the total number of the particles in subsystem A consists of one particle, and the remaining subsystem B is $n-1$ particles. The measurement operators are the same, and therefore the

procedure is fundamentally the same as the $N_A = 1$, $N_B = 1$ case.

$N_A = 2$, $N_B = N - 2$ case: For $N_A = 2$, the measurement of A returns three possible values: -1, 0 and 1. Each of such measurement operators are described as

$$\begin{cases} \pi^j_{-1}(\alpha,\beta) = \sum_{n,\mu} \mathrm{e}^{i\alpha(\mu-n)} d^{(1)}_{n,-1}(\beta) d^{(1)}_{\mu,-1}(\beta) \left|j,n\right\rangle \left\langle j,\mu\right| \\ \pi^j_{0}(\alpha,\beta) = \sum_{n,\mu} \mathrm{e}^{i\alpha(\mu-n)} d^{(1)}_{n,0}(\beta) d^{(1)}_{\mu,0}(\beta) \left|j,n\right\rangle \left\langle j,\mu\right| \\ \pi^j_{1}(\alpha,\beta) = \sum_{n,\mu} \mathrm{e}^{i\alpha(\mu-n)} d^{(1)}_{n,1}(\beta) d^{(1)}_{\mu,1}(\beta) \left|j,n\right\rangle \left\langle j,\mu\right| \end{cases} \tag{3.92}$$

n, μ that appear in the summations run from -1 to 1. Fig. 3-16 shows the sum of the von Nuemann entropy for $N_A = 2$ and $N_B = 2$.

many particle vs many particle case: Lastly, we consider the case where subsystems A and B both consist of more than two particles each. Fig. 3-17 shows the sum of the von Nuemann entropy for $N_A = 4$ and $N_B = 12$.

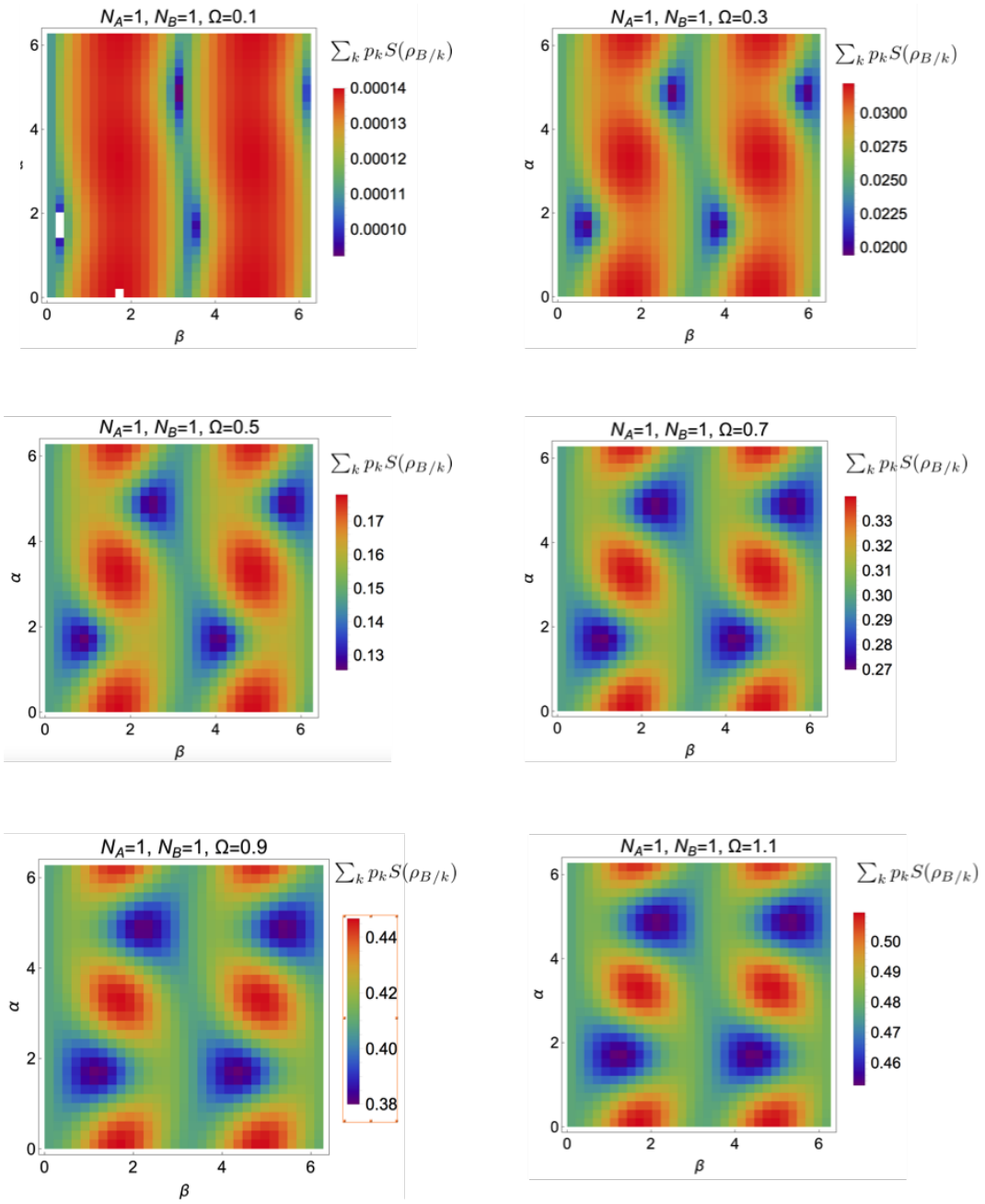

Figure 3-14: (Color online) Probabilistic sum of von Nuemann entropy of ρ_B after measurements, labeled by α and β, are performed on subsystem A. $N_A = 1, N_B = 1$

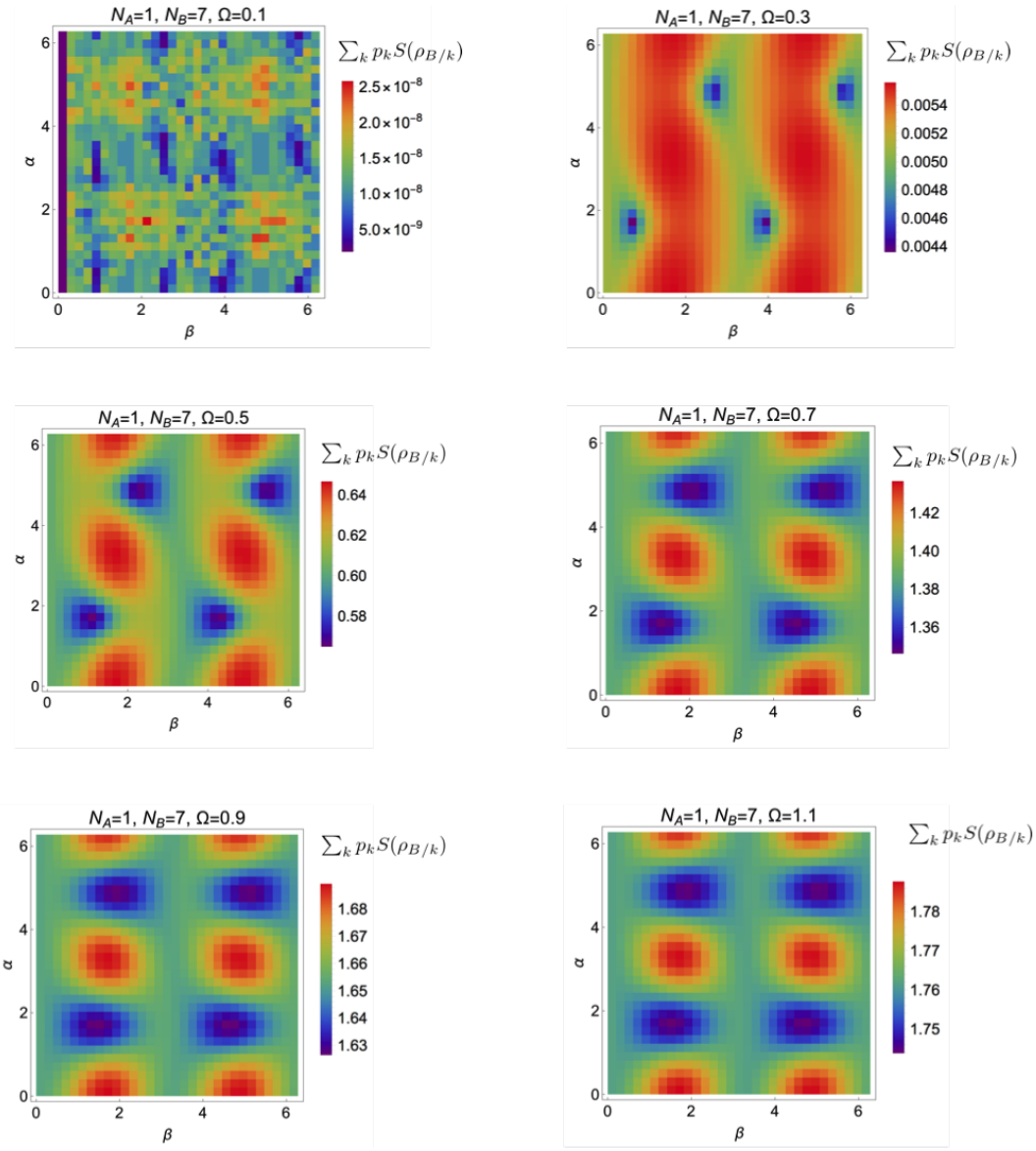

Figure 3-15: (Color online) Probabilistic sum of von Nuemann entropy of ρ_B after the measurements, labeled by α and β, performed on subsystem A. $N_A = 1, N_B = 7$

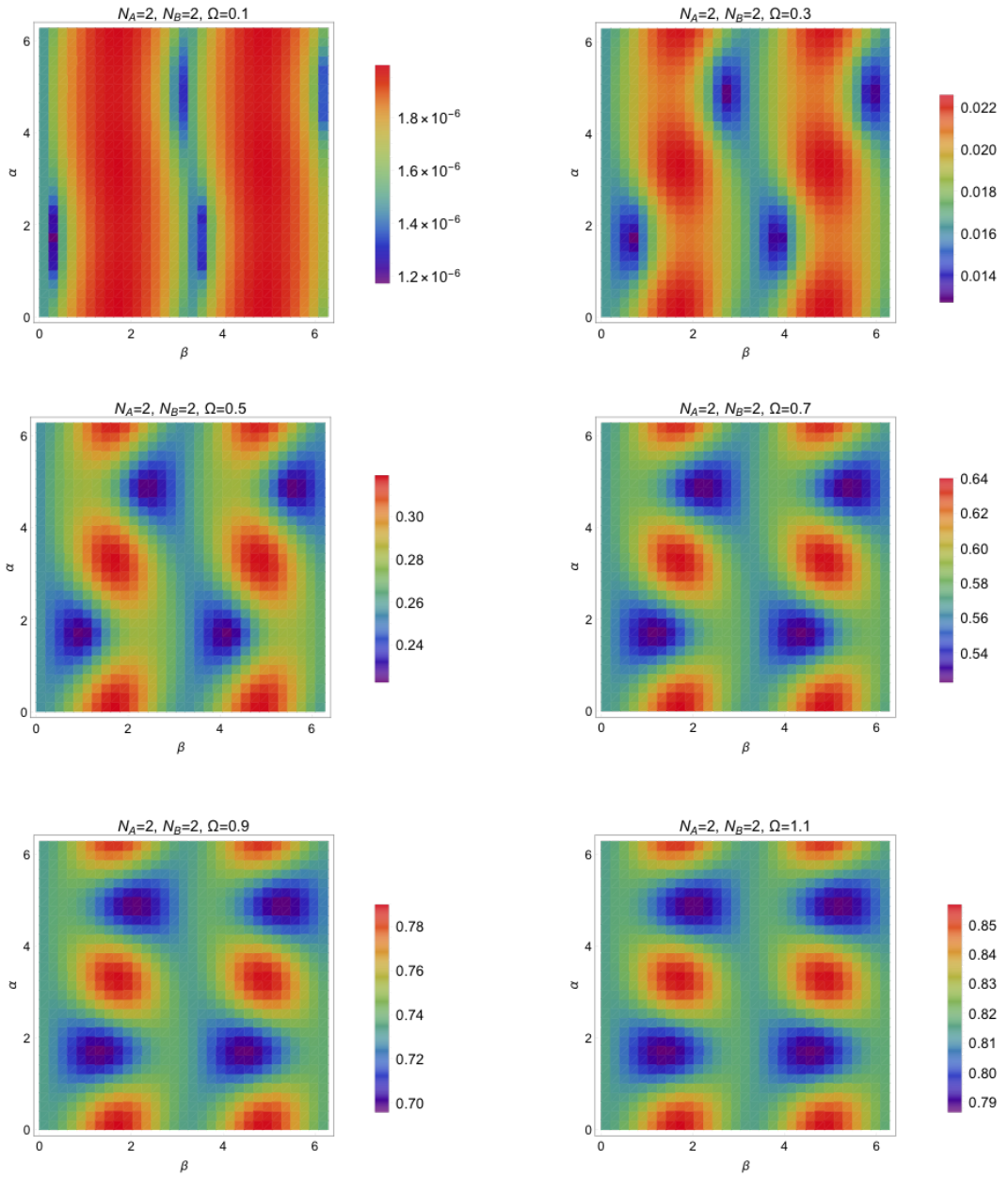

Figure 3-16: (Color online) probabilistic sum of von Nuemann entropy of ρ_B after the measurements, labeled by α and β, are performed on subsystem A. $N_A = 2, N_B = 2$

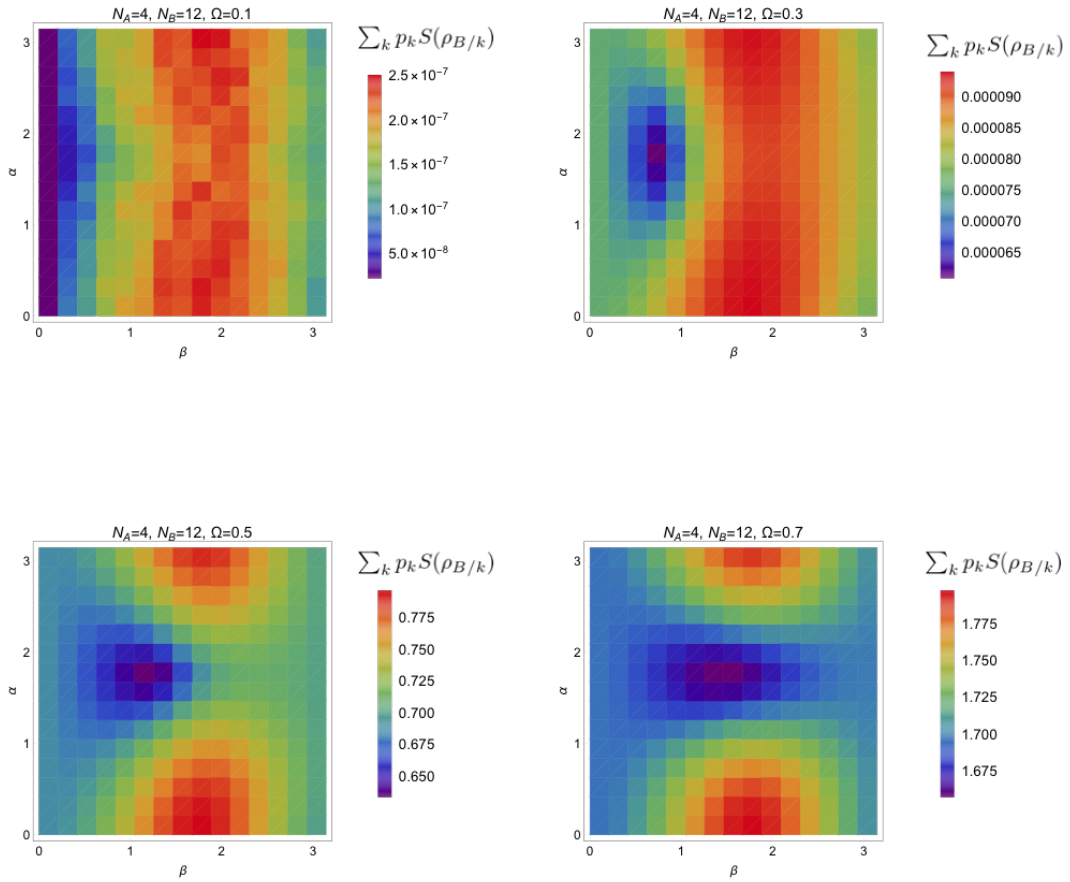

Figure 3-17: (Color online) probabilistic sum of von Nuemann entropy of ρ_B after the measurements, labeled by α and β, are performed on subsystem A. $N_A = 4, N_B = 12$

Computing correlations

The minimum value of the von Neumann entropies plotted in the previous subsection yields the conditional entropy ($S_{B|A}$). With that, we are finally able to compute the total correlation (I_{tot}), classical correlation (I_c) and the quantum discord ($D^{\rightarrow}(\rho_{AB}) = I_{tot} - I_c$). The results are shown for various subsystem sizes (Fig. 3-18 to Fig. 3-21).

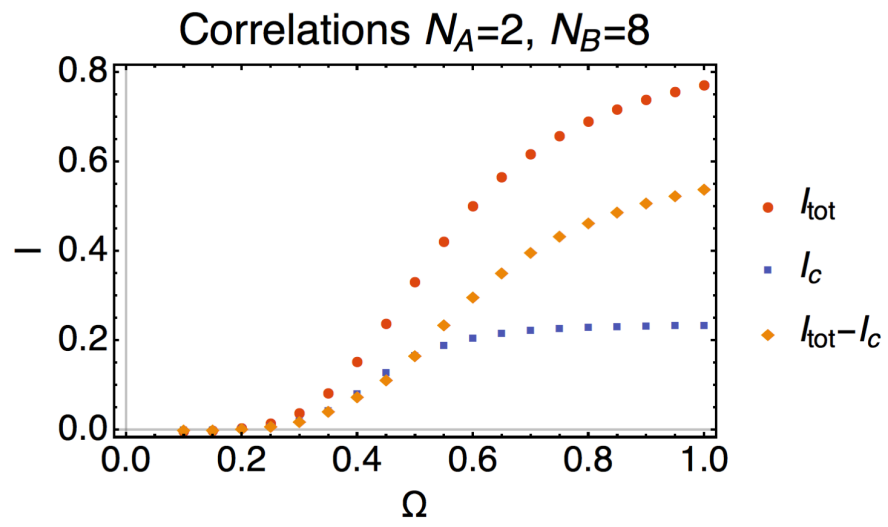

Figure 3-18: (Color online) Correlations between subsystem A and B plotted against Ω. N_A =2, N_B = 8

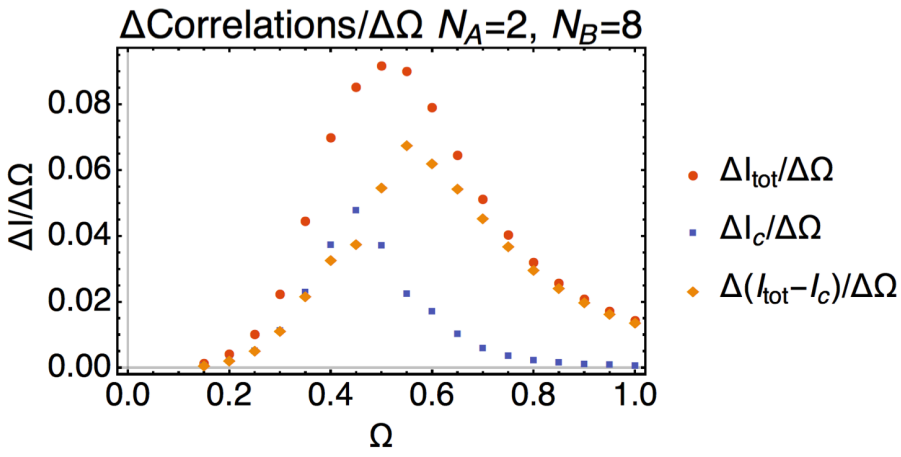

Figure 3-19: (Color online) Correlations between subsystem A and B differentiated by Ω. N_A =2, N_B = 8

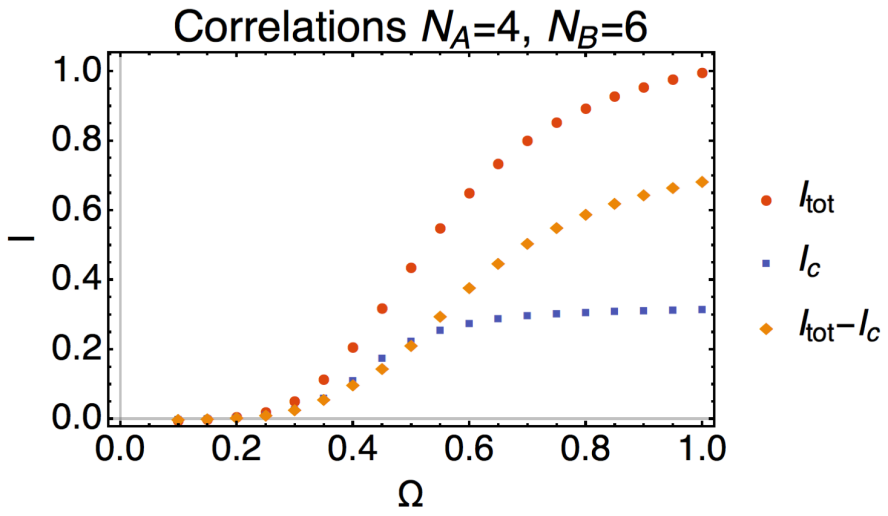

Figure 3-20: (Color online) Correlations between subsystem A and B plotted against Ω. N_A =4, N_B = 6

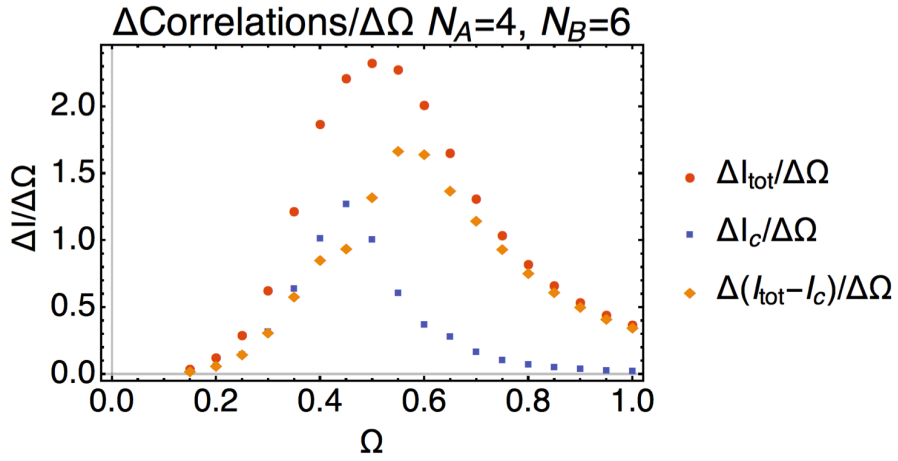

Figure 3-21: (Color online) Correlations between subsystem A and B differentiated by Ω. N_A =4, N_B = 6

3.5.3 Conclusion

The steady state of the driven dissipative model is believed to be entangled at $\Omega < 0.5$, when the purity of the system is close to 1. However, our $n-k$ separability arguments with various k suggests that even for $\Omega > 0.5$ and when the system is highly mixed, the system is still entangled. The entanglement seems to be peaked at the critical point, suggesting the phase transition is quantum-like. However, the results of correlation and quantum discord imply that the total correlation of the system is not peaked at the transition point, which contradicts with many of the cases of typical thermal phase transitions and pure quantum phase transitions. The correlation of the Dicke model does monotonically increase with respect to Ω, while classical correlation reaches plateau, suggesting for large Ω, the system builds up quantum discord that is different from entanglement.

We have shown that, despite its long history, from a relatively modern quantum information theory perspective, the semi-classical driven-dissipative Dicke model is still an interesting model in that its steady state can be tuned into 1. A pure state with no entanglement, 2. A pure state with entanglement 3. A mixed state with entanglement and 4. A mixed state with no entanglement but large nonclassical correlation. It is remarkable that these states can be accessed essentially by one parameter Ω, the Rabi frequency, which, in real experiments, would be easily manipulated by either by varying the power or the wavelength of the laser.

While the entanglement of the steady state in the pure state region can be useful in quantum technologies, such as enhanced sensitivity from spin squeezing [49] or quantum Fisher information, it is an interesting question to ask whether the entanglement in the mixed state region would be of any practical use. Along the line, the implication and application of the quantum discord of the model is an interesting topic that should be studied in the future.

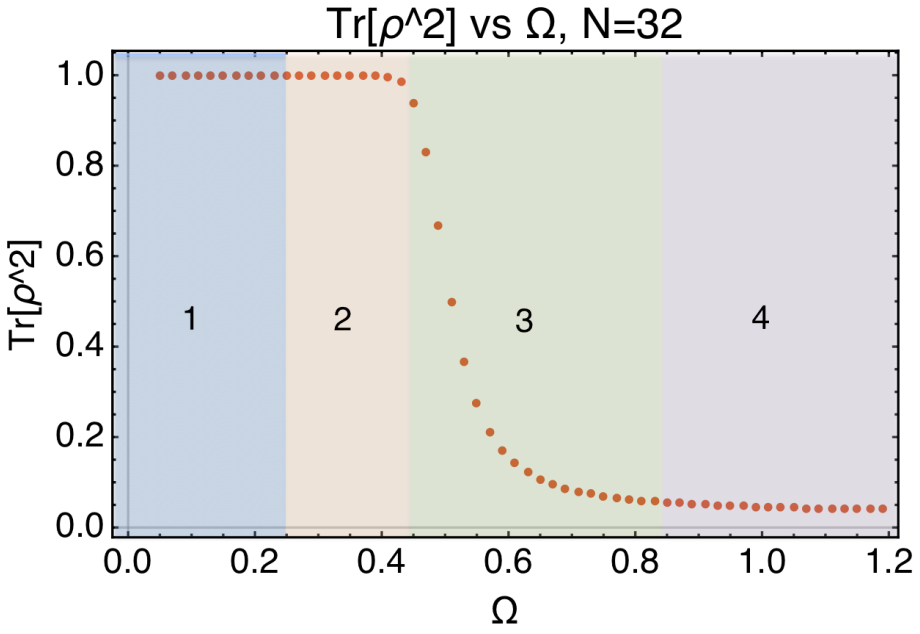

Figure 3-22: (Color online) Qualititative classification of the steady state based on the correlation between the atoms.

1. A pure state with little entanglement, 2. A pure state with entanglement 3. A mixed state with entanglement and 4. A mixed state with little entanglement but large nonclassical correlation.

Chapter 4

Summary

In summary, this study has shown that the dipole-dipole interacting atomic systems can access a variety of phases with relatively simple experimental controls, provided that the model is chosen appropriately. For example, in the zigzag system described in Chapter 2, it was demonstrated that a large number of phases can be realized depending on the depth of the optical lattice and the angle of the external field. In the driven-dissipative Dicke model of Chapter 3, it was shown that it is possible to create steady states with completely different correlation patterns between the atoms, including quantum entanglement, depending only on the Rabi frequency of the atoms in the laser field.

For the outlook of the study, the reader should refer to the conclusion section of each chapter.

Bibliography

[1] A F Albuquerque, D Schwandt, B Hetényi, S Capponi, M Mambrini, and A M Läuchli. Phase diagram of a frustrated quantum antiferromagnet on the honeycomb lattice: Magnetic order versus valence-bond crystal formation. Phys. Rev. B, 84(2):24406, 7 2011.

[2] Luigi Amico, Rosario Fazio, Andreas Osterloh, and Vlatko Vedral. Entanglement in many-body systems. Rev. Mod. Phys., 80(2):517–576, 5 2008.

[3] M. a. Baranov, M. Dalmonte, G. Pupillo, and P. Zoller. Condensed matter theory of dipolar quantum gases. Chemical Reviews, 112(9):5012–5061, 2012.

[4] Marianne Bauer and Meera M Parish. Dipolar Gases in Coupled One-Dimensional Lattices. Phys. Rev. Lett., 108(25):255302, 6 2012.

[5] C Becker, P Soltan-Panahi, J Kronjäger, S Dörscher, K Bongs, and K Sengstock. Ultracold quantum gases in triangular optical lattices. New J. Phys., 12(6):65025, 6 2010.

[6] Vineeth S Bhaskara and Prasanta K Panigrahi. Generalized concurrence measure for faithful quantification of multiparticle pure state entanglement using Lagrange's identity and wedge product. Quantum Information Processing, 16(5):118, 2017.

[7] Fernando G S L Brandão and Michał Horodecki. An area law for entanglement from exponential decay of correlations. Nature Physics, 9(11):721–726, 2013.

[8] F J Burnell, Meera M Parish, N R Cooper, and S L Sondhi. Devil's staircases and supersolids in a one-dimensional dipolar Bose gas. Phys. Rev. B, 80(17):174519, 11 2009.

[9] Lincoln D. Carr, David DeMille, Roman V. Krems, and Jun Ye. Cold and ultracold molecules: Science, technology and applications. New Journal of Physics, 11, 2009.

[10] Amodsen Chotia, Brian Neyenhuis, Steven A Moses, Bo Yan, Jacob P Covey, Michael Foss-Feig, Ana Maria Rey, Deborah S Jin, and Jun Ye. Long-Lived Dipolar Molecules and Feshbach Molecules in a 3D Optical Lattice. Phys. Rev. Lett., 108(8):80405, 2 2012.

[11] M Cross. A new theory of the spin-Peierls transition with special relevance to the experiments on TTFCuBDT. Phys. Rev. B, 19(1):402–419, 1979.

[12] P. D. Drummond. Observables and moments of cooperative resonance fluorescence. Physical Review A, 22(3):1179–1184, 1980.

[13] Volkan Erol. Quantum Fisher Information : Theory and Applications. (April), 2017.

[14] Shunsuke Furukawa, Masahiro Sato, and Akira Furusaki. Unconventional N??el and dimer orders in a spin- 1/2 frustrated ferromagnetic chain with easy-plane anisotropy. Physical Review B - Condensed Matter and Materials Physics, 81(9):1–9, 2010.

[15] Shunsuke Furukawa, Masahiro Sato, Shigeki Onoda, and Akira Furusaki. Ground-state phase diagram of a spin-12 frustrated ferromagnetic XXZ chain: Haldane dimer phase and gapped/gapless chiral phases. Physical Review B - Condensed Matter and Materials Physics, 86(9), 2012.

[16] J J Garc\'\ia-Ripoll, S Dürr, N Syassen, D M Bauer, M Lettner, G Rempe, and J I Cirac. Dissipation-induced hard-core boson gas in an optical lattice. New Journal of Physics, 11, 2009.

[17] T Giamarchi. Quantum Physics in One Dimension. Oxford University Press, 2004.

[18] Alexey V Gorshkov, Kaden R A Hazzard, and Ana Maria Rey. Kitaev honeycomb and other exotic spin models with polar molecules. Molecular Physics, 111(12-13):1908–1916, 2013.

[19] Berry Groisman, Sandu Popescu, and Andreas Winter. Quantum, classical, and total amount of correlations in a quantum state. Phys. Rev. A, 72(3):32317, 9 2005.

[20] L Henderson and V Vedral. Classical, quantum and total correlations. Journal of Physics A: Mathematical and General, 34(35):6899–6905, 8 2001.

[21] S Hofferberth, I Lesanovsky, B Fischer, T Schumm, and J Schmiedmayer. Non-equilibrium coherence dynamics in one-dimensional Bose gases. Nature, 449(7160):324–327, 2007.

[22] Michał Horodecki, Jonathan Oppenheim, and Andreas Winter. Quantum State Merging and Negative Information. Communications in Mathematical Physics, 269(1):107–136, 2007.

[23] Hai-Lin Huang. Entanglement Entropy Signature of Quantum Phase Transitions in a Multiple Spin Interactions Model. Communications in Theoretical Physics, 55(2):349–358, 2 2011.

[24] Bastian Jungnitsch, Tobias Moroder, and Otfried Gu. Taming Multiparticle Entanglement. 190502(May):1–4, 2011.

[25] Michael Knap, Erez Berg, Martin Ganahl, and Eugene Demler. Clustered Wigner-crystal phases of cold polar molecules in arrays of one-dimensional tubes. Phys. Rev. B, 86(6):64501, 8 2012.

[26] Thierry Lahaye, Tobias Koch, Bernd Fröhlich, Marco Fattori, Jonas Metz, Axel Griesmaier, Stefano Giovanazzi, and Tilman Pfau. Strong dipolar effects in a quantum ferrofluid. Nature, 448(7154):672–675, 8 2007.

[27] Elliott H. Lieb and Werner Liniger. Exact analysis of an interacting bose gas. I. the general solution and the ground state. Physical Review, 130(4):1605–1616, 1963.

[28] Shunlong Luo, Shuangshuang Fu, and Nan Li. Decorrelating capabilities of operations with application to decoherence. Phys. Rev. A, 82(5):52122, 11 2010.

[29] Jian Ma, Xiaoguang Wang, C P Sun, and Franco Nori. Quantum spin squeezing. Physics Reports, 509(2):89–165, 2011.

[30] Klaus Mattle, Harald Weinfurter, Paul G Kwiat, and Anton Zeilinger. Dense Coding in Experimental Quantum Communication. Phys. Rev. Lett., 76(25):4656–4659, 6 1996.

[31] Fabio Mezzacapo and Massimo Boninsegni. Ground-state phase diagram of the quantum J1-J2 model on the honeycomb lattice. Phys. Rev. B, 85(6):60402, 2 2012.

[32] A Micheli, G K Brennen, and P Zoller. A toolbox for lattice-spin models with polar molecules. Nat Phys, 2(5):341–347, 5 2006.

[33] Hans-Jürgen Mikeska and Alexei K. Kolezhuk. One-dimensional magnetism. 83:1–83, 2004.

[34] Florian Mintert, André R R Carvalho, Marek Kuś, and Andreas Buchleitner. Measures and dynamics of entangled states. Physics Reports, 415(4):207–259, 2005.

[35] K.-K. Ni, S Ospelkaus, M H G de Miranda, A Pe'er, B Neyenhuis, J J Zirbel, S Kotochigova, P S Julienne, D S Jin, and J Ye. A High Phase-Space-Density Gas of Polar Molecules. Science, 322(5899):231–235, 10 2008.

[36] Leonardo Novo, Tobias Moroder, and G Otfried. Genuine multiparticle entanglement of permutationally invariant states. 012305:1–8, 2013.

[37] Takahiro Ohgoe, Takafumi Suzuki, and Naoki Kawashima. Double peaks in the momentum distribution of cold polar molecules in the supersolid state. Journal of Physics: Conference Series, 400(1):012058, 2012.

[38] E Orignac and R Chitra. Mean-field theory of the spin-Peierls transition. Phys. Rev. B, 70(21):214436, 12 2004.

[39] E Orignac and T Giamarchi. Weakly disordered spin ladders. Phys. Rev. B, 57(10):5812–5829, 3 1998.

[40] Tobias J. Osborne and Michael A. Nielsen. Entanglement in a simple quantum phase transition. pages 1–14, 2002.

[41] Tobias J Osborne and Michael A Nielsen. Entanglement, Quantum Phase Transitions, and Density Matrix Renormalization. Quantum Information Processing, 1(1):45–53, 2002.

[42] Asher Peres. Separability Criterion for Density Matrices. Phys. Rev. Lett., 77(8):1413–1415, 8 1996.

[43] Giulio Racah. Theory of Complex Spectra. II. Phys. Rev., 62(9-10):438–462, 11 1942.

[44] K. O. Roberts, T. Mckellar, J. Fekete, a. Rakonjac, a. B. Deb, and N. Kjærgaard. Steerable optical tweezers for ultracold atom studies. Optics letters, 39(7):2012–5, 2014.

[45] Pranaw Rungta, V Bu\ifmmode \checkz\else ž\fiek, Carlton M Caves, M Hillery, and G J Milburn. Universal state inversion and concurrence in arbitrary dimensions. Phys. Rev. A, 64(4):42315, 9 2001.

[46] Subir Sachdev. Quantum Phase Transitions. Cambridge University Press, 2 edition, 2011.

[47] Erhard Schmidt. Zur Theorie der linearen und nichtlinearen Integralgleichungen. Mathematische Annalen, 63(4):433–476, 1907.

[48] S. Schneider and G. J. Milburn. Entanglement in the steady state of a collective-angular-momentum (Dicke) model. Physical Review A. Atomic, Molecular, and Optical Physics, 65(4):421071–421075, 2002.

[49] R J Sewell, M Koschorreck, M Napolitano, B Dubost, N Behbood, and M W Mitchell. Magnetic Sensitivity Beyond the Projection Noise Limit by Spin Squeezing. Phys. Rev. Lett., 109(25):253605, 12 2012.

[50] Y Sherkunov, Vadim V Cheianov, and Vladimir Fal'ko. Phase transitions in dipolar gases in optical lattices. Phys. Rev. A, 85(2):25603, 2 2012.

[51] J Sirker. THE LUTTINGER LIQUID AND INTEGRABLE MODELS. International Journal of Modern Physics B, 26(22):1244009, 9 2012.

[52] Anders S S\orensen and Klaus M\olmer. Entanglement and Extreme Spin Squeezing. Phys. Rev. Lett., 86(20):4431–4434, 5 2001.

[53] N Syassen, D M Bauer, M Lettner, T Volz, D Dietze, J J Garc\'\ia-Ripoll, J I Cirac, G Rempe, and S Dürr. Strong Dissipation Inhibits Losses and Induces Correlations in Cold Molecular Gases. Science, 320(5881):1329–1331, 2008.

[54] Denis Sych and Gerd Leuchs. A complete basis of generalized Bell states. New Journal of Physics, 11(1):13006, 1 2009.

[55] Tetsu Takekoshi, Markus Debatin, Raffael Rameshan, Francesca Ferlaino, Rudolf Grimm, Hanns-Christoph Nägerl, C Ruth Le Sueur, Jeremy M Hutson, Paul S Julienne, Svetlana Kotochigova, and Eberhard Tiemann. Towards the production of ultracold ground-state RbCs molecules: Feshbach resonances, weakly bound states, and the coupled-channel model. Phys. Rev. A, 85(3):32506, 3 2012.

[56] Géza Tóth. Multipartite entanglement and high-precision metrology. Phys. Rev. A, 85(2):22322, 2 2012.

[57] Géza Tóth, Christian Knapp, Otfried Gühne, and Hans J Briegel. Spin squeezing and entanglement. Phys. Rev. A, 79(4):42334, 4 2009.

[58] S Trotzky, Y-A. Chen, A Flesch, I P McCulloch, U Schollwöck, J Eisert, and I Bloch. Probing the relaxation towards equilibrium in an isolated strongly correlated one-dimensional Bose gas. Nature Physics, 8(4):325–330, 2012.

[59] Christopher N Varney, Kai Sun, Victor Galitski, and Marcos Rigol. Kaleidoscope of Exotic Quantum Phases in a Frustrated XY Model. Phys. Rev. Lett., 107(7):77201, 8 2011.

[60] Matthias Vojta. Quantum phase transitions. Reports on Progress in Physics, 66(12):2069–2110, 11 2003.

[61] A G Volosniev, J R Armstrong, D V Fedorov, A S Jensen, M Valiente, and N T Zinner. Bound states of dipolar bosons in one-dimensional systems. New J. Phys., 15(4):43046, 4 2013.

[62] Teng Long Wang, Ling Na Wu, Wen Yang, Guang Ri Jin, Neill Lambert, and Franco Nori. Quantum Fisher information as a signature of the superradiant quantum phase transition. New Journal of Physics, 16, 2014.

[63] Reinhard F Werner. Quantum states with Einstein-Podolsky-Rosen correlations admitting a hidden-variable model. Phys. Rev. A, 40(8):4277–4281, 10 1989.

[64] Patrick Windpassinger and Klaus Sengstock. Engineering novel optical lattices. Rep. Prog. Phys., 76(8):86401, 8 2013.

[65] Elie Wolfe and S F Yelin. Certifying Separability in Symmetric Mixed States of N Qubits, and Superradiance. Phys. Rev. Lett., 112(14):140402, 4 2014.

[66] Elie Wolfe and S. F. Yelin. Spin Squeezing by means of Driven Superradiance. Arxiv preprint, 1405.5288v(2):5, 2014.

[67] Bo Yan, Steven A Moses, Bryce Gadway, Jacob P Covey, Kaden R A Hazzard, Ana Maria Rey, Deborah S Jin, and Jun Ye. Observation of dipolar spin-exchange interactions with lattice-confined polar molecules. Nature, 501(7468):521–525, 9 2013.

[68] Nengkun Yu. Separability of a mixture of Dicke states. 060101:1–4, 2016.

[69] W H Zurek. Einselection and decoherence from an information theory perspective. Annalen der Physik, 9(11-12):855–864, 2000.